2011

Modeling of diesel particulate filter filtration and regeneration for transient driving schedules

Di Huang
Michigan Technological University

MODELING OF DIESEL PARTICULATE FILTER

FILTRATION AND REGENERATION FOR TRANSIENT

DRIVING SCHEDULES

By

Di Huang

A DISSERTATION

Submitted in partial fulfillment of the requirements for the degree of

DOCTOR OF PHILOSOPHY

(Chemical Engineering)

MICHIGAN TECHNOLOGICAL UNIVERSITY

2011

This dissertation "Modeling of Diesel Particulate Filter Filtration and Regeneration for Transient Driving Schedules," is hereby approved in partial fulfillment of the requirements for the degree of DOCTOR OF PHILOSOPHY IN CHEMICAL ENGINEERING

Department of Chemical Engineering

Signatures:

Dissertation Advisor   _____

Jason M. Keith

Department Chair   _____

Komar Kawatra

Date   _____

Table of Contents

List of Figures

List of Tables

Acknowledgements

I would like to take this opportunity to express my gratitude to all of those who have contributed for the successful completion of this dissertation.

First and foremost, I would like to thank my advisor, Dr. Jason M. Keith for his constant help during my study at MTU. I also thank Dr. Keith for his suggestion, understanding, encouragement, and financial support.

I also would like to thank the other committee members: Dr. Adrienne Minerick, Dr. Daniel A. Crowl, and Dr. Gordon G. Parker for their valuable suggestion and comments.

I would also like to give my sincere thanks to my parents, Yong Huang and Jing Geng, for their encouragement and love.

Special thanks also go to my wife, Qiaoyu Lu, for her encouragement, comments, love and understanding. I would also love to thank my little son,

Abstract

Due to their high thermal efficiency, diesel engines have excellent fuel economy and have been widely used as a power source for many vehicles. Diesel engines emit less greenhouse gases (carbon dioxide) compared with gasoline engines. However, diesel engines emit large amounts of particulate matter (PM) which can imperil human health. The best way to reduce the particulate matter is by using the Diesel Particulate Filter (DPF) system which consists of a wall-flow monolith which can trap particulates, and the DPF can be periodically regenerated to remove the collected particulates.

The estimation of the PM mass accumulated in the DPF and total pressure drop across the filter are very important in order to determine when to carry out the active regeneration for the DPF. In this project, by developing a filtration model and a pressure drop model, we can estimate the PM mass and the total pressure drop, then, these two models can be linked with a regeneration model which has been developed previously to predict when to regenerate the filter.

There results of this project were:

1 Reproduce a filtration model and simulate the processes of filtration. By studying the deep bed filtration and cake filtration, stages and quantity of mass accumulated in the DPF can be estimated. It was found that the filtration efficiency increases faster during

the deep-bed filtration than that during the cake filtration. A "unit collector" theory was used in our filtration model which can explain the mechanism of the filtration very well.

2 Perform a parametric study on the pressure drop model for changes in engine exhaust flow rate, deposit layer thickness, and inlet temperature. It was found that there are five primary variables impacting the pressure drop in the DPF which are temperature gradient along the channel, deposit layer thickness, deposit layer permeability, wall thickness, and wall permeability.

3 Link the filtration model and the pressure drop model with the regeneration model to determine the time to carry out the regeneration of the DPF. It was found that the regeneration should be initiated when the cake layer is at a certain thickness, since a cake layer with either too big or too small an amount of particulates will need more thermal energy to reach a higher regeneration efficiency.

4 Formulate diesel particulate trap regeneration strategies for real world driving conditions to find out the best desirable conditions for DPF regeneration. It was found that the regeneration should be initiated when the vehicle's speed is high and during which there should not be any stops from the vehicle. Moreover, the regeneration duration is about 120 seconds and the inlet temperature for the regeneration is 710K.

Chapter 1 Introduction

1.1 Diesel Particulate Matter (DPM)

Diesel particulate matter (DPM) is the solid particulate component of diesel engine exhaust. The majority of particulates in diesel exhaust consist of small particles. It is likely that inhaled particles can penetrate deep into the lungs. The roughness of the particles allows surface area to bind with other toxins in the environment. This can make particle inhalation a health hazard.

1.2 Heavy Diesel Emission Standard

1.2.1 US Emission Standard

In the United States, emission standards are regulated by the Environmental Protection

Agency (EPA). Also, California has a more stringent emission standard which is managed by the California Air Resources Board (CARB). Table 1.1 shows the EPA emission standards for the years of 1994, 1998, 2002, and 2007, respectively. (1)

1.2.2 Emission Standard in the European Union

The European Union has their own emission standards for diesel vehicles. The different standards for 2000, 2005, and 2008 are shown in Table 1.2. (1)

Table 1.1. EPA Emission Standard

Year	HC (g/bhp-hr)	CO (g/bhp-hr)	NO$_x$ (g/bhp-hr)	PM (g/bhp-hr)
1994	1.30	15.5	5.0	0.10
1998	1.30	15.5	4.0	0.10
2002	0.50	15.5	2.4	0.10
2007	0.14	15.5	0.2	0.01

Table 1.2. European Emission Standard

Year	HC (g/kWh)	CO (g/kWh)	NO$_x$ (g/kWh)	PM (g/kWh)
2000(Euro III)	0.78	5.45	5.0	0.16
2005(Euro IV)	0.55	4.00	3.5	0.03
2008(Euro V)	0.55	4.00	2.0	0.03

1.2.3 Emission Standard in China

The number of cars in China has been rapidly growing. To control emissions, China issued emissions standards in 2000 which were equivalent to Euro I standards. The standards were revised in 2005 and 2007 to Euro II and Euro III standards, respectively. Beijing requires vehicles obey the Euro IV standard as of January, 2008.
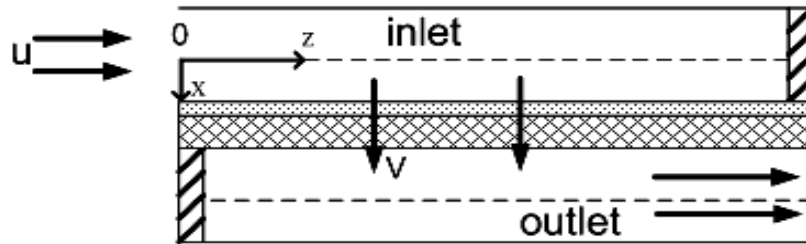
Figure 1.1 Schematic of a DPF channel. (2) (Permission from Elsevier. See Appendix A)

1.3 Diesel Particulate Filter (DPF) and Regeneration

A diesel particulate filter, also known as a DPF, is a design to trap diesel particulate matter (soot) from diesel engine exhaust. 90% or more of the soot can be removed by using a wall-flow monolith particulate filter, which is the best design as seen in Figure 1.1. This structure allows the exhaust to pass through a wall-flow monolith. The channel walls are porous with opposing ends of adjacent channels plugged. As the gas flows through the monolith, the deposit builds up in the inlet channel over time. Therefore, the DPF regenerated to burn off the deposit.

Regeneration is initiated either by adding heat (also called active regeneration) or a catalyst (also called passive regeneration) to the filter. Some filters are used only once (disposable), while others are capable of regenerating the accumulated particulates. There are two general ways, one is the passive method (through the use of a catalyst), while, the other is an active method which combusts fuel in a burner to heat the filter to the soot combustion temperature to burn the particulate off. This is known as "filter regeneration".

1.4 Filtration and Pressure Drop in DPF

Another problem for regeneration is to determine the time when the regeneration is to be carried out. In this work, two control parameters are studied: total mass accumulated in the DPF and pressure drop across the DPF. By assessing the theory of filtration and pressure drop in the DPF, one can estimate the mass accumulation and the changes of pressure drop in the DPF.

1.5 UDDS Driving Cycle

The UDDS stands for Urban Dynamometer Driving Schedule. The duration of the UDDS is 1400 seconds, the distance is around 7.5 miles, and the average speed and the maximum speed are 19.6 mi/h and 56.7mi/h, respectively as seen in Figure 1.2. This UDDS driving cycle will be used in our modeling work. By simulating the DPF regeneration under UDDS driving conditions, we found the best time to initiate the regeneration, also desirable regeneration duration, inlet temperature during the regeneration, exhaust gas flow rate, and deposit thickness for transient driving schedules. (1)
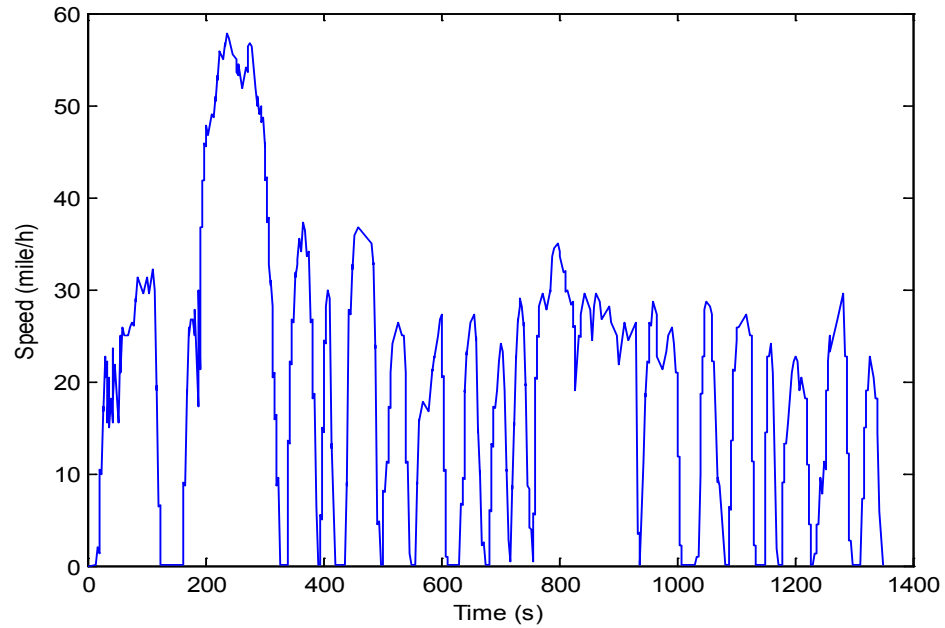
Figure 1.2 UDDS (FTP-72) Driving Cycle. (Data modified from (1))

1.6 Dissertation Outline

The following chapter, chapter 2 presents the reviews of research performed on diesel particulate filters (DPF), including experiments and modeling in filtration, regeneration, and pressure drop.

Chapter 3 presents the equations for a DPF filtration model, which is used to estimate the spatial and temporal distribution of PM within a DPF.

6

Chapter 4 involves the equations for a pressure drop model. The equations shown in this chapter can be solved to estimate the pressure drop for a given temperature and PM distribution within the DPF. Moreover, a parametric study will be taken in this chapter to find out reasonable critical parameters of this pressure drop model during DPF filtration and regeneration.

In chapter 5, real-world driving conditions using the urban dynamometer driving schedule (UDDS) as inlet boundary conditions for the DPF will be performed. Some values of parameters in the filtration model, the pressure drop model, and the regeneration model will be changed to non-uniform which fluctuate during the UDDS driving cycle. Also, in order to maximize the fuel economy, our work focuses on identifying an optimum time during the UDDS cycle to initiate the regeneration of the filter.

In Chapter 6, we develop three simple sinusoidal functions to approximate the vehicle speed for highway driving without stops, city driving without stops, start-and-stop city driving, respectively. This is meant to generalize the regeneration performance during different driving condition and to make comparisons between these simple driving cycles and the UDDS driving cycle.

Chapter 7 summarizes the conclusions of this work and provides recommendations for future work.

1.7 References

(1). Emission test cycles – DieselNet [Internet]. Urban Dynamometer Driving Schedule (UDDS). Available from http://www.dieselnet.com/standards/cycles/ftp72.html

(2). Zheng HS, Keith JM, Ignition analysis of wall-flow monolith diesel particulate filters. Catalysis Today. 2004:98(3):403-412

Chapter 2 Literature Review

2.1 Introduction

The diesel particulate filter (DPF) collects particulates from a diesel engine. In real world applications, the wall-flow monolith DPF is widely used because of its compact arrangement and high filtration and removal efficiency.

There are two models which are able to represent the process of trapping and removing PM from diesel engines: the filtration model and the regeneration model. Also, there is another important model for DPF—the pressure drop model which can be used to simulate the pressure drop across the filter.

In this chapter, the literature describing experiments and modeling of filtration, regeneration, and pressure drop will be reviewed.

2.2 Reviewed Papers

2.2.1 Review of paper "Emission Control Options to Achieve Euro IV and Euro V on Heavy Duty Diesel Engines" by Philip G. Blackman (3)

Due to their high thermal efficiency, modern diesel engines are widely used as vehicle power sources. Moreover, because of the high fuel economy and torque, diesel engines are devoted to heavy-duty applications. In addition, the high power and excellent drivability of today's turbo-charged small high-speed diesel engines becomes an increasing demand for diesel powered light-duty vehicles. Compared to gasoline engines, diesel engines also have lower CO_2 emissions. Diesel engines become the most applicable workhorses of freight and public transportation around the world. For instance, heavy-duty diesel vehicles account for only 2% of the vehicle population in California, but they carry 80% of the freight.

However, diesel engines produce more PM and NOx emissions. Since these emissions may affect human beings' health, future emission standards around the world for diesel vehicles are becoming more stringent. In order to help achieve the tighter emissions standards, advanced aftertreatment technology utilizing oxidation and reduction catalysts in systems capable of high conversion of all four pollutants are

being developed. Compared to NOx and PM, the HC and CO emission limits are not too difficult to meet the emission standards because of the low production from the engines.

It is understood that the diesel oxidation catalyst (DOC) and the DPF can significantly reduce PM, HC, and CO emissions from diesel engines. The key emission control technologies available for NOx control on Heavy Duty-Diesel (HDD) engines are Exhaust Gas Recirculation (**EGR**) and Selective Catalytic Reduction (**SCR**). EGR is one proven system to effectively reduce the NOx emission from diesel exhaust and has been used for light-duty engines for many years. By using ammonia, derived from urea, SCR has been demonstrated as highly effective in heavy duty applications as the reductant for NOx control.

There are three main reactions that consume NOx in the SCR:

$$4NH_3 + 4NO + O_2 \rightarrow 4N_2 + 6H_2O \tag{1}$$

$$4NH_3 + 2NO + 2NO_2 \rightarrow 4N_2 + 6H_2O \tag{2}$$

$$8NH_3 + 6NO_2 \rightarrow 7N_2 + 12H_2O \tag{3}$$
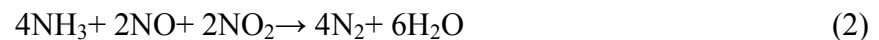
Each reaction is dominant under different conditions. If there is no NO_2 in the exhaust gas, reaction (1) is dominant and it is a fast reaction. When NO_2 is present in the NOx

(small fraction), a significant improvement in activity is observed due to reaction (2), which is very fast. However, the ratio of NO_2: NO in the NOx can influence reaction (2). At ratios up to 1:1, reaction (2) is dominant and the presence of NO_2 leads to improve low temperature NOx conversion in the SCR system. Once the ratio is larger than 1, reaction (3) becomes dominant, however, this reaction is very slow. Therefore, overall NOx reduction could decrease under conditions where NO_2: NO ratio is over 1.

2.2.2 Review of paper "Detailed Diesel Exhaust Particulate Characterization and Real-Time DPF Filtration Efficiency Measurements During PM Filling Process." by D. E. Foster and T. Kusaka (4)

The filtration efficiency of the DPF increases when the deposit layer forms on the substrate wall of the filter. In reality, the clean filter has poor filtration efficiency. It acts more as a facilitator to form a soot cake for the filtration of diesel particulates. From the experimental results, the authors found that different engine operating conditions results in variable PM concentration, as well as chemical composition of the particulates. In addition, the engine operation impacts PM size distribution and the gas flow rate and filtration velocity. DPF pressure drop and filtration performance are

impacted by all of these parameters.

There are two major steps in the DPF filtration process which are "deep bed filtration" and "cake filtration" as shown in Figure 2.1. Stage 1 shows a clean DPF. Stage 2 illustrates PM being collected inside the pores of the substrate. Finally, stage 3 is reached when a thin "cake layer" of PM begins to develop on the substrate walls of the inlet channels.
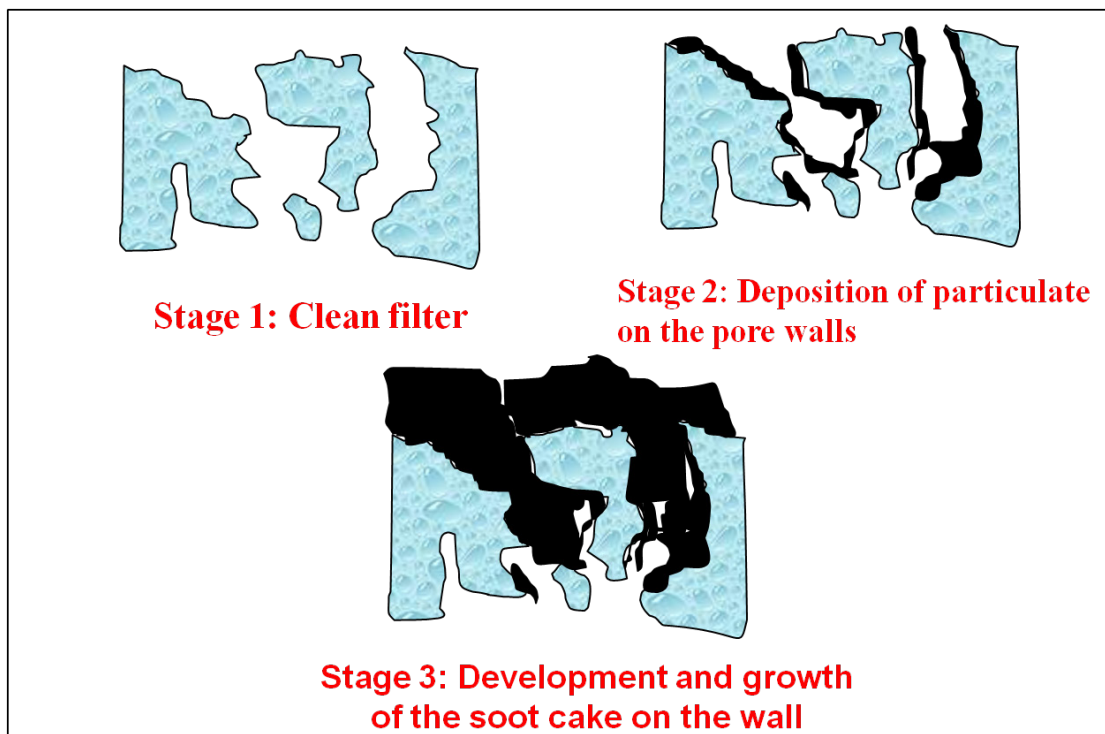
Figure 2.1 Stages of filtration in the inlet channel of DPF (Modified from (4))
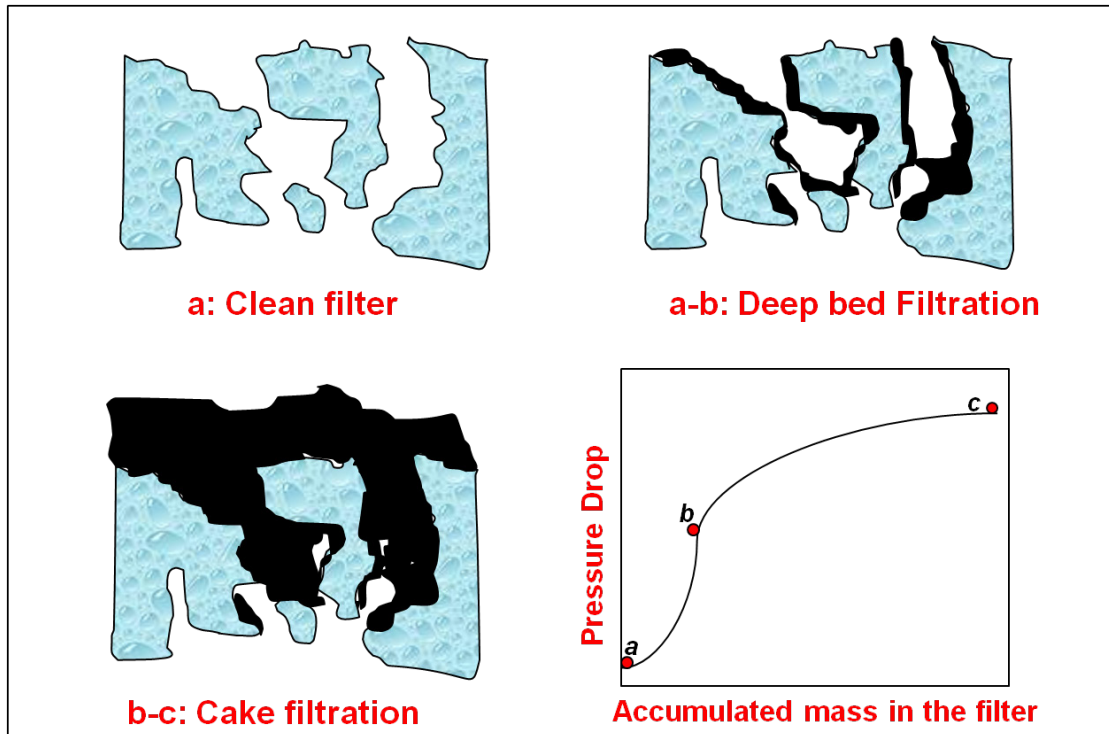
Figure 2.2 Pressure drop during DPF filing. (Modified from (4))

A general plot of pressure drop is shown in Figure 2.2. The pressure drop increases quickly as the pores become plugged in stages a and b which is the deep bed filtration. Pressure drop during stages a and b increases non-linearly. But during the cake filtration (from b to c), there is a linear and slower rise in the pressure drop curve as the cake layer becomes thicker.

2.2.3 Review of paper "Filtration Behavior of Diesel Particulate Filters" by H. Sakai, P. Busch, and C.D.Vogt (5)

In this paper, the effect of pore size and pore size distribution on the PM filtration efficiency of the ceramic monolith wall-flow DPF was studied. These researchers used small round plates with different average mean pore sizes (4.6, 9.4, 11.7, 17.7μm) with a narrow pore size distribution. During the DPF filtration efficiency tests, $ZnCl_2$ particles, whose diameter is in the range of 10 nm to 500 nm, were used instead of PM. Various sizes of $ZnCl_2$ particles were introduced into the gas flow. Performing a count of the numbers of particles upstream and downstream of the filter yielded a direct calculation of the filtration efficiency.

As shown in Figure 2.3, there are four kinds of filtration mechanisms: diffusion, interception, inertia and gravity. The **diffusion** collection mechanism arises as aerosol particles deviate from their line of flow due to Brownian diffusion, and are collected by coming into contact with the filter material. In the **interception** collection mechanism, particles that follow along their line of flow are collected by coming into contact with the filter material. The larger the aerosol particles, the easier it is for PM to be collected. The **inertial** collection mechanism is the condition whereby due to a

rapid change in flow angle (such as at the back end of a DPF inlet channel) the PM particles deviate from their flow line as a result of their inertia and are collected by colliding with the filter material. Finally, the **gravity** and electrostatic collection mechanisms also assume PM particles deviate from their flow line due to the respective forces.
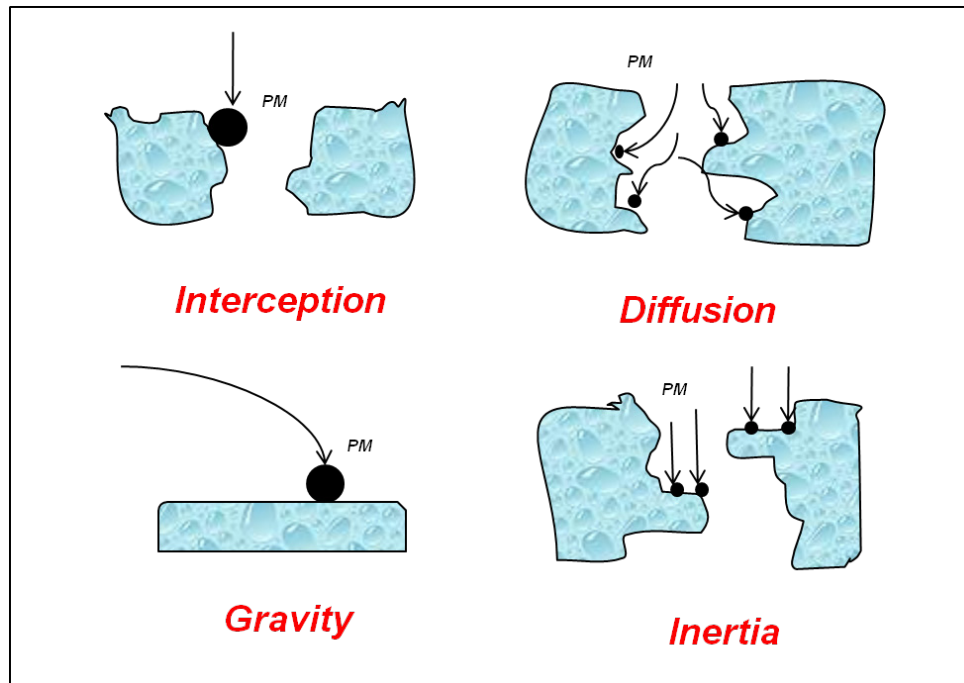
Figure 2.3 Filtration Mechanism. (Modified from (5))

Some of the results of the experiments are summarized below. A reduction in pore diameter and flow speed always raised the filtration efficiency. The filtration efficiency increases with decreasing the mean pore diameter. Comparing the filter with 25μm mean pore diameter and the filter with 15μm mean pore diameter, it can be noticed that there is a significant difference in PM filtration during preconditioning.

The filtration efficiency improved from 80% to 92% by reducing the mean pore diameter from 25 μm to 15 μm.   When the PM loading rate becomes more than 0.3 g/L, filtration efficiency with an optimized pore size in the filter exceeds 95%.

2.2.4 Review of "A Methodology to Estimate the Mass of Particulate Matter Retained in a Catalyzed Particulate Filter as Applied to Active Regeneration and On-Board Diagnostics to Detect Filter Failures". J. H. Johnson, J. D. Naber, and S.T. Bagley (6)

There are many different parameters which may influence the regeneration efficiency of Catalyzed Particulate Filter (CPF) such as: total pressure drop, volumetric flow rate, exhaust temperature, exhaust gas viscosity and the permeability of the cake and wall materials. In this paper, the authors discussed a computational methodology to estimate the regeneration efficiency.

The authors found that the mass of particulate matter (PM) in the wall can be oxidized under temperatures above 350 $^{\circ}$C and significantly affect the wall pressure drop and the total pressure drop. This effect would result in a poor correlation between

pressure-drop across the CPF and the mass accumulated in the CPF. The authors also found an accurate estimation of the PM mass retained in the CPF is important in order to determine the time to initiate the regeneration of CPF. At any given engine load, more than 98% of the PM mass retained in the CPF is in the cake layer and about only 2% of the particulates is inside the pores of the substrate wall. Although by the mass most of the PM is in the cake layer, the cake layer only accounts for 8-50% of the pressure drop.

Filter failures have always been a matter of concern as limited parameters would be available to indicate failure in an operating vehicle. One of the key requirements of a particulate filter system is durability. The material used for the CPF should have a high filtration efficiency, low thermal expansion, high strength design, high thermal capacity, and controlled regeneration conditions. (6)

One method currently used in the industry to estimates the mass accumulated in the CPF is from the total pressure drop and empirical relations. The authors suggest employing estimation of the mass retained in the CPF from the calculated cake pressure drop and the measured total pressure drop in order to give more accurate results, since 98% of the PM mass retained is in the cake. The pressure drop equations

for each phase are shown below:

$$\Delta P = \Delta P_{\text{fliter wall}} + \Delta P_{\text{soot layer}} + \Delta P_{\text{inlet channel}} + \Delta P_{\text{outlet channel}} \tag{2.1}$$

Equation 2.1 shows the total pressure drop across the DPF. The total pressure drop is equal to the summation of pressure drop across the substrate wall and deposit thickness, and pressure drop due to the inlet and outlet channels friction, which are shown below in Equations 2.2-2.5:

$$\Delta P_{\text{fliter wall}} = \frac{\mu Q}{2V_{\text{trap}}} (\alpha + w)^2 \left(\frac{w}{k_0 \alpha} \right) \tag{2.2}$$

$$\Delta P_{\text{soot layer}} = \frac{\mu Q}{L \pi D_f^2 k_{\text{soot}}} (\alpha + w)^2 \ln \left(\frac{\alpha}{\alpha - 2w_s} \right) \tag{2.3}$$

$$\Delta P_{\text{inlet channel}} = \frac{\mu Q}{2V_{\text{trap}}} (\alpha + w)^2 \left(\frac{4FL^2}{3(\alpha - 2w_s)^4} \right) \tag{2.4}$$

$$\Delta P_{\text{outlet channel}} = \frac{\mu Q}{2V_{\text{trap}}} (\alpha + w)^2 \left(\frac{4FL^2}{3\alpha^4} \right) \tag{2.5}$$

$$m_{\text{cake}} = \left[\frac{\Delta P}{\mu Q} - \frac{C_2}{k_t} - c_3 \right] * \frac{k_p}{C_1} \tag{2.6}$$

Equation 2.6 shows the mass of cake layer which is used to calculate the deposit thickness.

$$C_1 = \frac{1}{\rho_p} \frac{1}{16(n\alpha L)^2} \tag{2.7}$$

$$C_2 = \frac{w_s}{4n\alpha L} \tag{2.8}$$

$$C_3 = \frac{2}{3} \frac{LF}{n\alpha^4} \tag{2.9}$$

$C_1,$ $C_2,$ and C_3 are three constants where the authors made an assumption that the density of the PM cake (ρ_p) does not vary considerable with load. In these equations,

the following symbols are used as seen in table 2.1.

Table 2.1 Symbols in pressure drop model

ΔP	Pressure Drop, kPa
D_f	Filter diameter, 24 cm
F	Factor equal to 28.454
k_0	Clean filter wall permeability, 3×10^{-9} cm^2
k_{soot}	Particulate layer permeability, 1.1×10^{-11} cm^2
k_t	Loaded wall permeability, m^2
L	Filter length, 32 cm
m_{cake}	Mass retained in the cake layer, gms
Q	Actual exhaust volumetric flow rate, m^3/s
V_{trap}	Total filter filtration volume, cm^3
w	Filter wall thickness, 4.76×10^{-2} cm
w_s	Particulate matter layer thickness, 1.2×10^{-3} cm
α	Filter cell width, 0.211 cm
μ	Exhaust dynamic viscosity, Ns/m^2
ρ_p	PM cake layer packing density, 1.1 g/cm^3

2.2.5 Review of "Experimental Study of DPF Loading and Incomplete Regeneration" by D. Pinturaud, A. Charlet, C. Caillol, P. Higelin, P. Girot, and A. Briot (7)

In this paper, to study partial regeneration, the authors designed two specific experiments. The first apparatus is used to observe the radial distribution of soot after loading and the remaining soot after a controlled partial regeneration. The second apparatus is used to observe the localization of soot in the longitudinal direction.

The controlled regeneration was initiated when the filter is loaded at 7 g/l. The authors set up this controlled regeneration experiment as the following conditions: 10 minutes post-injection period; engine speed of 1700 rpm and the engine torque is 95 N-m. During the regeneration, the amount of oxidized soot depends upon the DPF inlet temperature which is controlled by the volume of injected fuel.

In Figure 2.4, the mass regeneration efficiency which is the ratio between the mass of soot regenerated and mass of soot loaded is shown as a function of the filter feed temperature. The method of controlled regeneration can be used to choose the amount of soot that it expects to oxidize with great accuracy. Similarly, to increase the inlet

temperature after 10 minutes of post-injection a larger amount of post-injection is needed. By using these methods, the spatial and temporal behavior of the regeneration can be observed.

The authors found that the soot layer has a uniform distribution on the four sides of the channel wall which indicates that the gas flow is equally divided to the four walls of the channel.
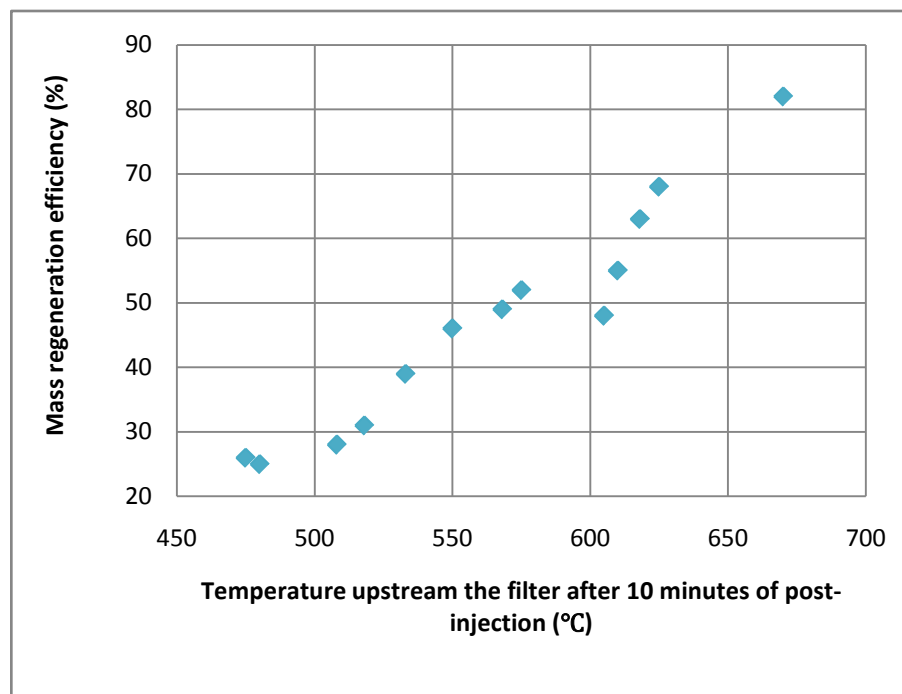
Figure 2.4 Mass regeneration efficiency as a function of upstream DPF exhaust gas temperature (Data reproduced from (7)).

From Figure 2.5 shown below, the authors found that more particulates are deposited at the end of the channel than those at the entrance of the channel. When the loading is low, the distribution of soot is not completely uniform. Otherwise, the thickness becomes more uniform when the loading increases.

Figure 2.6 shows the evolution of soot along the filter after a controlled regeneration. The dotted line is the reference curve which represents regeneration efficiency of 0% i.e. a loading at 7 g/L. For regenerations corresponding to mass regeneration efficiency less than 45%, one can find that the deposit thickness after regeneration is larger. This may be explained by the fact that the temperature of the exhaust gas is too low to burn off the soot which is not in contact with the catalyst. Fresh soot is then deposited on top of the remaining soot. The mass decrease at higher regeneration efficiencies is due to soot which is oxidized inside the wall and near the wall surface (7)
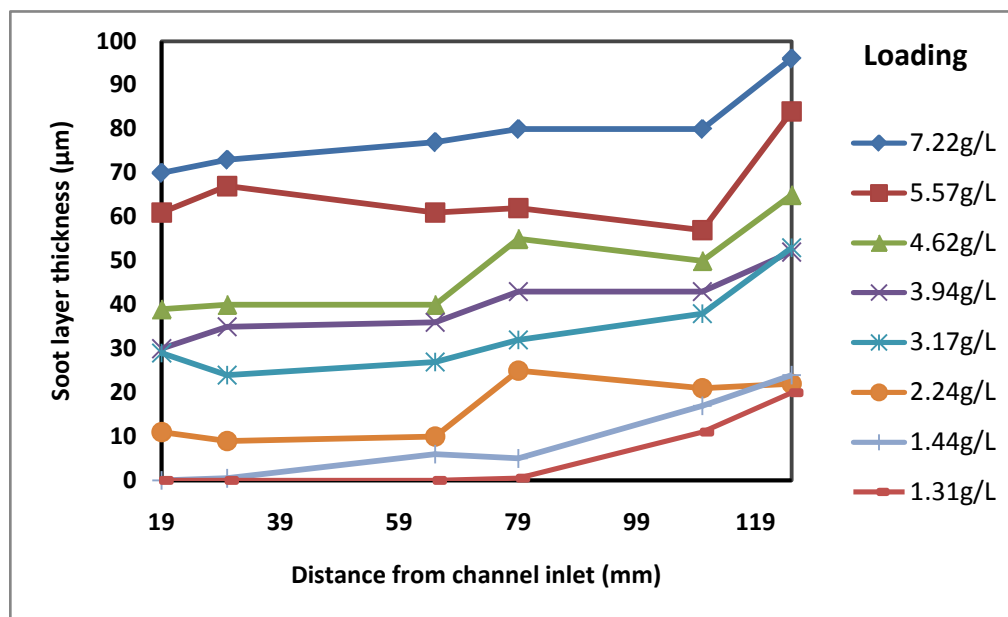
Figure 2.5 Soot layer thickness along the filter as a function of loading. (Data reproduced from (7))
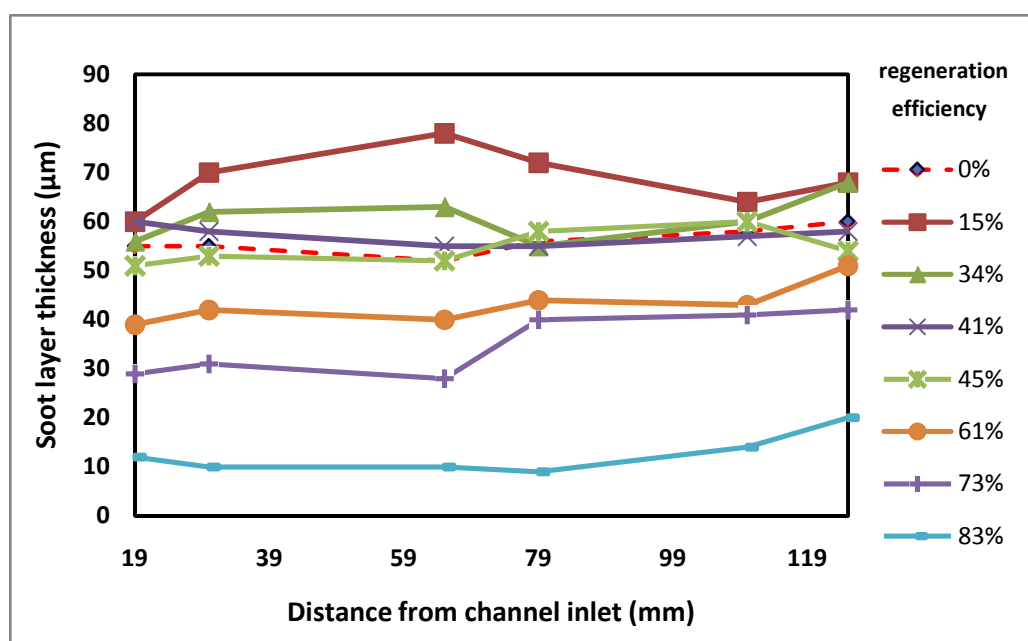
Figure 2.6 Soot layer thickness along the filter as a function of mass regeneration efficiency.

(Data reproduced from (7))

2.2.6 Review of "Filtration Behavior of Diesel Particulate Filters (2)" by T. Mizutani, A. Kaneda, S. Ichikawa, H. Kurachi, C. D. Vogt, M. Tanaka, A. Martin, S. Fujii and P. Busch (8)

The authors described the characteristics of the DPF and how the design of the DPF affects PM filtration efficiency, emissions levels, and the pressure drop in the DPF. Results show that filter MPS (mean pore size) smaller than 15μm results in 100% filtration efficiency. They also note that the filtration efficiency decreases with increasing MPS up to 20μm, after which there is no impact on filtration efficiency.

It can be noticed that when the total area of the flow passage is very small, the pressure drop goes up sharply. Because the pore area is proportional to MPS squared, the effect is large especially for small pores. For a clean filter there is a considerable increase in pressure drop if MPS < 10μm. However, the rate of pressure drop decrease is nearly negligible if MPS > 10μm. As soot fills the pores during deep bed filtration, the pressure drop increases a significant amount. Then, soot accumulates on the substrate wall and forms a soot cake layer resulting in a smaller pressure drop increase proportional to the cake thickness. It also can be found that the pressure drop with soot loading depends on porosity, such that for higher porosity values, the pressure drop is

lower. However, the pore size has very little effect on pressure drop with soot loading (during cake filtration).

2.2.7 Review of "Diesel Particulate Filter Optimization" by C. Barataud, S. Bardon, B. Bouteiller, V. Gleize, A Charlet and P. Higelin (9)

Recrystallized Silicon carbide (R-SiC) honeycombs have been widely used for DPFs. Although this kind of filter design is very reliable, existing aftertreatment devices can still be improved.

In this paper, the author describes several new features developed for R-SiC diesel particulate filters in order to increase their durability and reduce their cost. Durability can be improved by optimizing the different filter properties, such as thermo-mechanical resistance and thermal diffusivity.

During the thermal regeneration of a DPF, heat released from the soot combustion results in an increasing temperature in the filter and strong thermal gradient across the filter. When silicon carbide is used for the filter material, uniform temperature increase

will not result in filter damage. One reason is that SiC is a refractory material with extreme resistance to high temperatures. However, thermal gradients might lead to filter damage if the filter is not correctly designed. Today, R-SiC filters with segmented structures are used in order to improve the thermo-mechanical resistance and the durability of the filters.

The filter assembly method will now be described. Because of the temperature fields occurring within a filter during thermal regenerations, they used a "two-zone" assembling method. The filter is separated in two zones (so-called 'entrance' and 'exit') where the properties are different: for the "entrance" it has good mechanical strength, no soot leakage, high thermal diffusivity, thermal stability, and chemical stability, while, for the "exit", it has low elastic modulus, low resistance to shear, good thermal diffusivity, thermal stability, and chemical stability. This "two-zone" assembling has better thermo-mechanical strength and radial thermal diffusivity when compared to conventional technology. For this "two-zone" assembly method, the "entrance zone" is used to improve filters' integrity and durability, while, the "exit zone" is for reinforcing the mechanical stress relaxation of the filter. However, both zones have good thermal and chemical stability.

2.2.8 Review of "Pressure Drop of Segmented Diesel Particulate Filters" by M. Masoudi (10)

This work analyzes performance of a DPF with monolithic and segmented designs.

Monolithic vs. Segmented Filters

Recently, most of the DPFs are made of refractory ceramics. The two most common materials are: Cordierite (Cd) and Silicon Carbide (SiC). Cordierite filters are manufactured through an extrusion process so that it is a single piece monolithic filter. On the other hand, many SiC filters are extruded in smaller 'segments' and the joined together to form the filter full.

For the same DPF cross-section, wall thickness, and cell density, there is a higher flow resistance in the segmented filter and therefore a larger pressure drop.

From Darcy law of pressure drop due to flow through a porous wall, one can obtain:

$$\Delta P = \frac{\mu \bar{U} w_S}{k_{wall}} \tag{2.10}$$

Equations (2.11)-(2.14) represent the pressure drop for substrate wall, soot layer, inlet

channel, and outlet channel for the segmented DPF, respectively.

$$\Delta P_{wall} = \frac{\mu Q w_S}{k_{wall}} \frac{1}{\overline{n_4}(4D_h L)} \tag{2.11}$$

$$\Delta P_{soot} = \frac{\mu Q}{8 k_{soot} \, \overline{n_4} L} \ln \frac{D_h}{(D_h - 2w_{soot})} \tag{2.12}$$

$$\Delta P_{inlet\ channel} = \frac{F \mu L}{3(D_h - 2w_{soot})^4} \frac{Q}{\overline{n_4}} \tag{2.13}$$

$$\Delta P_{outlet\ channel} = \xi \frac{\rho}{2} \left(\frac{Q}{\overline{n_4} D_h^2}\right)^2 \tag{2.14}$$

The total pressure drop for the segmented DPF is shown below in Eqn. 2.15 which is

equal to the summation of the pressure drop shown above in Eqns. 2.11-2.14.

$$\Delta P = \frac{\mu Q}{\overline{n_4} L} \left[\frac{w_S}{k_{wall}\ D_h} + \frac{1}{8 k_{soot}} \ln \frac{D_h}{(D_h - 2w_{soot})} + \frac{F L^2}{3} \left(\frac{1}{D_h^4} + \frac{1}{(D_h - 2w_{soot})^4} \right) \right] + \xi \frac{\rho}{2} \left(\frac{Q}{\overline{n_4} D_h^2} \right)^2 \tag{2.15}$$

Segmented filters generate higher pressure drop than monolithic filters by up to 30%

for clean cases and up to 35% for the loaded filters. A higher cell density filter could

results in the reduction of this higher pressure drop.

In both loaded segmented and loaded monolithic filters, 80% or higher of the pressure

drop is due to the substrate wall and the deposit layer. The impacts of channel friction

and flow contraction / expansion are less important. For the clean filter, the opposite is

true, as the majority of the pressure drop is from flow in the channel.

Table 2.2 Symbols of pressure drop model for segmented filter

D_h	hydraulic diameter of filter channel
F	laminar flow friction factor for square channels
k_{wall}	filtration wall permeability
k_{soot}	soot permeability
L	filter length
$\overline{n_4}$	a fictitious number of inlet channels
Q	exhaust gas volumetric flow rate
w_{soot}	particulate (soot) layer thickness deposited on the filtration wall
w_s	filtration wall thickness
μ	exhaust gas dynamic viscosity
ρ	exhaust gas density
ξ	flow contraction and expansion coefficient
ΔP	pressure drop

2.2.9 Review of "Microwave-Regenerated Diesel Exhaust Particulate Filter" by R. D Nixdorf (11)

The Wall-flow DPF has a limited capacity to trap carbon which means the filtration efficiency is low for the clean filter itself. Also, additional thermal energy must be applied to the filter to combust the carbon particles and clean the filter. Carbon particles can be removed in the range of 400-450 °C during the regeneration.

Small diesel engines, such as those equipped on diesel engine vehicles, are commonly operated under low load conditions. Under these conditions, the exhaust gas temperature is too low to initiate the combustion for PM. An external heating source is required to achieve reliable particulate filter regeneration. Electrical resistance, fuel burners, or engine controls have been used to apply the additional heat to increase the exhaust temperature. Microwave power has been used to heat trapped carbon particles but the problems are unpredictable carbon deposition on the filter and uneven microwave heating. When the filter reaches its designed capacity for particulate matter, the microwave power is activated for the time period required to reach the temperature which is able to initiate the regeneration. The silicon carbide fiber filter reacts with the microwave energy to rapidly combust the pollutants to harmless carbon dioxide and

water.

A low-load operating condition in smaller diesel engines is a significant percentage of the driving cycle. An active heating source will be needed in many applications. The silicon carbide fiber microwave regenerated DPF has demonstrated a PM regeneration efficiency of 80-95%. The regeneration efficiency of the microwave-regenerated filter PM is not affected by transient cycles or gas flow rates. Moreover, the active microwave regeneration at low loads and idle conditions also can be combined with the passive catalyst filter regeneration at high loads.

2.2.10 Review of paper "Simultaneous PM and NOx Reduction System for Diesel Engines" by K. Nakatani, S. Hirota, S. Takeshima, K. Itoh , T. Tanaka and K. Dohmae (12)

In this paper, the authors present a new after-treatment system known as the DPNR (Diesel Particulate -NOx Reduction System) which is able to reduce particulate matter (PM) and nitrogen oxides simultaneously and continuously in diesel engine exhaust gas. This system employs novel catalytic and combustion technologies to allow for

rich operating conditions in diesel engines.

The new catalytic converter for DPNR is a fine porous ceramic, which is monolithic honeycomb structure coated with a NOx storage reduction catalyst. This kind of catalytic converter is used for lean burn gasoline engines. This structure is similar as that in the DPF in which filter channels are alternatively plugged to force the gas flow through the porous walls. The structure of this substrate is optimized for particulates to go into the substrate pores. In addition, the catalyst is coated both inside and on the substrate walls of the filter.

PM mass loading in the DPNR catalyst was estimated by the total pressure drop across the converter. The PM oxidation rate was determined by measuring the decreasing rate of pressure drop. It was found that PM oxidation rate is faster with smaller the PM mass loading in the DPNR catalyst. The oxidation rate decreased gradually with increasing amount of PM loaded.

The authors found that the DPNR (Diesel Particulate-NOx Reduction system) can reduce PM and NOx in diesel exhaust simultaneously. The structure of this kind of system is similar as the DPF consists of a porous ceramic but the porous wall is coated

with a NOx storage-reduction catalyst. In addition, this system is able to reduce of NOx and PM continuously, using a repetitive control of lean and rich operating conditions. The PM oxidation rate becomes higher when the amount of PM accumulated is smaller. Appropriate control of the PM emission level or exhaust temperature is necessary to keep the PM oxidation rate high.

2.2.11 Review of paper "Measurement of the Local Gas Velocity at the Outlet of a Wall Flow Particle Filter" by B. Benker, A. Wollmann, and M. Claussen (13)

Recent studies show that the soot distribution in the inlet channel of the DPF depends on the selected engine operating points during both loading and regeneration. However, in actual practice only the overall pressure drop of the DPF is measured. In this paper, authors measured the outlet channel velocity profile to find out whether or not aging and thermal instability of the diesel particle filter correlate with inhomogeneous flow conditions.

The literature contains data such as pressure drop, particle size distribution, and gas composition, but almost all the data are for the overall performance of many DPF

channels. A thicker deposit results in a higher local pressure drop and a measurement of the overall performance of each channel is very helpful for modeling and the practical improvement of DPF design with respect to long-term stability.

The test was carried out about the loading of a DPF with and without DOC. The difference between those cases is: after 8 hours of loading the overall velocity profile from a DPF (without DOC) is nearly flat. When using a DOC+DPF under the same conditions a similar state is reached after 12 hours.

From the experiment it can be found that the gas flow rate decreases with the increasing of radius of the DPF which means gas flow rate is higher in the central area of the DPF. However, since more mass was collected in the center, as the soot layer being built up, the flow rate in the central region becomes smaller.

2.2.12 Review of "Study on Next Generation Diesel Particulate Filter", Y. Furuta, T. Mizutani, Y. Miyairi, K. Yuki and H. Kurach (14)

In this paper, the authors present a new method which can not only improve the

filtration efficiency but also reduce the pressure drop with PM accumulation. This method is also capable of providing a linear relationship between PM loading and pressure drop: an inlet membrane having smaller pores is set up on the substrate walls in the inlet channel. Using this method, the pressure drop is not dependent on the wall material but the filtration inlet membrane. Using this kind of membrane, one can pick an appropriate porosity for the filter materials. In this paper, the authors use the filtration membrane and formed it into a honeycomb structure for use as a DPF.

As mentioned above this kind of inlet membrane structure is able to meet both the high filtration efficiency and low pressure drop with PM filtration. The relationship between pressure drop and PM accumulation was also found to be linear for an Inlet-Membrane structure. High pressure drop across the filter may lead to a reduction in engine output and decrease the fuel economy. In this paper the authors also mentioned another problem about the pressure drop characteristics of the DPF - hysteresis in the relationship between the PM amount and pressure drop. During the regeneration step, not all of the PM is removed from inside the substrate walls (deep-bed filtration) which will lead to a higher post-regeneration pressure drop than the clean filter.

It is known that the pressure drop decreases with increasing porosity. It is also known that the filtration efficiency increases with reducing pore diameters. However, high porosity reduces the heat capacity of the filter which can impact regeneration. The inlet membrane, composed of material having small pore diameters, can be used to solve this problem. One can just put the inlet membrane structure on the inlet channel wall's surface. With this inlet membrane concept, a low pressure drop with PM accumulation and high initial filtration efficiency can be achieved. From the figures (Fig.2.7 and Fig.2.8) shown below it can be noticed that the standard design (without the inlet membrane) has a sharp initial increase in pressure drop. However, for the system with the added inlet membrane has a filtration efficiency increase of 20%, Furthermore, the filtration efficiency is higher, therefore the relationship between pressure drop and the accumulated PM amount becomes more linear.
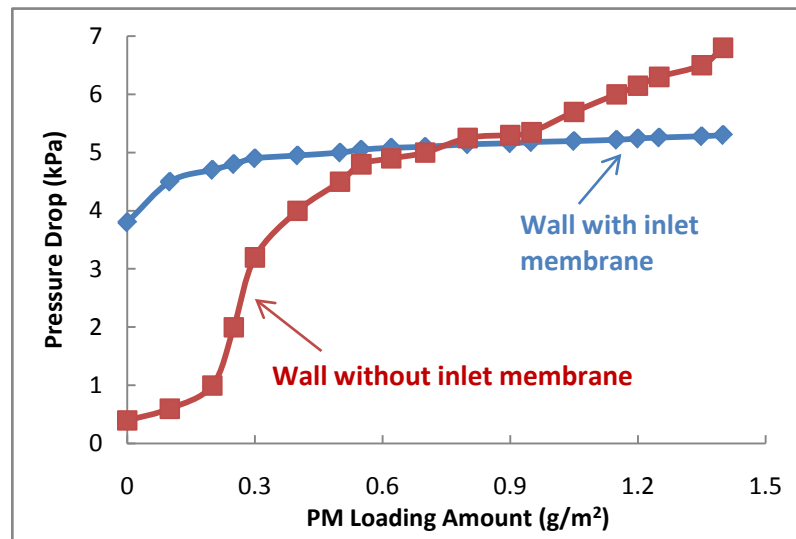
Figure 2.7 PM Amount vs. pressure drop (plate) (Figure reproduced from (14))
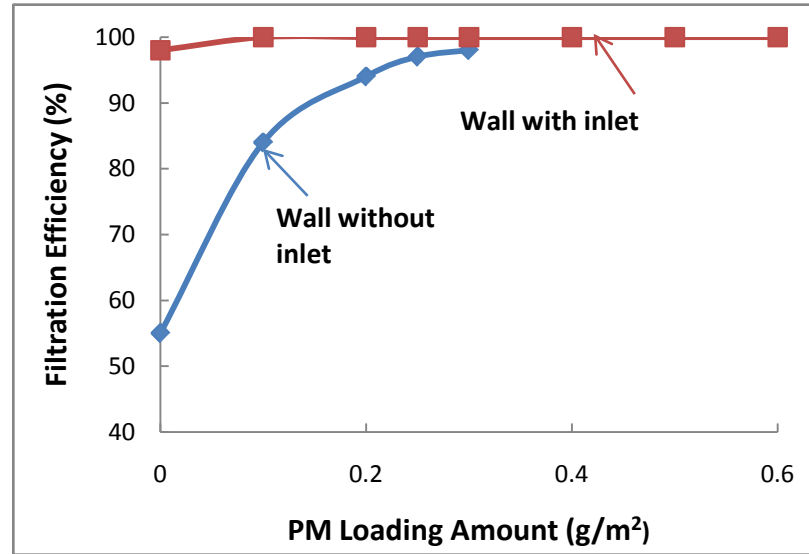
Figure 2.8 PM Amount vs. filtration efficiency (plate) (Figure reproduced from (14))

2.2.13 Review of "Study on Reliability of Wall-Flow Type Diesel Particulate Filter" by T. Kuki, Y. Miyairi, Y. Kasai, M. Miyazaki and S. Miwa (15)

In active regeneration, heat released from PM regeneration causes the filter to heat up to high temperatures and creates temperature gradients which results in thermal stress. If the filter is damaged due to thermal stress, it will render the DPF useless; therefore, a suitable filter material and configuration are required to prevent this problem during filter regeneration.

Since the heat released from the regeneration increases as the deposit layer increases, the temperature gradient in the filter will also increase resulting in higher thermal stress. Therefore, it is important to prevent the filter from breaking down by controlling the total amount of PM in the filter before regeneration.

The DPF must be regenerated by forced combustion. This is done by increasing the inlet gas temperature to burn off the particulate accumulated in the filter. There are some parameters to estimate the DPF temperature during regeneration: the amount of PM, exhaust gas flow rate, and exhausts gas temperature. Pressure loss with the amount of PM (deposit thickness) may be used to determine the rate of PM reacting. In addition, since fuel economy can be affected if the regeneration is initiated with small deposit thickness, it is very important to define the appropriate PM deposit thickness. In this paper, the authors present that a pressure drop history over several PM accumulations (Fig. 2.9). At the beginning of the first accumulation, the PM filtration occurs within the wall and leads to a steep pressure drop. This is due to the deep bed filtration mechanism. After the pores are filled, the PM begins to build up on the substrate wall (cake filtration) and the pressure drop increases linearly. After regeneration, the pressure drop does not decrease to the initial value of the clean filter. This is because some of the particulate remains inside of the filter walls. Then the mass further builds up within the walls and then on the cake layer. (15)
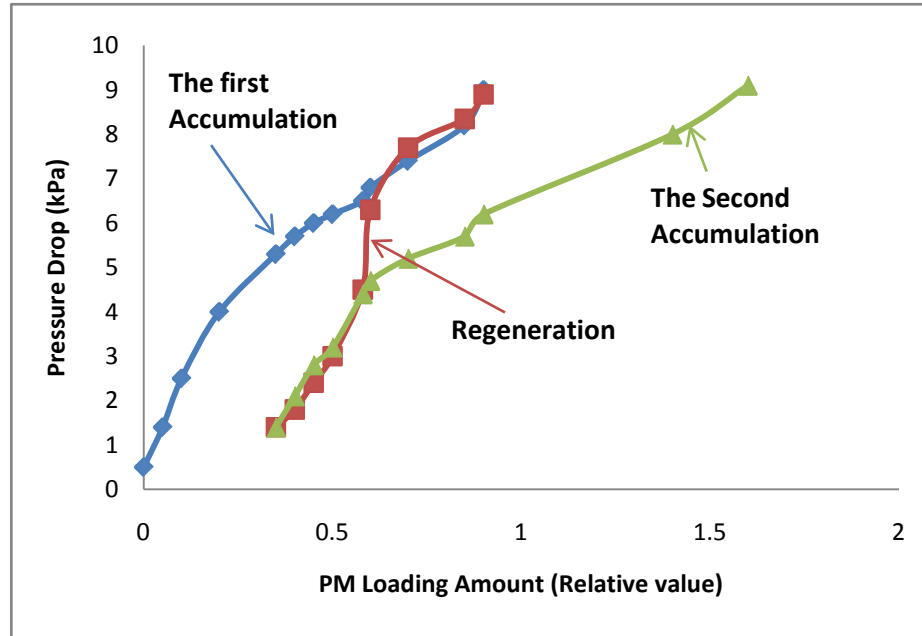
Figure 2.9 Pressure loss hysteresis (Figure reproduced from (15))

2.2.14 Review of "Parametric and Sensitivity Analysis of Diesel Particulate Filter Regeneration" by D. Huang and J. M. Keith (16)

Particulate matter emissions from diesel-fueled cars, trucks, and buses are regulated by state and federal government agencies. Although improvements in engine performance have taken place, aftertreatment is necessary to meet the existing emissions standards. In order for a particulate emissions control system to function under real driving conditions, real-time model predictive control is needed.

In this paper, at first, the authors perform a parametric study to compare two existing models of DPF regeneration: Bisset one-dimensional model and the average model which uses averaging theory to focus solely on the thermal evolution in the diesel particulate trap developed by Zheng and Keith. Then, the authors estimate the sensitivity of the ignition time and ignition length to changes in the gas flow rate and initial deposit thickness under various conditions using the averaged model.

For the parametric study, there are nine cases (including the standard case $G_f = 0.272$ g/(cm^2·s) and $w_b = 1.117 \times 10^{-3}$cm. This gives rise to nine different conditions including the base case):

• Half deposit particle thickness (w_b/2), half gas mass flux (G_f/2)

• Half deposit particle thickness (w_b/2), same gas mass flux (G_f)

• Half deposit particle thickness (w_b/2), double gas mass flux ($2G_f$)

• Same deposit particle thickness (w_b), half gas mass flux (G_f/2)

• Same deposit particle thickness (w_b), same gas mass flux (G_f)

• Same deposit particle thickness (w_b), double gas mass flux ($2G_f$)

• Double deposit particle thickness ($2 w_b$), half gas mass flux (G_f/2)

• Double deposit particle thickness ($2 w_b$), same gas mass flux (G_f)

• Double deposit particle thickness (2 w_b), double gas mass flux (2G_f)

First of all, for most cases (standard deposit thickness w_b and double the standard deposit thickness 2 w_b at any gas mass flux G_f) there was good agreement between the Bissett model, averaged model, and the analytical model. Thus, it is acceptable to use the averaged model to estimate DPF regeneration. However, it can be noted that the modified Bissett model and averaged model do not agree at half of the standard deposit thickness (w_b/2) and for double the standard gas mass flux (2G_f) for feed temperatures less than 700 K, as seen in Figure 2.10. This result is due to incomplete regeneration.
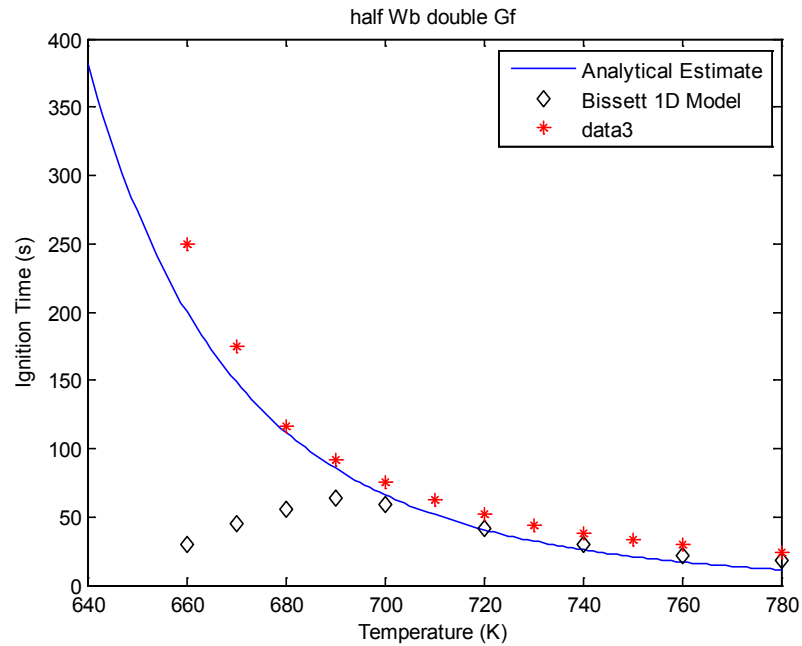
Figure 2.10 Model comparison of the ignition time for various temperatures for cases with

double the standard gas flow rate and half of the standard initial deposit thickness.

42

Sensitivity analysis will be used to assess how sensitive the ignition time (t_{ig}) and ignition length (L_{ig}) are to changes in the exhaust gas mass flux (G_f) and the particulate deposit thickness (w_b). There are four cases:

The data in Table 2.3 shows that the predicted ignition time and ignition length are most sensitive to changes in deposit thickness for 1/2 w_b and G_f. We note that all the numbers in Table 2.3 are negative, meaning that increasing w_b leads to a decrease in the ignition time (t_{ig}) and the ignition length (L_{ig}). Investigation of the columns in Table 2.3 shows that the sensitivity of t_{ig} changes little as the gas mass flux changes. On the other hand, investigation of the rows in Table 2.3 suggests a large sensitivity of both t_{ig} and L_{ig} as the deposit thickness changes. Therefore, we conclude that the sensitivity of the ignition time changes more with changes in the particulate deposit thickness than the exhaust gas mass flux. There is no sensitivity analysis for w_b /2 and 2 G_f when the averaged model is not valid.

Table 2.3 Sensitivity of the ignition time and the ignition length to changes in deposit thickness for a feed temperature of 670 K and variable G_f and w_b.

Sensitivity of ignition time, $\dfrac{\partial t_{ig}}{\partial(w_b/w_{b0})}$ (s)			
	$\dfrac{1}{2}w_b$	w_b	$2\,w_b$
$\dfrac{1}{2}\,G_f$	-159	-71	-26
$1\,G_f$	-160	-69	-25
$2\,G_f$	No Ignition	-64	-24

Sensitivity of ignition length, $\dfrac{\partial(L_{ig}/L_0)}{\partial(w_b/w_{b0})}$ (dimensionless)			
	$\dfrac{1}{2}w_b$	w_b	$2\,w_b$
$\dfrac{1}{2}\,G_f$	-0.48	-0.20	-0.06
$1\,G_f$	-0.84	-0.36	-0.12
$2\,G_f$	No Ignition	-0.68	-0.22

As shown in Table 2.4, under this condition, the most sensitive result occurs at half the standard gas flow rate and half the standard deposit thickness for the ignition time. However, for the ignition length, this happens at standard flow rate and half deposit

thickness. The values in this table for ignition time are negative, which means that increasing the gas flow rate (G_f) leads to a decrease in t_{ig}. However, all the positive numbers, for the ignition length, mean that the ignition length increases as the gas flow rate increases. Since the DPF ignites downstream under these conditions an increase in G_f leads to an increase in L_{ig}. Unlike the previous section, neither of the gas flow rate nor the deposit thickness dominates the sensitivity. The sensitivity changes with the gas flow rate almost as much as with the deposit thickness.

In this section, the study focuses on the sensitivity at different inlet temperatures and gas flow rates at the same deposit thickness ($W_b = W_{b0}$). The inlet temperature is another important parameter of the averaged model. From the data shown below in Table 2.5, it is clearly noticed that, for both ignition time and length, the most sensitive results occurs at 670K. However, for ignition time it occurs at half of the standard gas flow rate, while, for ignition length it happens at double the standard gas flow rate. Also, it is noticed that the sensitivity changes more with different temperatures than with the gas flow rate. The numbers shown in Table 5 are negative, which means that the ignition time and ignition length decrease with increasing inlet temperature. Also it can be noticed that the sensitivity of both the ignition time and ignition length changes much more with the inlet temperature than the gas flow rate. Therefore, the inlet

temperature impacts t_{ig} and L_{ig} more.

Table 2.4 Sensitivity of the ignition time and the ignition length to changes in gas mass flux for a feed temperature of 670 K and variable G_f and w_b.

Sensitivity of ignition time, $\dfrac{\partial t_{ig}}{\partial(G_f/G_{f0})}$ (s)			
	$\dfrac{1}{2}G_f$	$1\,G_f$	$2\,G_f$
$\dfrac{1}{2}W_b$	-17	-10	No Ignition
W_b	-13	-7	-5
$2\,W_b$	-8	-5	-2
Sensitivity of ignition length, $\dfrac{\partial L_{ig}/L_0}{\partial(G_f/G_{f0})}$ (dimensionless)			
	$\dfrac{1}{2}G_f$	$1\,G_f$	$2\,G_f$
$\dfrac{1}{2}W_b$	0.7	0.9	No Ignition
W_b	0.4	0.4	0.8
$2\,W_b$	0.2	0.2	0.2

Table 2.5 Sensitivity of the ignition time and the ignition length to changes in deposit thickness for variable feed temperature and G_f.

Sensitivity of ignition time, $\left.\dfrac{\partial t_{ig}}{\partial(w_b / w_{b0})}\right|_{w_b = w_{b0}}$ (s)			
	670K	690K	710K
$\dfrac{1}{2} G_f$	-71	-44	-28
$1 G_f$	-69	-41	-26
$2 G_f$	-64	-40	-25
Sensitivity of ignition length, $\dfrac{\partial L_{ig} / L_0}{\partial(G_f / G_{f0})}$ (dimensionless)			
	670K	690K	710K
$\dfrac{1}{2} G_f$	-0.20	-0.12	-0.06
$1 G_f$	-0.36	-0.20	-0.12
$2 G_f$	-0.68	-0.36	-0.22

In this section, the authors assess the sensitivity of the ignition time and length under different inlet temperatures with variable deposit thickness at the same exhaust gas

flow rate ($G_f = G_{f0}$). As shown in table 2.6, for both ignition time and ignition length, the most sensitive results are under the condition of half the standard deposit thickness at 670K. The numbers in Table 2.6 for the ignition time are negative, which means the ignition time decreases with increasing inlet temperature. However, for the ignition length, the positive numbers indicate L_{ig} increases as the inlet temperature increases. It also can be noticed that, under this condition, the deposit thickness and inlet temperature are both important to the sensitivity. (16)

Table 2.6 Sensitivity of the ignition time and the ignition length to changes in gas mass flux

for variable feed temperature and G_f.

Sensitivity of ignition time, $\left.\dfrac{\partial t_{ig}}{\partial (G_f / G_{f0})}\right|_{G_f = G_{f0}}$ (s)			
	670K	690K	710K
$\dfrac{1}{2} W_b$	-10	-8	-7
$1 W_b$	-7	-6	-4
$2 W_b$	-5	-4	-3
Sensitivity of ignition length, $\left.\dfrac{\partial L_{ig} / L_0}{\partial (G_f / G_{f0})}\right|_{G_f = G_{f0}}$ (dimensionless)			
	670K	690K	710K
$\dfrac{1}{2} W_b$	0.86	0.36	0.22
$1 W_b$	0.38	0.22	0.12
$2 W_b$	0.22	0.12	0.06

2.3 References

(3). Blackman PG. Emission Control Options to Achieve Euro IV and Euro V on Heavy Duty Diesel Engines. SAE Journal. 2008;2008280021.

(4). Foster DE, Kusaka T. Detailed Diesel Exhaust Particulate Characterization and Real-Time DPF Filtration Efficiency Measurements during PM Filling Process. SAE Journal. 2007;2007010320.

(5). Sakai H, Busch P, Vogt CD. Filtration Behavior of Diesel Particulate Filters. SAE Journal. 2007;2007010921.

(6). Johnson JH, Naber JD, Bagley ST. A Methodology to Estimate the Mass of Particulate Matter Retained in a Catalyzed Particulate Filter as Applied to Active Regeneration and On-Board Diagnostics to Detect Filter Failures. SAE Journal. 2008;2008010764.

(7). Pinturaud D, Charlet A, Caillol C, Higelin P, Girot P, Briot A. Experimental Study of DPF Loading and Incomplete Regeneration, SAE Journal. 2007;2007240094.

(8). Mizutani T, Kaneda A, Ichikawa S, Kurachi H, Vogt CD, Tanaka M, Martin A, Fujii S, Busch P. Filtration Behavior of Diesel Particulate Filters (2). SAE Journal. 2007;2007010923.

(9). Barataud C, Bardon S, Bouteiller B, Gleize V, Charlet A, Higelin P. Diesel Particulate Filter Optimization. SAE Journal. 2003;2003010376.

(10). Masoudi M. Pressure Drop of Segmented Diesel Particulate Filters. SAE Journal. 2005;2005010971.

(11). Nixdorf RD. Microwave-Regenerated Diesel Exhaust Particulate Filter. SAE Journal. 2001;2001010903.

(12). Nakatani K, Hirota S, Takeshima S, Itoh K, Tanaka T Dohmae K, Simultaneous PM and NOx Reduction System for Diesel Engines. SAE Journal. 2002;2002010957.

(13). Benker B, Wollmann A, Claussen M. Measurement of the Local Gas Velocity at the Outlet of a Wall Flow Particle Filter. SAE Journal. 2005;200524001.

(14). Furuta Y, Mizutani T, Miyairi Y, Yuki K,Kurach H. Study on Next Generation Diesel Particulate Filter. SAE Journal. 2009;2009010292.

(15). Kuki T, Miyairi Y, Kasai Y, Miyazaki M, Miwa S. Study on Reliability of Wall-Flow Type Diesel Particulate Filter. SAE Journal. 2004;2004010959.

(16). Huang D, Keith JM. Parametric and Sensitivity Analysis of Diesel Particulate Filter Regeneration. International Journal of Chemical Reactor Engineering. 2009;7 (A56).

Chapter 3 Filtration Model

In this chapter, a filtration model is used to calculate the filtration efficiency of a Diesel Particulate Filter (DPF). However, this filtration model only can be used to calculate the filtration efficiency and the fraction of mass which will be accumulated inside the porous substrate wall and on the surface of the wall. It is not able to describe the mechanisms of particle deposition inside the wall and on the wall surface. The filtration model equations will be reproduced from the SAE literature (17).

In general, there are two types of filtration: "deep bed filtration" and "cake filtration". A filter material with large pores can filter small particles by the physical mechanisms of impaction and diffusion: this is called "deep bed filtration" and occurs within the pores of the DPF. After the wall is filled with particles, they build up on the inlet channel walls by "cake filtration. Theoretically, there are four types of filtration: gravity, inertia, interception and diffusion, which are shown in Figure 3.1. The mechanisms of deep bed filtration are interception, diffusion and inertia and the mechanism of cake filtration is gravity.

In this study, the filter wall is divided into a series of layers, and we use a "unit collector" filtration theory, which is shown in Figure 3.2.
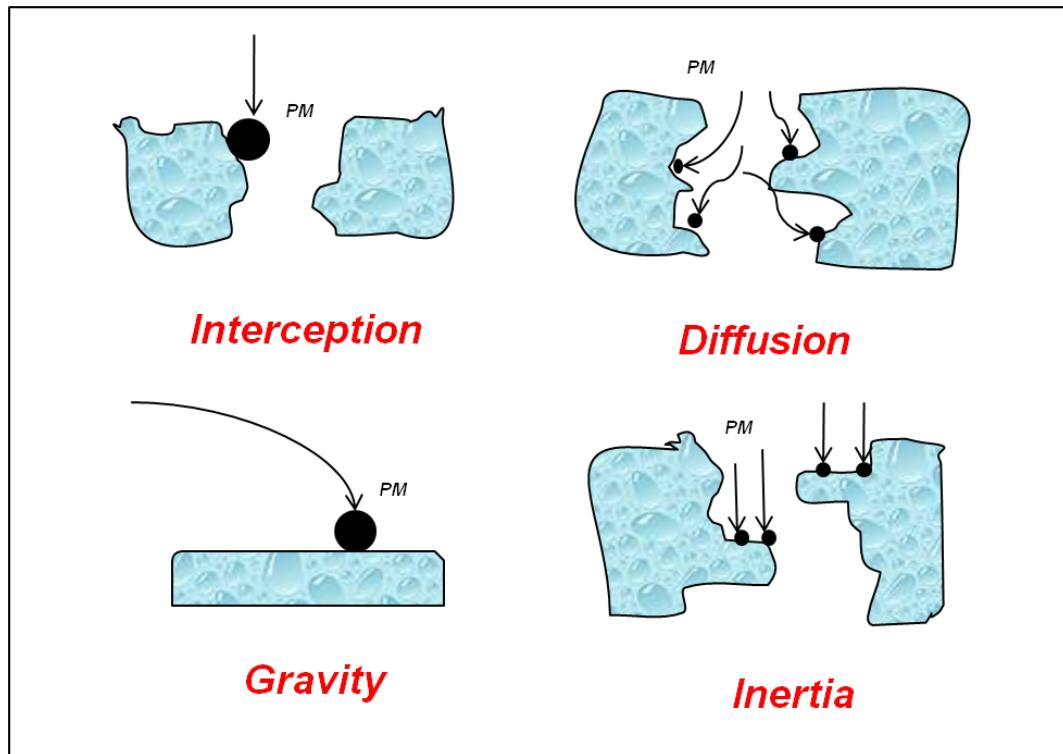
Figure 3.1 Filtration Mechanism: interception, diffusion, gravity and inertia. (Figure modified from (5))

3.1 Filtration Model Equations

This model is based upon the work proposed by Johnson et al (17). In this filtration

model, a "unit collector" theory will also be presented to describe the mechanisms of

deep bed filtration and cake filtration processes.

3.1.1 Clean filter
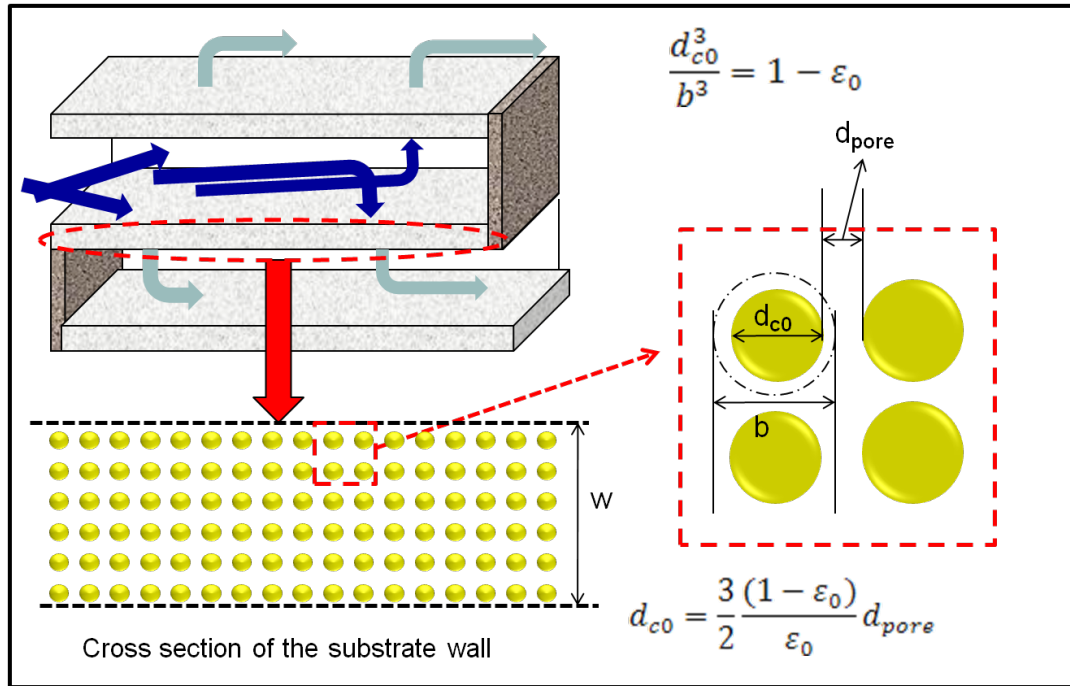
Figure 3.2 Illustration of a "packed bed" of unit collectors in the DPF

The relationship of d_{c0}, d_{pore}, and b is shown in figure 3.2, where the substrate wall is

assumed to be a packed bed with a thickness of w. Each sphere is one "unit collector"

with an initial diameter d_{c0}, and the dashed line circle around the sphere is its boundary

which is the "unit cell" with a diameter of b. Finally, d_{pore} shown in Figure 3.2

represents the average pore size of this packed bed.

By drawing a concentric spherical boundary at a certain distance around the collection sphere, the volume fraction of the packed bed is given by (18):

$$\frac{d_{c0}^3}{b^3} = 1 - \varepsilon_0 \tag{1}$$

Where ε_0 is the porosity of "unit collector" whose value is around 0.5 for most of the DPF materials.

There is a simple approximation to obtain the relationship between d_{c0} and d_{pore} which will be shown below:

The volume of a single sphere is given by $V_{\text{sphere}} = \frac{1}{6}\pi(d_{c0})^3$. Thus, in a unit volume the total volume of spheres is $(1 - \varepsilon_0)$. Furthermore, the number of spheres N_s in this unit volume is given by the volume of all spheres divided by the volume of one sphere:

$$Ns = \frac{6(1-\varepsilon_0)}{\pi(d_{c0})^3} \tag{2}$$

Furthermore, the surface area of one sphere is $\pi(d_{c0})^2$, so the total surface area of all the spheres is $N_s\pi(d_{c0})^2$ which is equivalent to:

$$S_v = \frac{6(1-\varepsilon_0)}{d_{c0}} \tag{3}$$

In a unit volume, the total pore volume is ε_0. Then, the simple approximation is to use the pore diameter d_{pore} as four times the ratio of the pore volume to the total surface area. Therefore, the pore diameter can be obtained as:

$$d_{pore} = 4 * \frac{\varepsilon_0}{\frac{6(1-\varepsilon_0)}{d_{c0}}} = \frac{2}{3}\frac{\varepsilon_0}{(1-\varepsilon_0)}d_{c0} \tag{4}$$

During the filtration process, Brownian diffusion and direct interception are considered two primary collection mechanisms to accumulate the particles in the filter. η_{DR} is the combined efficiency of Brownian efficiency η_D and collection efficiency η_R:

$$\eta_{DR} = \eta_D + \eta_R - \eta_D * \eta_R \tag{5}$$

Where, Brownian diffusion efficiency is given by (17, 19):

$$\eta_D = 3.5 * \text{g}(\varepsilon) * Pe^{-2/3} \tag{6}$$

In Equation (6), *Pe* is the Peclet number and defined as:

$$Pe = \frac{U_i d_{c0}}{D} \tag{7}$$

Where, U_i is the "pore" velocity in cm/s related to the approach velocity u_w (cm/s) and the porosity ε:

$$U_i = \frac{u_w}{\varepsilon} \tag{8}$$

and *D* in Equation (7) is the particle diffusion coefficient in cm²/s and is given below:

$$D = \frac{k_B T}{3\pi\mu\, d_p} SCF \tag{9}$$

Where, k_B is the Boltzman's constant which is in unit of (cm²*kg/(s²*K)), μ is the exhaust dynamic viscosity in g/cm*s, T (K) is the filter temperature and SCF is the Stokes-Cunningham slip correction factor, that describes transitional and slip flow effects at the surface of the "unit collector":

$$SCF = 1 + Kn_P(1.257 + 0.4e^{-1.1/Kn_P}) \tag{10}$$

and Kn_P is the particle Knudsen number defined by:

$$Kn_P = \frac{2\lambda}{d_p} \tag{11}$$

Where, d_p is the particle size (PM2.5 is used in this study which means average d_p =2.5 μm) and λ (cm) is the mean free path of the exhaust gas:

$$\lambda = v\sqrt{\frac{\pi(MW)}{2\bar{R}T}} \tag{12}$$

Where, v is the exhaust kinematic viscosity in cm^2/s, $\bar{R}$ is the universal gas constant (g*cm^2/(s^2*mol*K)), and MW is the molecular weight (g/mol) which can be calculated as below:

$$MW = \sum_i y_i MW_i \tag{13}$$

Where, y_i is the mole fraction of each of the exhaust gases and MW_i is the molecular weight of these gases.

In Eq. (6), $g(\varepsilon)$ is a geometric function for the Kuwabara "unit cell" model and is defined as (17, 19):

$$g(\varepsilon) = \left[\frac{\varepsilon}{2-\varepsilon-\frac{9}{5}(1-\varepsilon)^{1/3}-\frac{1}{5}(1-\varepsilon)^2}\right]^{1/3} \tag{14}$$

Note that when ε is equal to 0, 0.5, and 1, $g(\varepsilon)$ is equal to 0, 2.86, and 1

respectively.

As mentioned above, direct interception is another dominant collection mechanism during the filtration and its efficiency. An empirical correlation for the collection efficiency is given by (17, 19):

$$\eta_R = 1.5 * N_R^2 \frac{[g(\varepsilon)]^3}{(1+N_R)^{\frac{3-2\varepsilon}{3\varepsilon}}} \qquad (15)$$

Where, the interception parameter N_R can be calculated as:

$$N_R = \frac{d_p}{d_c} \qquad (16)$$

In equation (16), d_c is the "unit collector" diameter, which is initially equal to d_{c0}.

By defining the Brownian diffusion efficiency η_D and direct interception efficiency η_R, the combined efficiency η_{DR} can be calculated from Eq. (5).

Once the combined efficiency is obtained, the total collection efficiency for the clean filter wall can be calculated related to the single unit collector filtration efficiency as

follow (17):

$$E = 1 - exp\left[-\frac{3\eta_{DR}(1-\varepsilon_0)w}{2\varepsilon_0 d_{c0}}\right] \tag{17}$$

Where w is the wall thickness of the filter.

3.1.2 Loaded filter

As the particulate was collected by the filter, the diameter of each "unit collector" with time t for the *i*th slab (See Figure 3.3, i=1, 2 …n) is given below. Note that in this study n is equal to 10 which means there are ten layers in the substrate wall. As mass was accumulated in each slab the diameter of the unit collector related to time is given by (17):

$$d_c(i,t) = 2\left[\frac{3}{4\pi}\frac{m_w(i,t)}{\rho_{soot,w}} + \left(\frac{d_{c0}}{2}\right)^3\right]^{1/3} \tag{18}$$
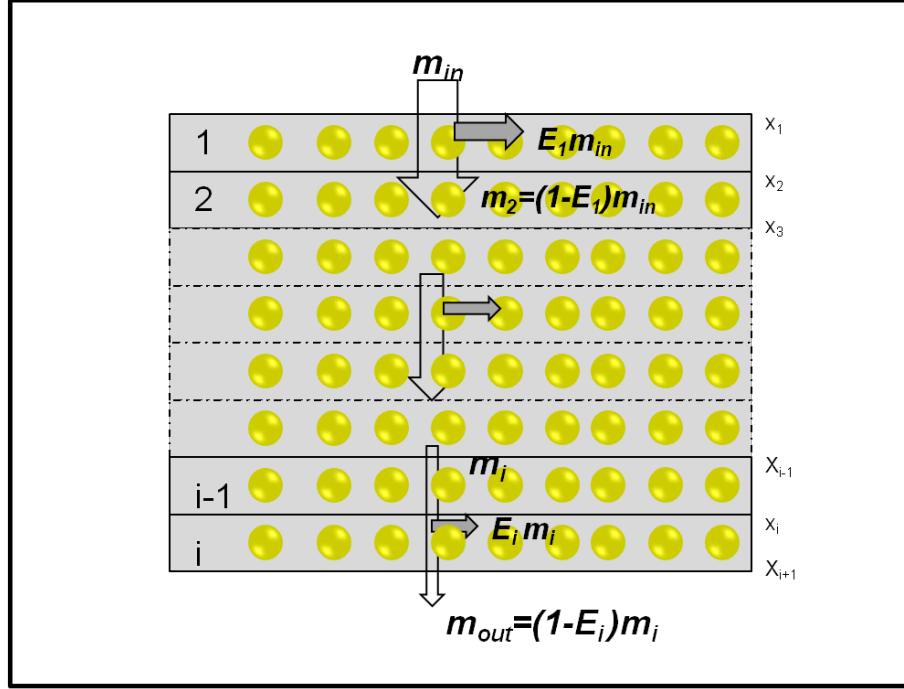
Figure 3.3 Schematic of the filter wall discretized into slabs of "unit collectors".

In Eq. (18), $\rho_{soot,w}$ represents the particulate packing density inside the filter wall

and it depends upon the experimental conditions, which is in units of g/cm^3. Also, the

porosity for each slab changes with time according to the relationship (17):

$$\varepsilon(i,t) = 1 - \left(\frac{d_c(i,t)}{d_{c0}}\right)^3 (1 - \varepsilon_0) \tag{19}$$

Moreover, the loaded filter permeability k (cm^2) for each slab also changes with time

(17):

$$\frac{k(i,t)}{k_0} = \left(\frac{d_c(i,t)}{d_{c0}}\right)^2 \frac{f(\varepsilon(i,t))}{f(\varepsilon_0)} \tag{20}$$

Where, here, k_0 is the permeability of the clean filter.

In the equation shown above, $f(\varepsilon)$ is another geometric function for the Kuwabara "unit cell" model and it is defined as (17):

$$f(\varepsilon) = \frac{2}{9} \frac{\left[2-\varepsilon-\frac{9}{5}(1-\varepsilon)^{1/3}-\frac{1}{5}(1-\varepsilon)^2\right]}{(1-\varepsilon)} \tag{21}$$

Note that when ε is equal to 0, 0.5, and 1, $f(\varepsilon)$ is equal to 0, 0.01, and ∞, respectively.

Finally, the loaded filter collection efficiency at each slab can be calculated as following (17):

$$E(i,t) = 1 - exp\left[-\frac{3\eta_{DR}(i,t)(1-\varepsilon(i,t))(x_{i+1}-x_i)}{2\varepsilon(i,t)d_c(i,t)}\right] \tag{22}$$

All the equations shown above and the theory of the "unit cell" and "unit collector" are applied to the particles which were accumulated inside the pore of the filter wall, this process is named "deep-bed" filtration as discussed before. Then, the particulate will be accumulated on the surface of the filter wall and build a deposit layer, which is called "cake" filtration. During the filtration, mass accumulated by "deep-bed" filtration was much less than that of "cake" filtration, however, the filtration efficiency increases during "deep-bed" filtration, which will be discussed in a later section. The partition coefficient shown below can predict the fraction of the inlet mass that will be

accumulated on the surface of the filter wall. It is given by:

$$\Phi(t) = \frac{(d_c(1,t))^2 - d_{c0}{}^2}{(\Psi b)^2 - d_{c0}{}^2} \tag{23}$$

Where, Ψ is a dimensionless constant which should be estimated from the experimental data, and b is the "unit cell" diameter. In this study, we made an assumption that $\Psi = 0.8$.

3.2 Filtration Model Results

Figure 3.4 shows the stages of filtration proposed by Foster et al. (4), while Figure 3.5 shows the filtration efficiency vs. pore size of the filter wall. From these two figures, it can be found that in figure 3.5, the filtration efficiency increases remarkably during the "deep-bed" filtration which is the process from stage 1 to stage 2 shown in figure 3.4. This is because most of the pores in the substrate wall were blocked by the particulates accumulated inside so that particles are not able to pass through the blocked wall and get into the outlet channel of DPF. Then, the filtration will become "cake" filtration which is from stage 2 to stage 3, when the filtration efficiency will increase uniformly and approach unity.
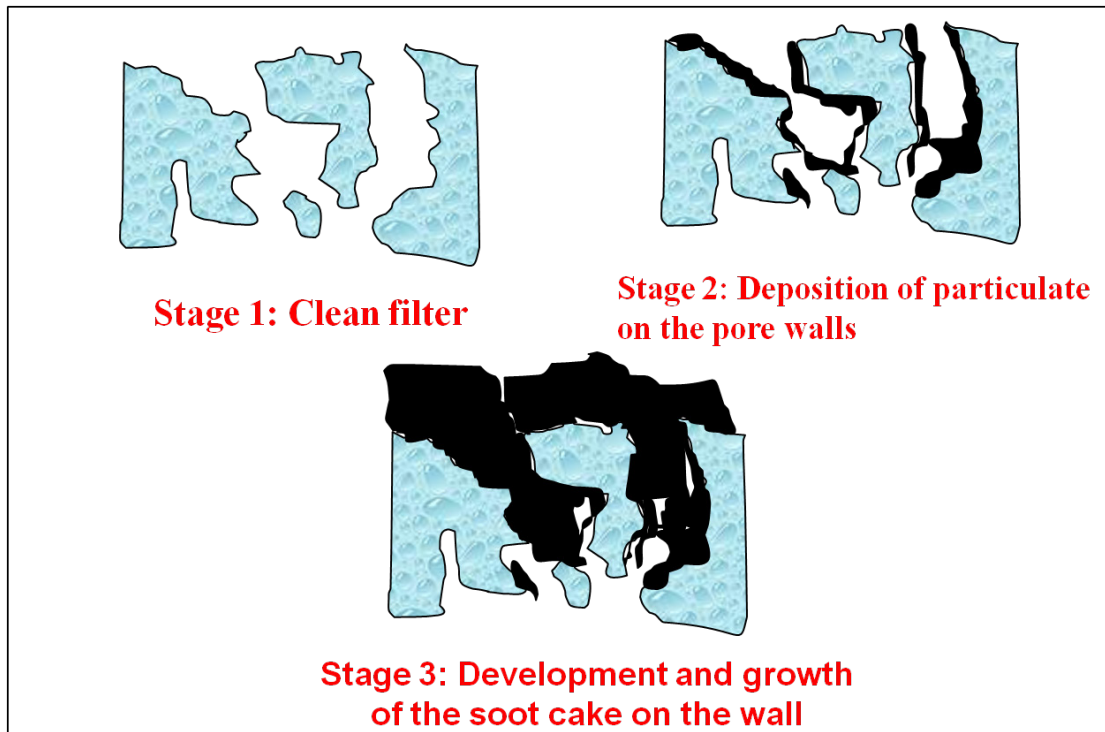
Figure 3.4. Stages of filtration in the inlet channel of DPF. (Figure modified from (4))
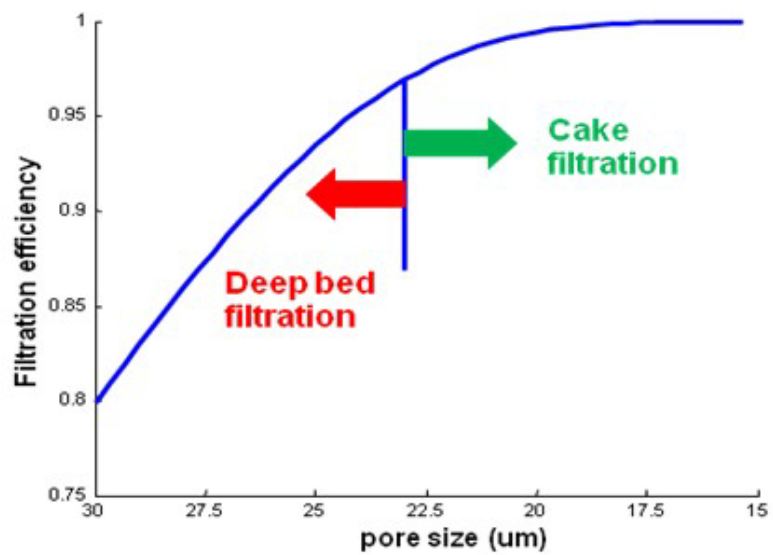
Figure 3.5. Filtration efficiency vs. pore size of the wall

In the section below, we perform a filtration study at constant inlet mass flow rate (G_f=0.42 g/cm^{2}s) and inlet temperature (T_{inlet}=435 K). Furthermore, the inlet particulate concentration is set at a constant value of 12.75 g/m^3 (Std.). The UDDS driving cycle will be discussed in the next chapter. From figure 3.6 it can be found that the filtration efficiency achieves unity at around 3800 seconds. Values used for the symbols and the numerical parameters are listed in the notation at the end of this chapter.
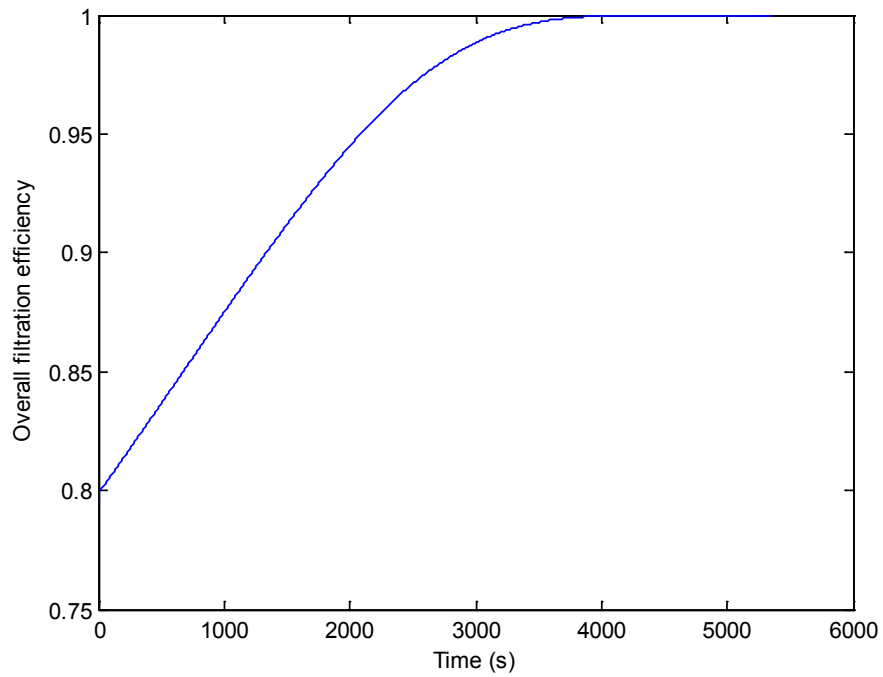
Figure 3.6. Overall filtration efficiency vs time. (Gf=0.42 g/cm2s, Tinlet=435 K, Cin=12.75 g/m3 (Std))

Figure 3.7 shows one single unit collector diameter in the first slab changes with time

in the four driving cycles. It can be noticed that the diameter increases from 45μm to 53μm in about 3800 seconds. After 3800 seconds, the diameter of the unit collector does not change since the filtration is only due to cake filtration.
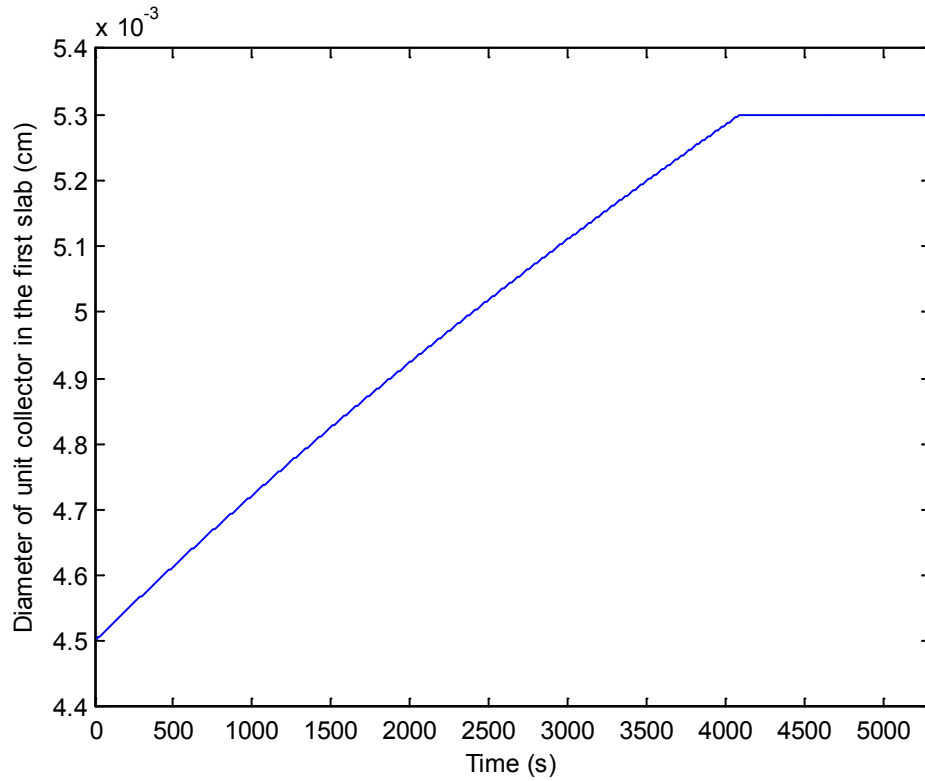
Figure 3.7. Overall single unit collector diameter in the first slab. (Gf=0.42 g/cm2s, Tinlet=435 K, Cin=12.75 g/m3 (Std))

Figures 3.8 shows the mass accumulated in each slab as a function of time (Note that for convenience the plots are shown in time increments of 1340 seconds which is the duration of the UDDS cycle). It can be found that the mass accumulated in each slab decreases along the vertical axial direction through the wall, because particulates will

be trapped in each slab and the mass which goes into the next slab will decrease. At first, the collection efficiency for each slab is the same, therefore, mass would be accumulated more in the top slabs. Also, we can notice that after about one hour, mass accumulated in each slab increases very slowly. This is because the filtration will switch to cake filtration and less amount of mass can go into the walls. Finally, no particulate can pass through the layer on the wall; therefore, the mass in each slab will remain the same.
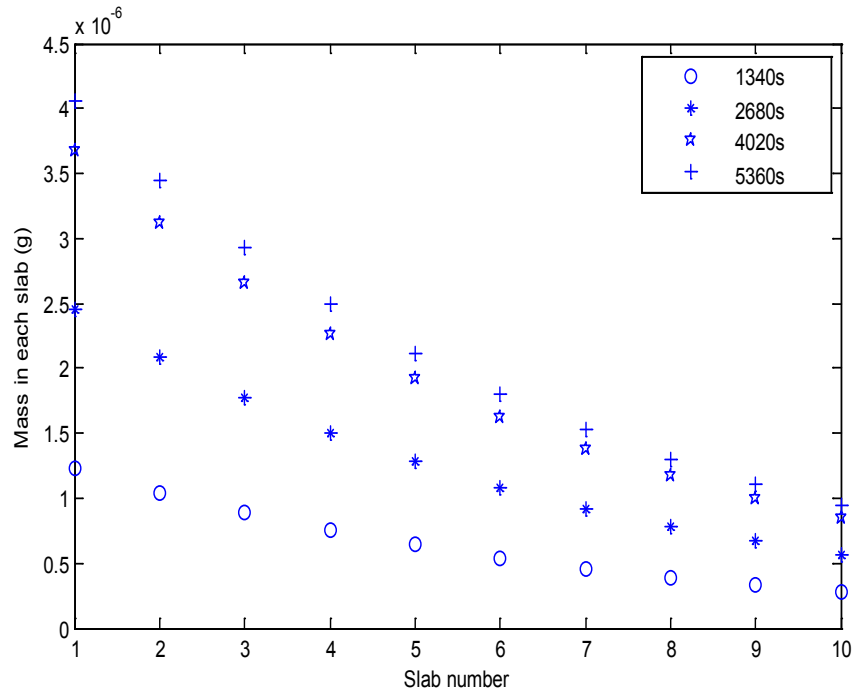
Figure 3.8.Accumulated mass in each slab as a function of time. (Gf=0.42 g/cm2s, Tinlet=435 K, Cin=12.75 g/m3 (Std))

Figure 3.9 shows the diameter of one unit collector for each slab. Because of the decreasing mass in each slab, the diameter of the unit collectors decreases and approaches the value for a clean filter (Eqn. 18). Also, as mentioned above, since the mass increases slowly in each slab after about one hour the diameter of the unit collector will also increase slowly and then remain constant.
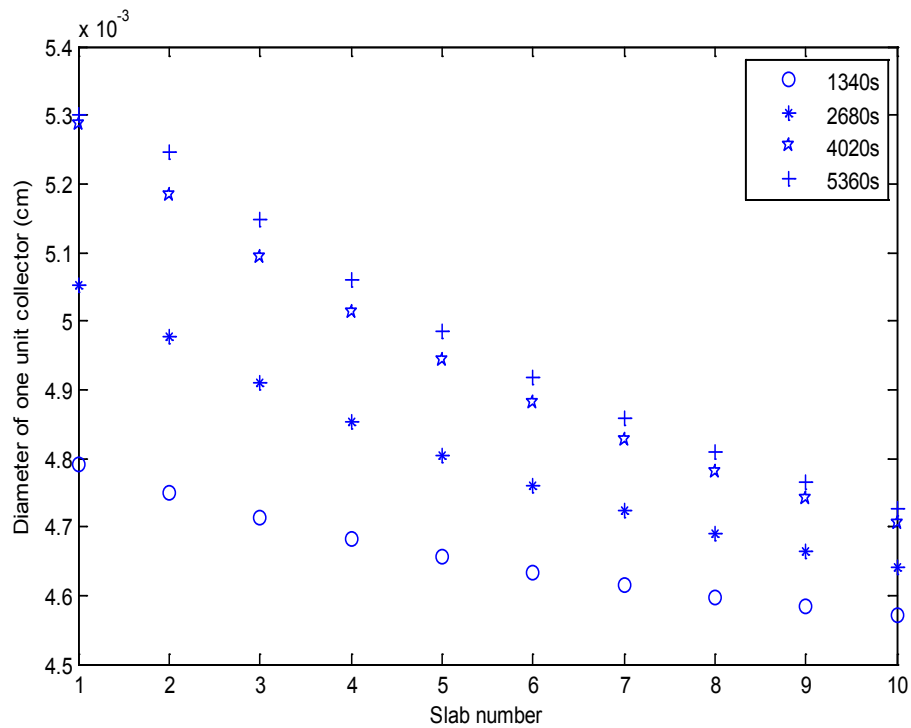
Figure 3.9.Single unit collector diameter for each slab as a function of time. (Gf=0.42 g/cm2s, Tinlet=435 K, Cin=12.75 g/m3 (Std))

Figures 3.10 and 3.11 show the porosity (ε), and filtration efficiency for each slab (E_i) as a function of time, respectively. Since the diameter of the unit collector decreases through the wall, on the other hand, the porosity of each slab will increase which also results in decreasing of the filtration efficiency for each slab.
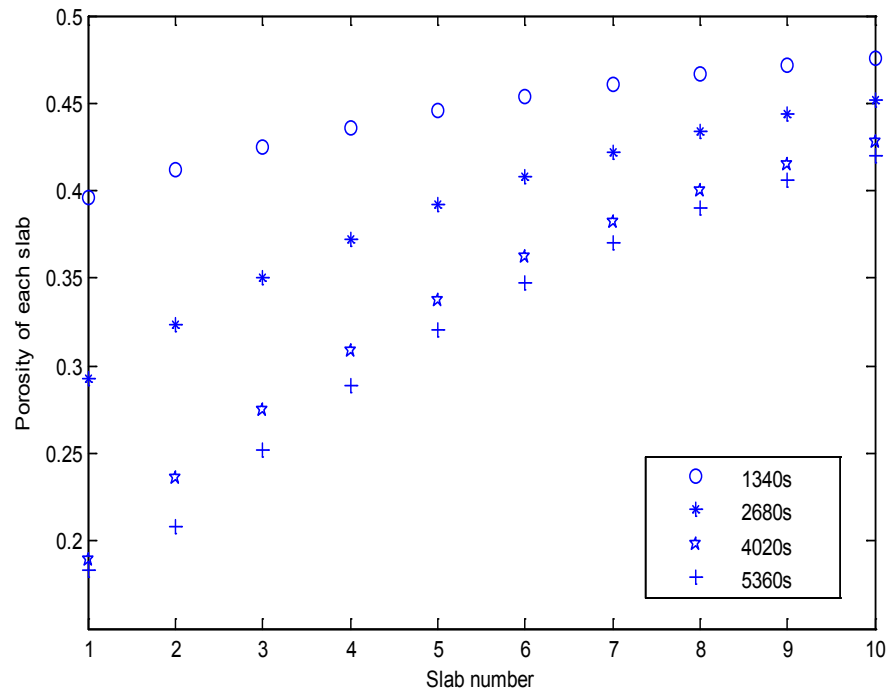
Figure 3.10.Porosity for each slab as a function of time. (Gf=0.42 g/cm2s, Tinlet=435 K
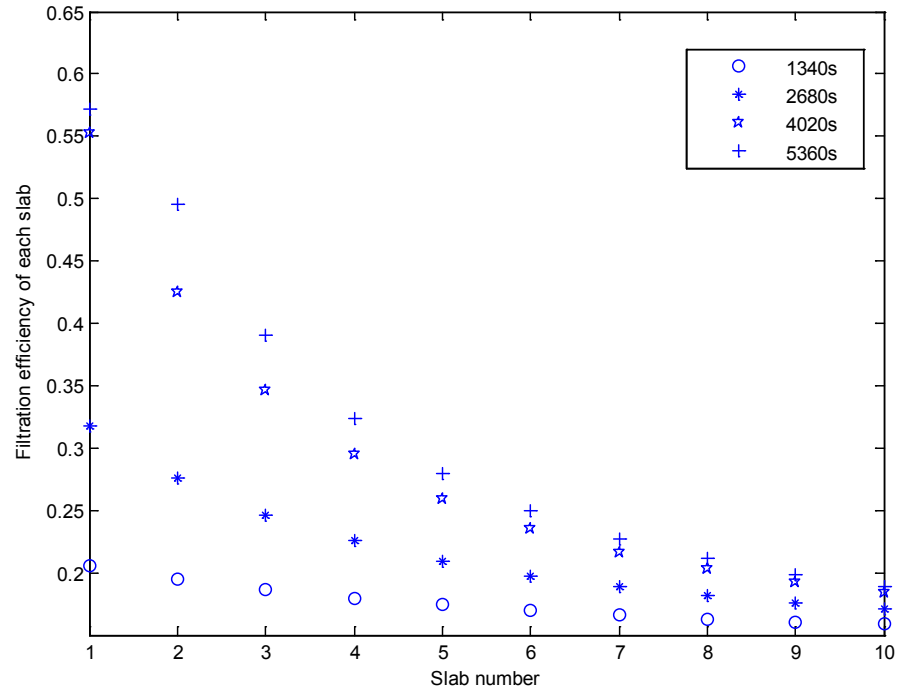
Cin=12.75 g/m3 (Std))

Figure 3.11. Filtration efficiency for each slab as a function of time. (Gf=0.42 g/cm2s,

Tinlet=435 K, Cin=12.75 g/m3 (Std))

In the above section, the input variables of the filtration model are constant. In the next

chapter, these constant input variables will be switched to real-world data (UDDS

driving cycle data).

3.3 Notation

b	"Unit cell" diameter
d_c	"Unit collector" diameter
d_p	Particle diameter, 2.5μm
d_{pore}	Pore diameter, 30μm
D	Diffusion coefficient
E	Filter collection efficiency
$f(\varepsilon)$	Geometric function by Kuwabara
$g(\varepsilon)$	Geometric function by Kuwabara
G_f	Inlet gas flow rate
k_B	Boltzman's constant,$1.38*10^{-19}$ cm^2*kg/s^2*K
k_0	Clean filter wall permeability, $3*10^{-9}$ cm^2
k	Loaded filter wall permeability
Kn_P	Particle Knudsen number
m_w	Deposit particulate mass per unit collector

MW	Molecular weight
N_R	Interception parameter
N_s	Number of spheres in unit volume
Pe	Peclet number
$\bar{R}$	Universal gas constant, $8.314*10^7$ g*cm^2/(s^2*mol*K)
SCF	Stoles-Cunningham slip correction factor
S_v	Specific surface area
T	Filter temperature
U_i	Interstitial or pore velocity
u_w	Filter wall/approach velocity
W	Filter wall thickness, 0.476mm
X	Filter wall thickness coordinate
Y	Mole fraction of each individual species in the exhaust
ε_0	Porosity of "unit collector", 0.5
ε	Filter porosity
η_D	"Unit collector" collection efficiency due to Brownian diffusion
η_R	"Unit collector" collection efficiency due to interception

λ	Exhaust gas mean free path
M	Exhaust dynamic viscosity
v	Exhaust kinematic viscosity
$\rho_{soot,w}$	Packing density of particulate matter in wall, $1.92 g/cm^3$
Φ	Partition coefficient
Ψ	Percolation constant,0.8

3.4 References

(17). Johnson JH, Konstandopoulos AG. A Study Describing the Performance of Diesel Particulate Filters During Loading and Regeneration- A Lumped Parameter Model for Control Applications. SAE Journal. 2003;2003010842.

(18). Dullien FAL. Porous Media- Fluid Transport and Pore Structure. New York (NY). Academic Press. 1979. (Chapter 3).

(19). Lee KW, Gieseke JA. Collection of Aerosol Particles by Packed Beds, Environmental Science and Technology. 1979;13(4):466-470.

Chapter 4 Pressure Drop Model

The pressure drop across the Diesel Particulate Filter (DPF) is one of the most important critical parameters in the design of a DPF regeneration strategy. When the pressure drop is too high, there is a significant amount of particulate accumulated on the filter wall. If this DPF is regenerated, there may be a large heat release which may cause a crack in the DPF. Also, the additional particulate needs more thermal energy to complete the regeneration. This energy is often provided by combusting diesel fuel, which leads to a lower fuel economy, which is an issue that should be considered at the same time. Therefore, a reasonable pressure drop is required for the DPF during both filtration and regeneration. In this chapter, we describe the pressure drop model equations that were used in a reproduction of the work of Johnson and Konstandopoulos from the SAE literature (17). The total pressure drop of the filter channel can be divided into four parts: inlet channel pressure drop, pressure drop across the soot deposit, the pressure drop across the substrate wall, and the outlet channel pressure drop. Moreover, a parametric analysis of this pressure drop model

will be presented.

4.1 Pressure Drop Model Equations

This pressure drop model used to calculate the pressure drop across the DPF is first derived for a clean filter, and then extended to a loaded filter. Please refer to Figure 4.1 for a cross-sectional view of a DPF inlet channel. In this system, the channel has a width α and a wall thickness w, both measured in m. The accumulated deposit is the form of a cake layer and is of thickness w_s. Thus, the area for gas flow has been reduced considerably.
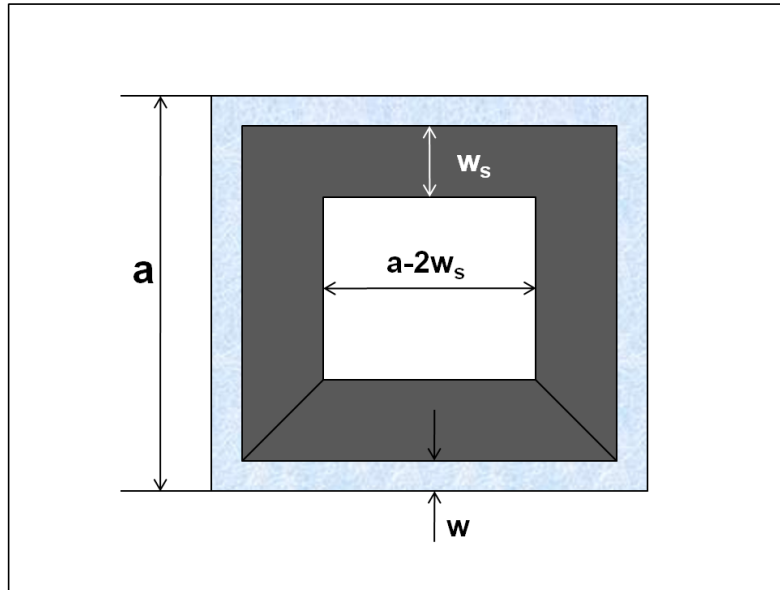
Figure 4.1 Cross section of a loaded filter channel

4.1.1 Clean Filter Pressure Drop Equations

The basic pressure drop equation for a clean filter (w_s) is shown below:

$$\Delta P_{clean} = \frac{\mu}{k_0}\frac{U\alpha}{4L}w + \frac{2\mu F}{3\alpha^2}UL \tag{1}$$

The terms in this expression are the filter wall pressure drop and the inlet and outlet channel pressure drop. In this equation, μ is the exhaust dynamic viscosity (g/cm*s), F is a factor equal to 28.454, L is the length of the filter (cm), k_0 is the clean filter wall permeability (cm^2), and U is the inlet velocity in cm/s which is shown in equation (2):

$$U = \frac{8Q}{\pi D_f{}^2 \sigma \alpha^2} \tag{2}$$

Where D_f is the filter diameter (cm), Q is the actual exhaust volumetric flow rate (cm^3/s), and σ is the filter cell density with the unit of $1/cm^2$ and given by:

$$\sigma = \frac{1}{(\alpha+w)^2} \tag{3}$$

Where α and w are the filter cell width and the wall thickness, in cm, respectively.

The total volume (cm^3) of the filter can be calculated as:

$$V_{trap} = \frac{\pi D_f{}^2 L}{4} \tag{4}$$

Therefore, equation (1) can be rewritten as:

76

$$\Delta P_{clean} = \frac{\mu Q}{2V_{trap}}(\alpha + w)^2 (\frac{w}{k_0 \alpha} + \frac{8FL^2}{3\alpha^4}) \tag{5}$$

or

$$\Delta P_{clean} = \frac{\mu Q}{2V_{trap}}(\alpha + w)^2 (\frac{w}{k_0 \alpha} + \frac{4FL^2}{3\alpha^4} + \frac{4FL^2}{3\alpha^4}) \tag{6}$$

Please note that the term $\frac{8FL^2}{3\alpha^4}$ of equation (5) is split into two terms in equation (6): one represents the frictional losses along the inlet channel, while the other one represents the frictional losses along the outlet channel.

4.1.2 Loaded Filter Pressure Drop Equations

In this subsection, the pressure drop model will be extended from a clean filter to a loaded filter. As mentioned above, the total pressure drop can be divided into four parts:

$$\Delta P = \Delta P_{filter\ wall} + \Delta P_{soot\ layer} + \Delta P_{inlet\ channel} + \Delta P_{outlet\ channel} \tag{7}$$

In eqn. (7), the terms of $\Delta P_{filter\ wall}$, $\Delta P_{soot\ layer}$, $\Delta P_{inlet\ channel}$, and $\Delta P_{outlet\ channel}$ represent the pressure drop across the substrate wall, the pressure drop across the soot deposit, the inlet channel pressure drop, and the outlet channel pressure drop, respectively.

The pressure drop due to the filter wall and soot layer are given below:

$$\Delta P_{\text{filter wall}} = \frac{\mu Q_0}{2V_0}(\alpha + w)^2 \left(\frac{w}{k_0 \alpha}\right) \tag{8}$$

$$\Delta P_{\text{soot layer}} = \frac{\mu Q_0}{8Lk_{\text{soot}}}\ln\left(\frac{\alpha}{\alpha - 2w_s}\right) \tag{9}$$

In equation (8), Q_0 and V_0 are volume gas flow rate and volume for a single channel, respectively. And the deposit soot layer thickness w_s can be calculated from the soot volume in unit of m^3:

$$V_{\text{soot}} = \frac{m_c}{N_{\text{cell}}\,\rho_{\text{soot},c}} \tag{10}$$

Where, N_{cell} is the number of total cells in the filter and m_c is the particulate mass in the soot layer.

From Figure 4.1, equation (10) can be rewritten as follow:

$$V_{\text{soot}} = 4w_s(\alpha - w_s)L \tag{11}$$

Finally, w_s can be obtained:

$$w_s = \frac{\alpha - \sqrt{\alpha^2 - \dfrac{m_c}{N_{\text{cell}}\,L\rho_{\text{soot},c}}}}{2} \tag{12}$$

Since the inlet channel is loaded, eqn. (2) for the inlet velocity is modified as below:

$$U = \frac{8Q}{\pi D_f{}^2 \sigma (\alpha - 2w_s)^2}$$

(13)

Then, the inlet channel pressure drop and outlet channel pressure drop, which are split from equation (5), are given below:

$$\Delta P_{\text{inlet channel}} = \frac{\mu Q_0}{2V_0}(\alpha + w)^2 \left(\frac{4FL^2}{3(\alpha - 2w_s)^4}\right)$$

(14)

$$\Delta P_{\text{outlet channel}} = \frac{\mu Q_0}{2V_0}(\alpha + w)^2 \left(\frac{4FL^2}{3\alpha^4}\right)$$

(15)

The only difference between inlet channel pressure drop and outlet channel is the fact that a deposit layer is not built up on the substrate wall of the outlet channel.

4.1.3 Sample Calculations

In this subsection, sample calculations about pressure drop for clean and loaded filter will be presented. The values of the parameters used in this section are from the Bissett model (20) and pressure drop model from J. Jonhson et. al. (6, 17) which are constants. (See the section 4.3 and Table 2.1).

Clean Filter

For the clean filter, there are no particulates accumulated in or on the substrate walls of the filter which means the regeneration is completed.

$$\Delta P_{clean} = \frac{\mu Q_0}{2V_0}(\alpha + w)^2 \left(\frac{w}{k_0\alpha} + \frac{8FL^2}{3\alpha^4}\right) = 0.83 \text{ kPa}$$

Here, $V_0 = 2.14 \text{ cm}^3$, and gas viscosity $u = 0.334\text{e-}3 \text{ g/cm*s}$

Loaded Filter

For the loaded filter, the pressure drop shown below is immediately before the regenration. Thus, the soot pressure drop can be estimated with a uniform initial deposit thickness.

$$\Delta P_{filter\ wall} = \frac{\mu Q_0}{2V_0}(\alpha + w)^2 \left(\frac{w}{k_0\alpha}\right) = 0.61 \text{ kPa}$$

$$\Delta P_{soot\ layer} = \frac{\mu Q_0}{8Lk_{soot}} \ln\left(\frac{\alpha}{\alpha - 2w_s}\right) = 1.65 \text{ kPa}$$

$$\Delta P_{inlet\ channel} = \frac{\mu Q_0}{2V_0}(\alpha + w)^2 \left(\frac{4FL^2}{3(\alpha - 2w_s)^4}\right) = 0.16 \text{ kPa}$$

$$\Delta P_{outlet\ channel} = \frac{\mu Q_0}{2V_0}(\alpha + w)^2 \left(\frac{4FL^2}{3\alpha^4}\right) = 0.15 \text{ kPa}$$

$$\Delta P_{total} = \Delta P_{filter\ wall} + \Delta P_{soot\ layer} + \Delta P_{inlet\ channel} + \Delta P_{outlet\ channel} = 2.57 \text{ kPa}$$

From the equations shown above, it can be noticed the total pressure drop across the fiter is equal to the summation of pressure drop of filter wall, soot layer, inlet channel,

and outlet channel. Moreover, from the sample calculation of loaded filter, one can also find that the pressure drop of soot layer takes significant fraction of the total pressure drop and it followed by the pressure drop of filter wall. While, inlet channel pressure drop and outlet channel pressure drop are small fractions of the total pressure drop. The slight difference between these two channels are caused by the different geometries which is due to the built deposit layer.

4.2 Parametric Study of Pressure Drop Model

In this part, we will perform a parametric study of the pressure drop model. Since the pressure drop is one of the most important DPF operating parameters during both filtration and regeneration, a reasonable pressure drop is needed to achieve good fuel economy and help ensure a complete regeneration which can extend the service life of the DPF. Therefore, parameters in the pressure drop model will be studied and one can compare the impact of each parameter on the pressure drop.

4.2.1 Uniform Gas Flow Rate and Deposit Thickness

There are several critical parameters in the pressure drop models. These include the inlet temperature, deposit thickness, and gas flow rate, which are three operating parameters, while the filter wall thickness is a design parameter which cannot be changed. Therefore, we do not consider the impact of changing the wall thickness in our simulation. In this study, the standard inlet temperature (T_{inlet}), deposit thickness (w_b), and gas flow rate per open frontal area (G_f) are 710K, $1.117*10^{-3}$ cm, and $0.272g/(cm^2*s)$, respectively. And the inlet pressure drop shown in the following figures is the summation of inlet channel pressure drop, particulate deposit pressure drop and the filter substrate wall pressure drop.

4.2.1.1 Effect of the Inlet Temperature on the Pressure Drop

The inlet temperature is the most dominant variable in the pressure drop model during the regeneration, as shown in Figure 4.2 (uniform gas flow rate). In these figures shown below, z/L=0 is the inlet and z/L=1 is the outlet.

From Figures 4.2- 4.5, one can notice that the pressure drop decreases faster when the

inlet temperature is higher. That is because a higher inlet temperature can supply more energy to initiate the regeneration for the same time. From Figure 4.2, it can be found that the pressure drop near the entrance of the filter decreases when the inlet temperature is equal to 800K or 900K. However, when the inlet temperature is lower (600K or 710K), the pressure drop did not change much since the particulate layer thickness does not change near the entrance. That means the regeneration is more rapid when the inlet temperature is higher. In other words, the regeneration efficiency increases with increasing inlet temperature during the same time.

The regeneration efficiency is one of the most important issues; however, fuel economy is another problem we need to consider since higher inlet temperature requires more thermal energy from burning the additional fuel. Moreover, the filter may crack during the regeneration if the inlet temperature is too high.

Figure 4.2 Pressure drop across the filter along the channel for different inlet temperatures

at the same time (30s).
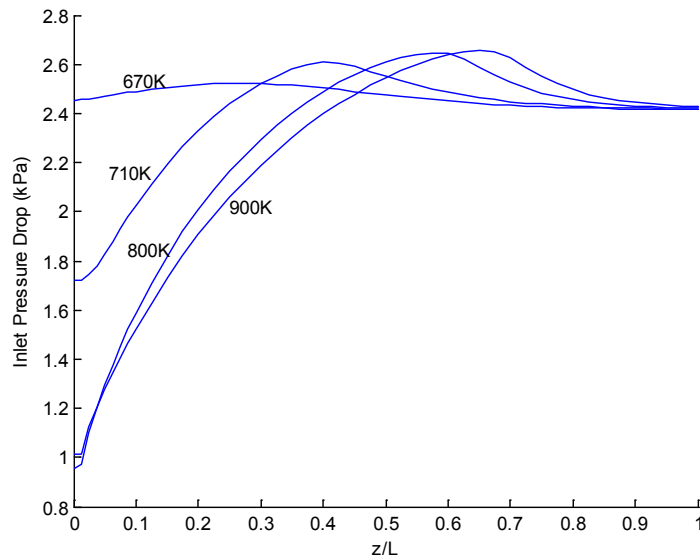
Figure 4.3 Pressure drop across the filter along the channel for different inlet temperatures
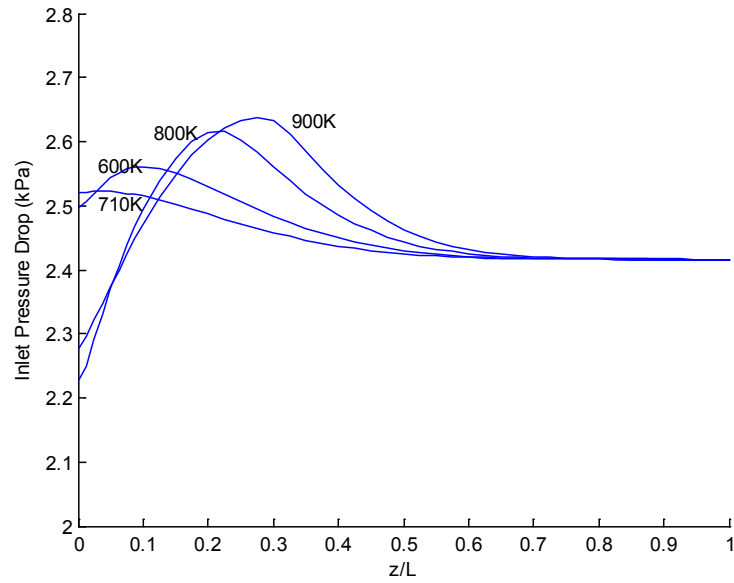
at the same time (60s).

84
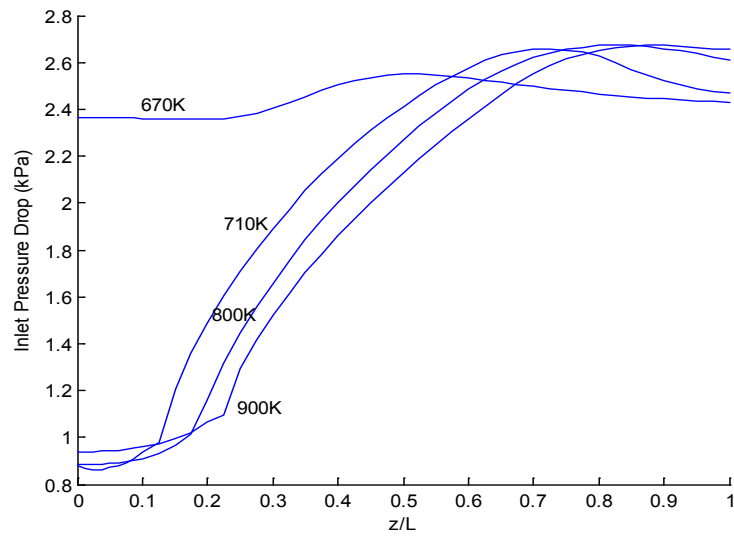
Figure 4.4 Pressure drop across the filter along the channel for different inlet temperatures at

the same time (90s).
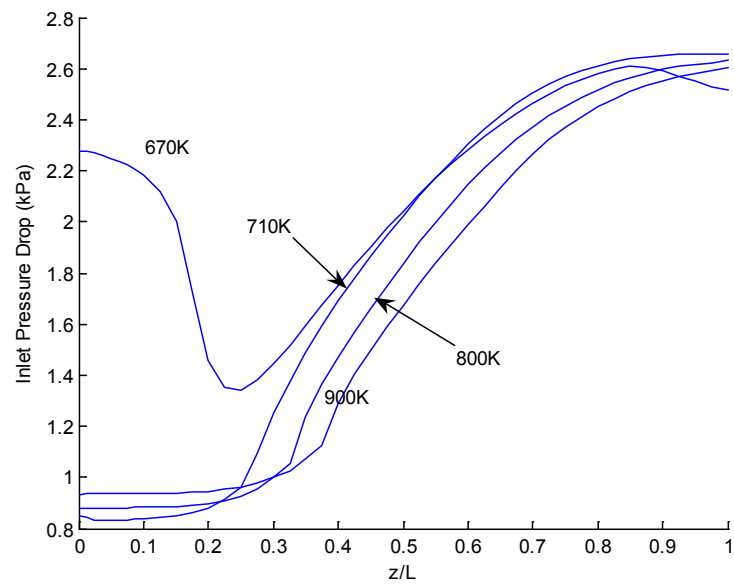
Figure 4.5 Pressure drop across the filter along the channel for different inlet temperatures

at the same time (120s).

4.2.1.2 Effect of the Initial Deposit Thickness (Uniform) on the Pressure Drop

The deposit thickness (w_b) affects the $\Delta P_{soot\ layer}$ term directly in the pressure drop model. It can be noticed that a thicker deposit layer can cause the regeneration to initiate faster (See Figures 4.6- 4.9). From Figure 4.8, it can be noticed that at t=60s, the pressure drop near the entrance of the filter channel decreases about 1, 0.8, 0.2, and 0.1 kPa for deposit thickness is of $2w_b$, w_b, $0.5w_b$, and $0.25w_b$, respectively. This is because more thermal energy is released from the combustion of the thicker particulate layer.

However, a thicker particulate deposit results in a higher pressure drop in the inlet channel, but at the same time a larger thermal energy release from thicker particulate deposit may also result in a crack formation in the DPF. On the other hand, we should not initiate the regeneration either when there is little particulate in the inlet channel of the filter. This is because less thermal energy released from the particulate is not enough for the regeneration and filter needs more energy to complete the regeneration from additional fuel which will also reduce the fuel economy.

Figure 4.6 Pressure drop across the filter along the channel for different deposit thickness.

(wb=1.117*10-3 cm, Tinlet=710K, Time=10s)

Figure 4.7 Pressure drop across the filter along the channel for different deposit thicknesses.

(wb=1.117*10-3 cm, Tinlet=710K, Time=30s)

Figure 4.8 Pressure drop across the filter along the channel for different deposit thicknesses.

(wb=1.117*10-3 cm, Tinlet=710K, Time=60s)
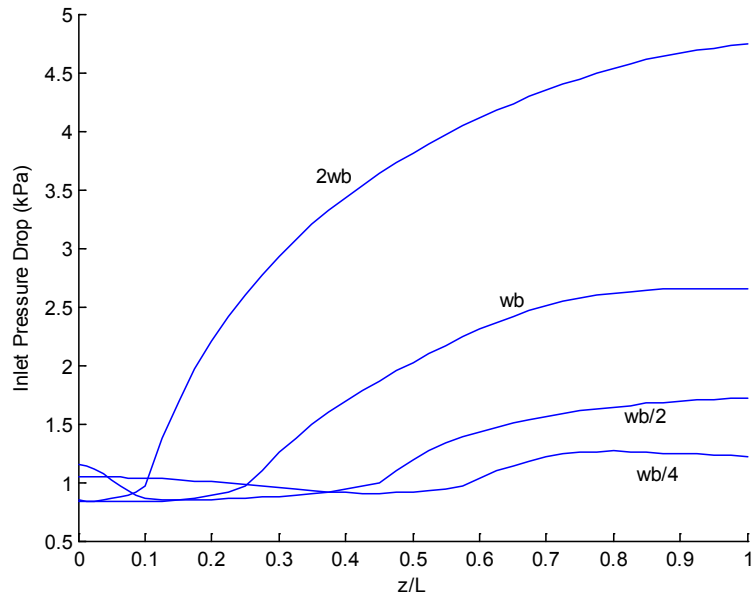
Figure 4.9 Pressure drop across the filter along the channel for different deposit thicknesses.

(wb=1.117*10-3 cm, Tinlet=710K, Time=120s)

Figures 4.10-4.13 show the inlet pressure drop along the inlet channel for different values of w_b for a feed temperature of 670K at different times. As we know, a higher inlet temperature leads to a leading edge ignition, while a lower inlet temperature causes a downstream ignition. Figures 4.10-4.13 show the downstream ignition situations comparing to those shown in Figures 4.6-4.9 which are leading edge ignition.

For the regeneration, one needs to make sure the reaction is leading edge since a leading edge reaction is necessary for a completed regeneration and also it can avoid higher pressure drop near the entrance of the filter channel or crack of the DPF.
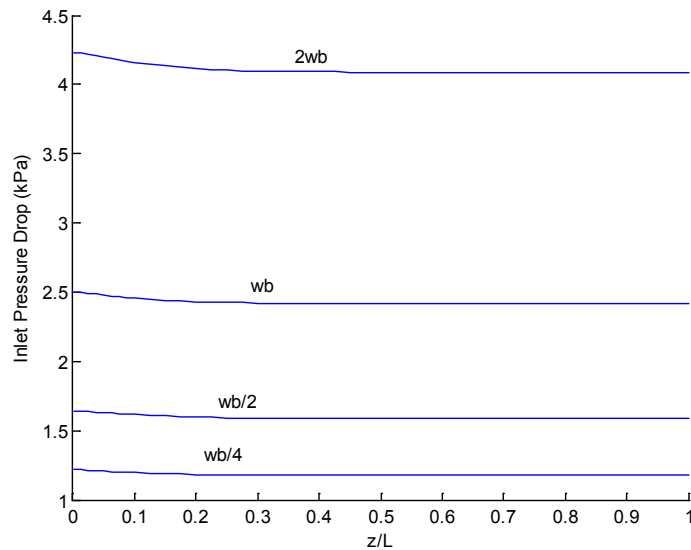
Figure 4.10 Pressure drop across the filter along the channel for different deposit thickness.

(wb=1.117*10-3 cm, Tinlet=670K, Time=10s)
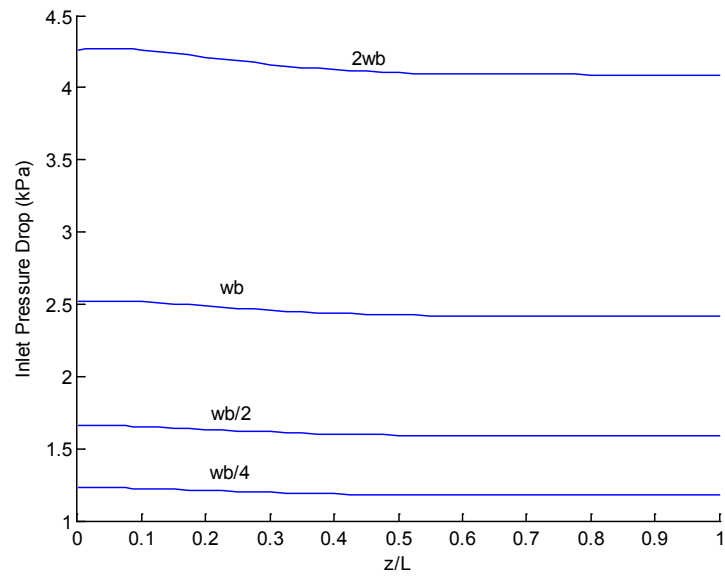
Figure 4.11 Pressure drop across the filter along the channel for different deposit thicknesses.

(wb=1.117*10-3 cm, Tinlet=670K, Time=30s)
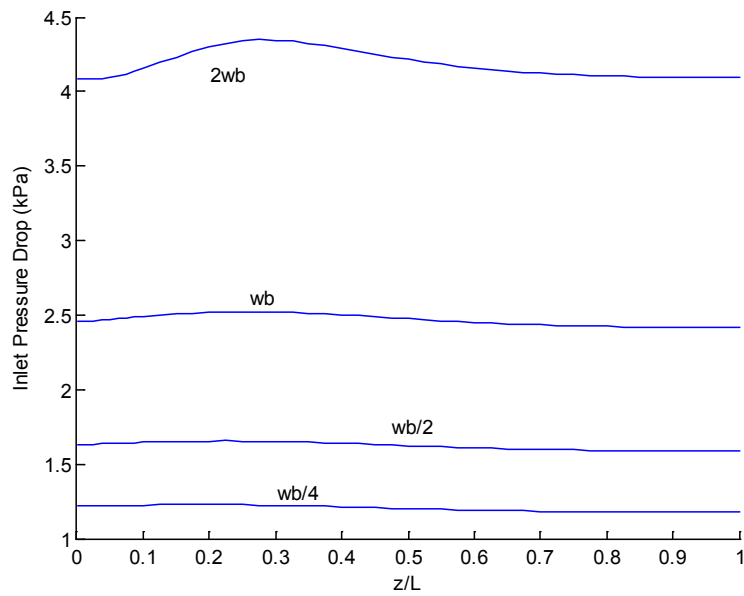
Figure 4.12 Pressure drop across the filter along the channel for different deposit thicknesses.

(wb=1.117*10-3 cm, Tinlet=670K, Time=60s)

90

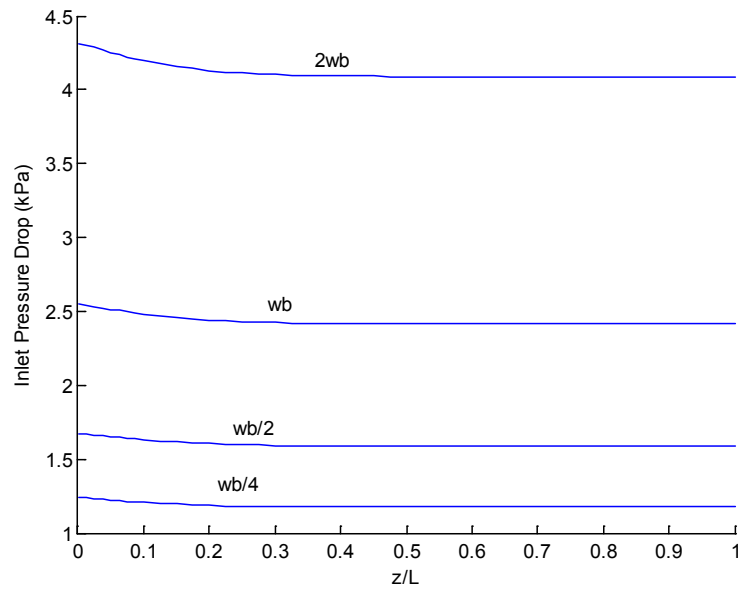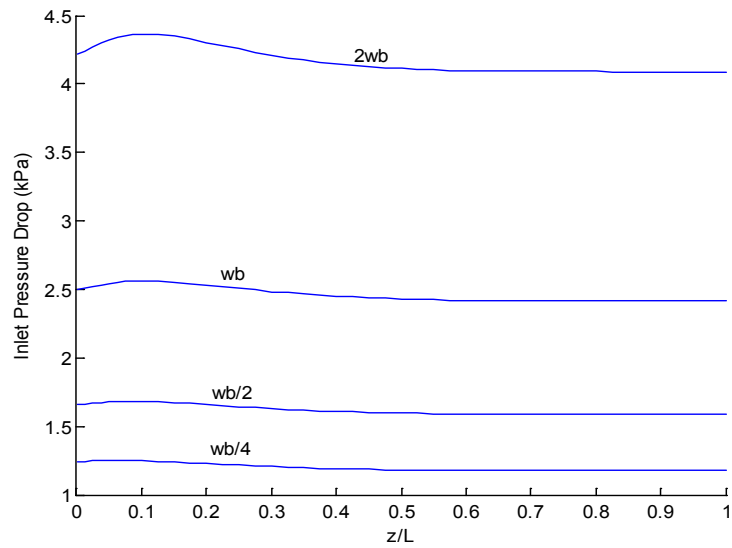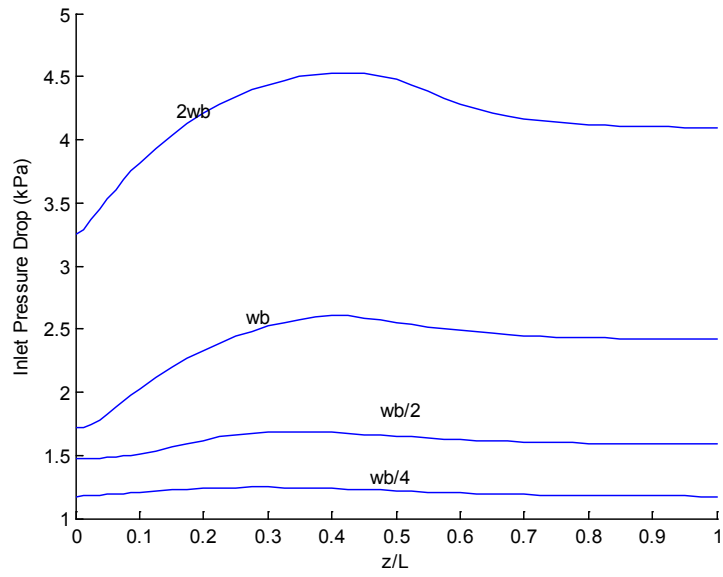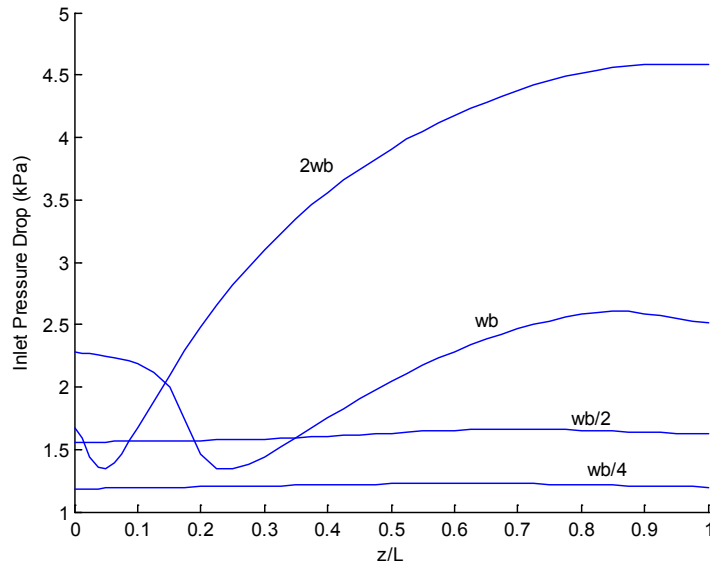**Figure 4.13 Pressure drop across the filter along the channel for different deposit thicknesses.**

(wb=1.117*10-3 cm, Tinlet=670K, Time=120s)

4.2.1.3 Effect of Gas Flow Rate on Pressure Drop

From the figures shown below (Figures 4.14- 4.16), we can find that increasing the gas flow rate results in an increasing pressure drop. Because more thermal energy is released from a larger gas flow rate, the regeneration reaction takes place faster. For instance, at t=120s, the regeneration efficiency is about 80%, 60%, and 30% under the conditions of double the standard gas flow rate, standard gas flow rate, and half the standard gas flow rate, respectively. However, from the results shown in Figure 2.10

(16, 21), one can notice that a large gas flow rate may quench the regeneration. Also, a

smaller gas flow rate may not be able to initiate the regeneration. Therefore, neither a

large nor a small gas flow rate is desirable.
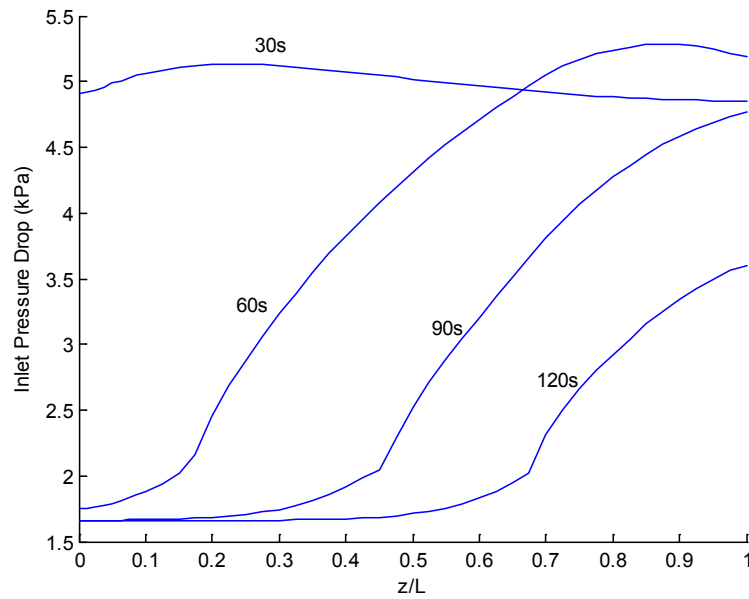
Figure 4.14 Pressure Drop across the filter under the same Inlet Temperature (710K) for

Double Q. (wb=1.117*10-3 cm, Q=0.272g/cm2*s)
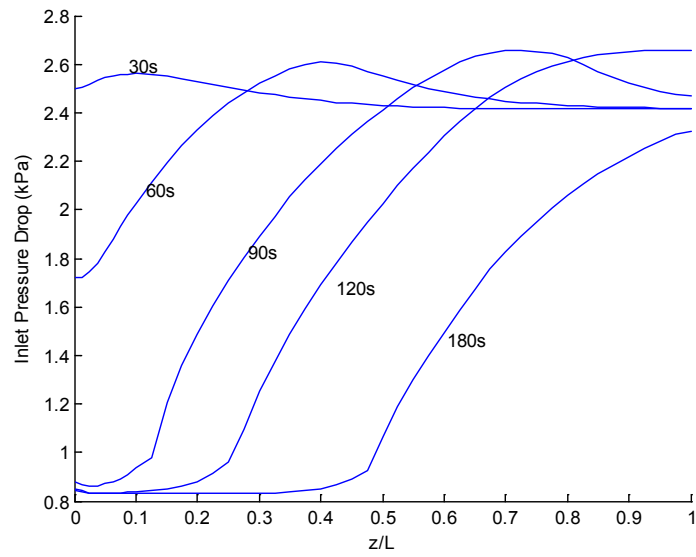
Figure 4.15 Pressure Drop across the filter under the same Inlet Temperature (710K) for

Standard Q. (wb=1.117*10-3 cm, Q=0.272g/cm2*s)
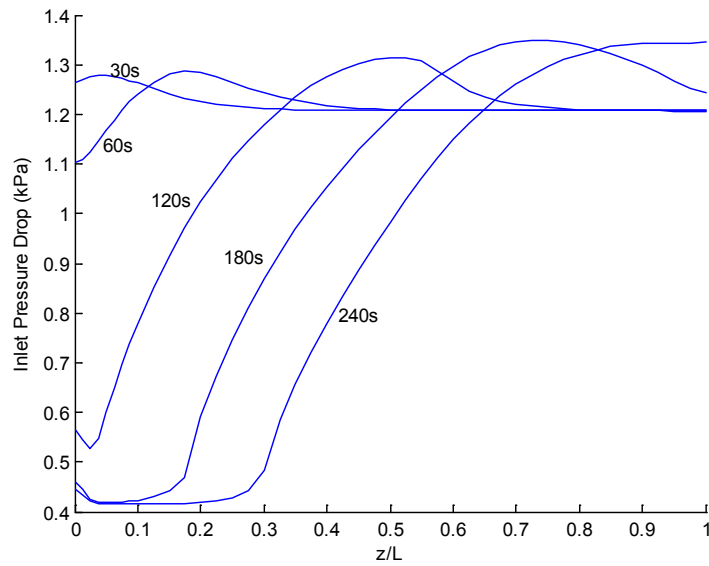
Figure 4.16 Pressure Drop across the filter under the same Inlet Temperature (710K) for Half

Q. (wb=1.117*10-3 cm, Q=0.272g/cm2*s)

4.2.2 Effect of Non- Uniform Deposit Thickness in Engine Aftertreatment Applications on the Pressure Drop

In this subsection, experimental data on the deposit thickness is obtained from the SAE literature (7). These series of data will be used to simulate the axial distribution of carbon deposit in the inlet channel in our pressure drop and regeneration models as shown in Figure 4.17.

In real driving conditions, the particulate deposit layer is not uniform in DPF. It will be accumulated more at the end of the channel than that near the entrance. Therefore, the pressure drop in the inlet channel and the pressure drop across the deposit layer will vary from the entrance to the end of the filter. There are two possible reasons: the first one is that the inertia of the exhaust gas will 'push' the particulate from the entrance to the end; the second one may be due to an incomplete regeneration which may have taken place before this loading. If the regeneration occurs at the leading edge of the DPF, the particulate which is accumulated near the entrance of the channel will be burnt off first. However, if there is a drop in the DPF feed temperature, the particulate near the end of the channel may not be burnt off during this incomplete regeneration and remain on the substrate wall.
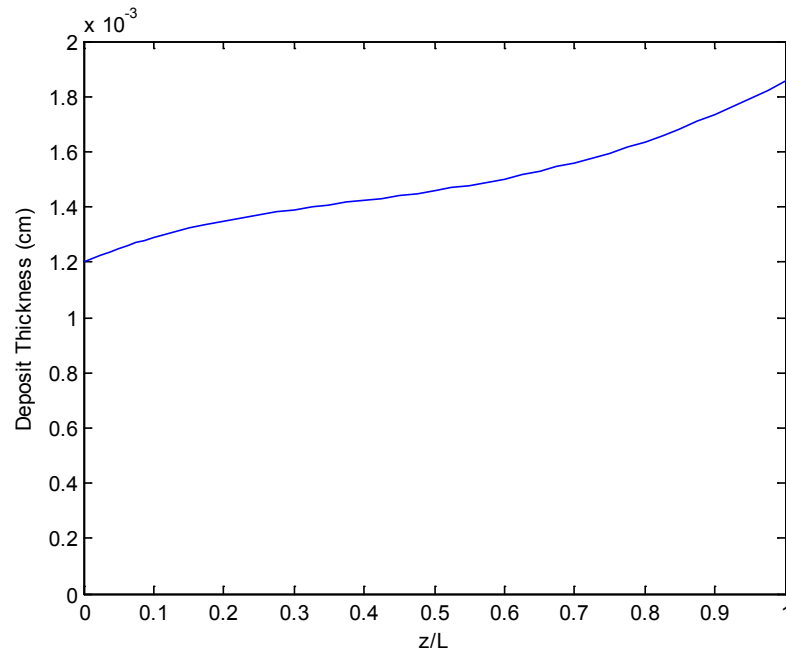
Figure 4.17 Actual Deposit Thickness along the Inlet Channel. Data obtained from (7).

Figure 4.18 shows the deposit thickness distribution along the channel during the regeneration from which it can be noticed that the regeneration is a leading edge reaction and the regeneration efficiency is about 95% at 180 seconds.

Temperature profiles along the inlet channel for different times during the regeneration process for the initial loading shown in Figure 4.18 is given in Figure 4.19. One can find that it takes more than 30 seconds to heat up the channels and the temperature peak happens at t= 180s which is equal to 1298K.
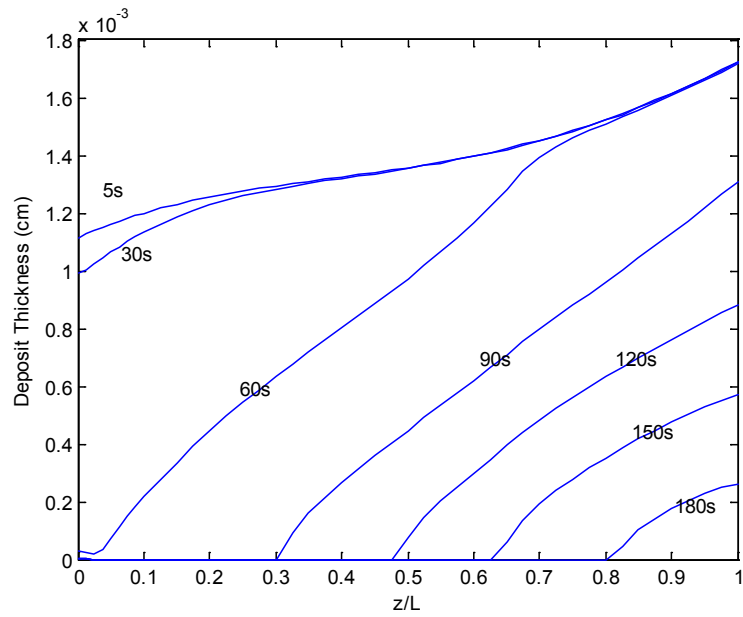
Figure 4.18 Deposit Thickness Distribution along the Channel during the Regeneration

(Tinlet=710K, Q=0.272g/cm2*s)
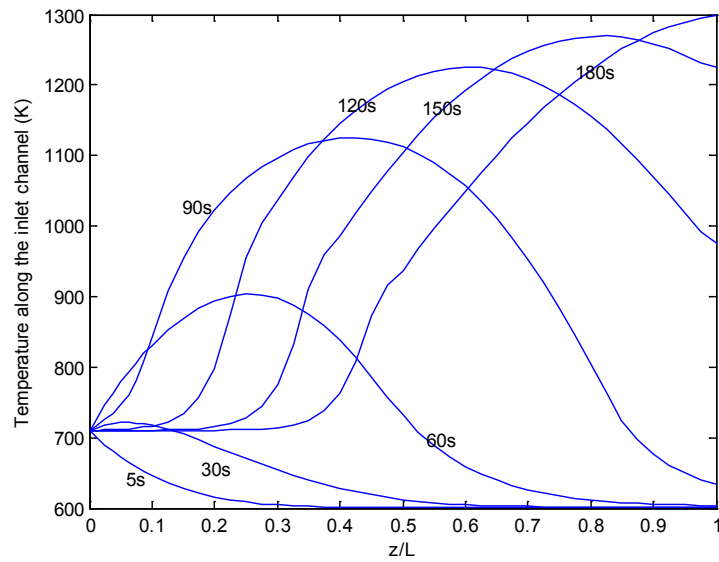
Figure 4.19 Temperature along the Inlet Channel during the Regeneration as the Same

Conditions Shown in Figure 4.15

Figure 4.20 shows the pressure drop along the channel for this case. The regeneration is a leading-edge ignition which means the ignition is initiated near the entrance of the filter. Therefore we can notice that the pressure drop decreases faster near the entrance of the filter. From the experimental data we can notice that the there is more particulate deposit near the end of the filter. Also more particulate can result in high temperature during the combustion which may cause a crack or even melting of the filter materials. If the filter materials cannot sustain a 1300K temperature then the regeneration should occur with a smaller loading than shown in Figure 4.17.
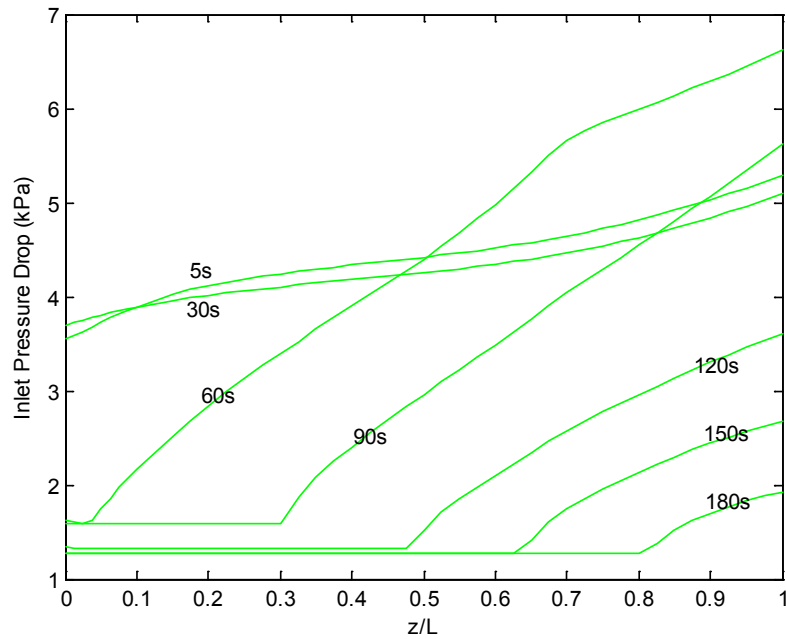
Figure 4.20 Inlet Pressure Drop across the filter along the Channel during the Regeneration

(Tinlet=710K, Q=0.272g/cm2*s)

97

4.3 Notation

D_f	Filter diameter, 24cm.
F	Factor equal to 28.454
k_0	Clean filter wall permeability, $3*10^{-9}$ cm^2.
k_{soot}	Particulate layer permeability, $1.3*10^{-11}$ cm^2.
k_t	Loaded wall permeability
L	Filter length, 32cm.
m_c	Mass retained in the cake layer
N_{cells}	Number of total cells in filter, 700.
ΔP	Pressure Drop
ΔP_{clean}	Clean filter pressure drop
$\Delta P_{filter\ wall}$	Pressure drop across the substrate wall
$\Delta P_{soot\ layer}$	Pressure drop across the soot deposit
$\Delta P_{inlet\ channel}$	Inlet channel pressure drop
$\Delta P_{outlet\ channel}$	Outlet channel pressure drop

Q	Actual exhaust volumetric flow rate, 0.094 m^3/s.
Q_0	Actual single channel exhaust volumetric flow rate, 13.99 cm^3/s.
U	Inlet velocity, cm/s
V_{trap}	Total filter volume
V_0	Single channel volume, 2.14 cm^3
w	Filter wall thickness, $4.76*10^{-2}$ cm.
w_s	Particulate matter layer thickness, $1.117*10^{-3}$ cm.
α	Filter cell width, 0.211 cm.
μ	Exhaust dynamic viscosity
σ	Filter cell density, 100 cpsi.

4.4 References

(20). Bissett EJ. Mathematical Model of the Thermal Regeneration of a Wall-flow Monolith Diesel Particulate Filter. Chemical Engineering Science. 1984;39 (7/8):1233-1244.

(21). Huang D. Parametric and Sensitivity Study of Wall-Flow Monolith Diesel Particulate Filter Regeneration. M.S. Thesis. 2008. Michigan Technological University. Houghton (MI).

Chapter 5 Real-World Driving Conditions

5.1 Urban Dynamometer Driving Schedule (UDDS)

Due to their high thermal efficiency and good reliability, diesel engines are equipped on larger motor vehicles such as heavy trucks and buses. However, particulate matter (PM) emission from diesel fuel is a major concern regarding the diesel engines. It is necessary to simulate diesel engine emissions under real-world driving conditions. Also, all the heavy-duty engines, including on-road and off-road, should meet the emission standard either from California emission standards or EPA (U.S. Environmental Protection Agency) standards.

In this chapter, the regeneration model will be studied under the Urban Dynamometer Driving Schedule (UDDS) which is a driving cycle used to test diesel engine vehicles under certain real-world driving conditions. Figure 5.1 shows the vehicle speed (mph) as a function of time. This cycle simulates an urban route of 7.5 mi (12.07 km). The

maximum speed is 56.7 mi/h (91.2km/h) and the average speed is 19.6 mi/h (31.5 km/h). The cycle duration is 1340 seconds (22).
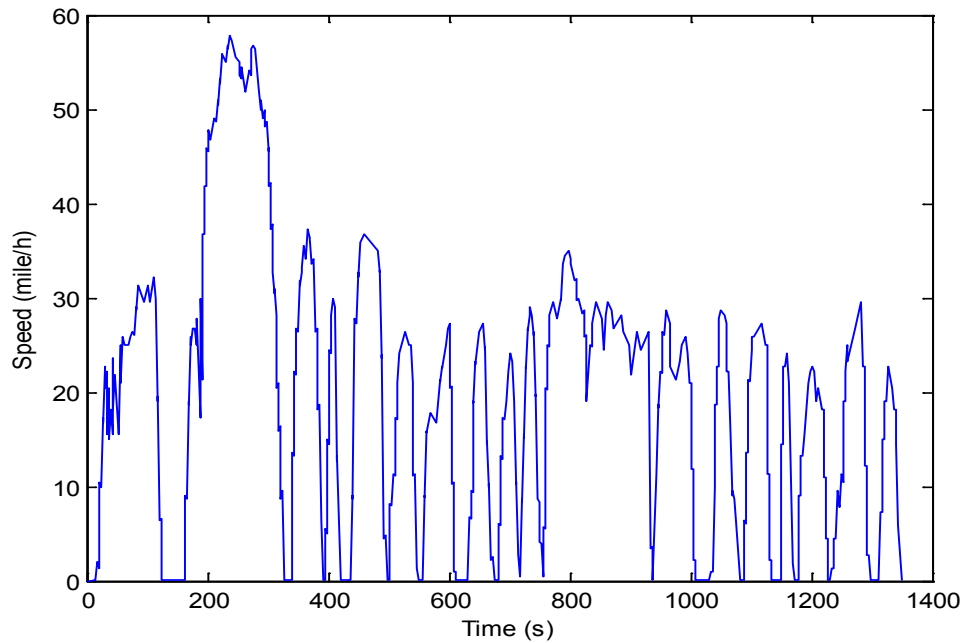
Figure 5.1. Vehicle speed as a function of time for Urban Dynamometer Driving Schedule (UDDS). (Data reproduced from (1))

5.2 Diesel Engine Exhaust Analysis

The test diesel engine is a Duramax 6.6L engine which is equipped on a 2002 Chevrolet Silverado 2500 series pick-up truck. By testing the vehicle and engine under UDDS driving cycle, real data were obtained such as engine speed, engine torque, and

engine exhaust temperature (22). Using the data, we can produce plots of engine speed vs. time, engine torque vs. time, and exhaust gas temperature vs. time under the Urban Dynamometer Driving Schedule (UDDS), shown below in Figures 5.2-5.4, respectively. Moreover, these realistic driving data will also be used in our simulations, shown in later sections.
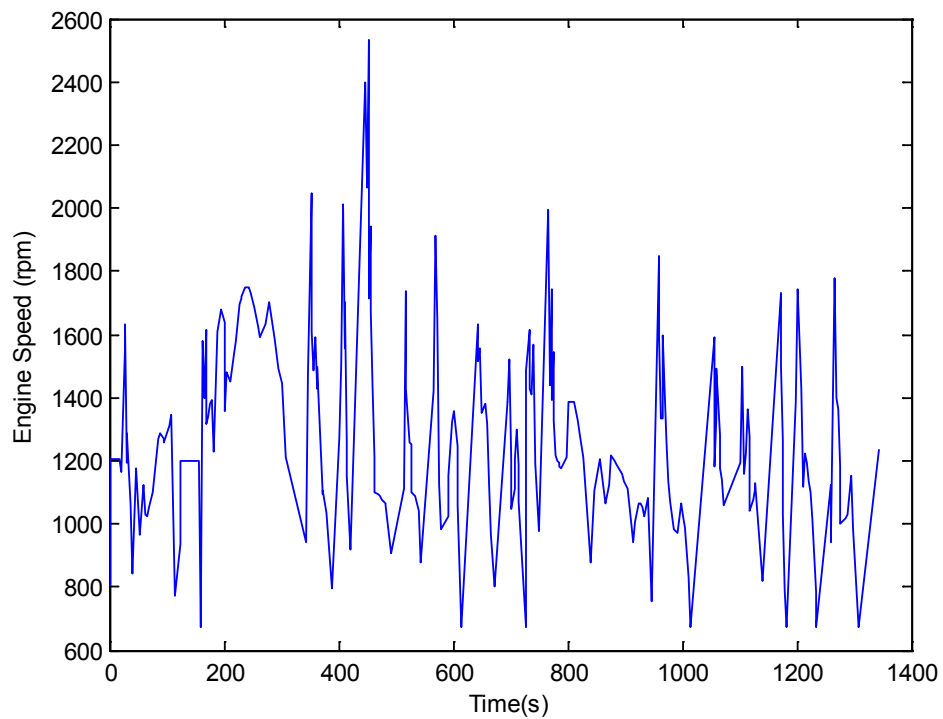
Figure 5.2. Engine speed vs. time for UDDS driving conditions.

(Data reproduced from (22))
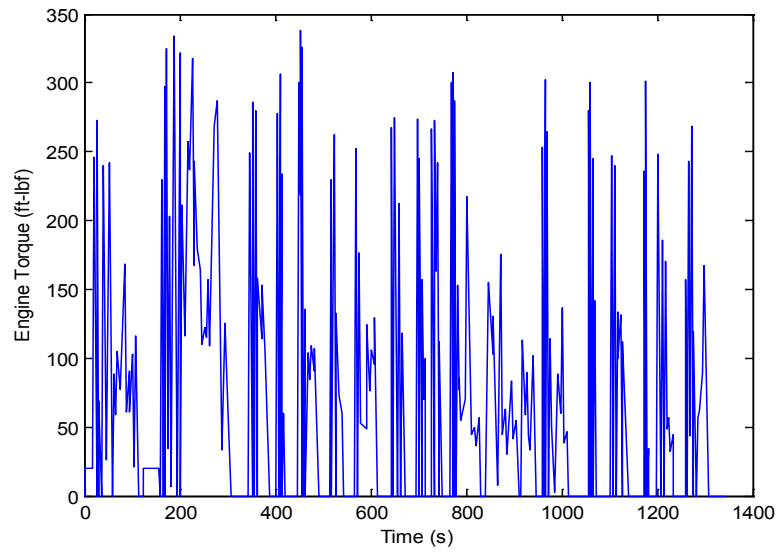
Figure 5.3. Engine torque vs. time for UDDS driving conditions.

(Data reproduced from (22))
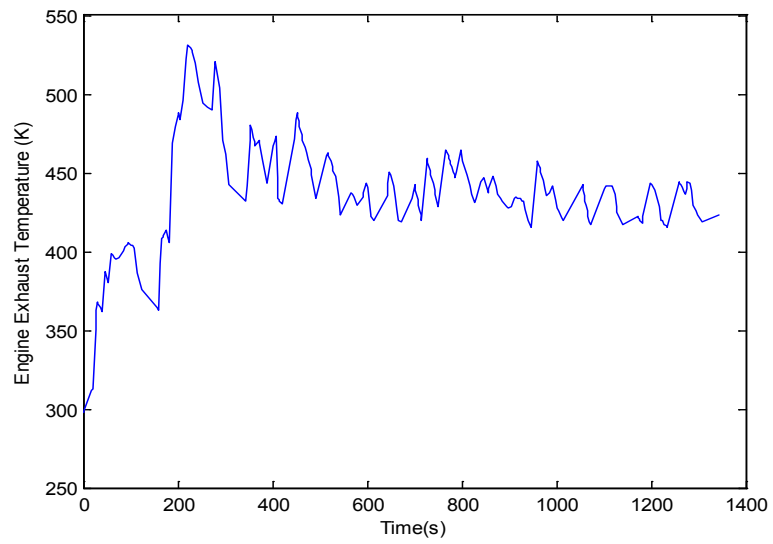
Figure 5.4. Engine exhaust temperature vs. time for UDDS driving conditions.

(Data reproduced from (22))

Figure 5.5 and Figure 5.6 show the correlations between engine exhaust gas temperature and engine torque, and between particulate matter (PM) concentration and engine torque (23). These relationships will be used to calculate some of the input parameters for our models.
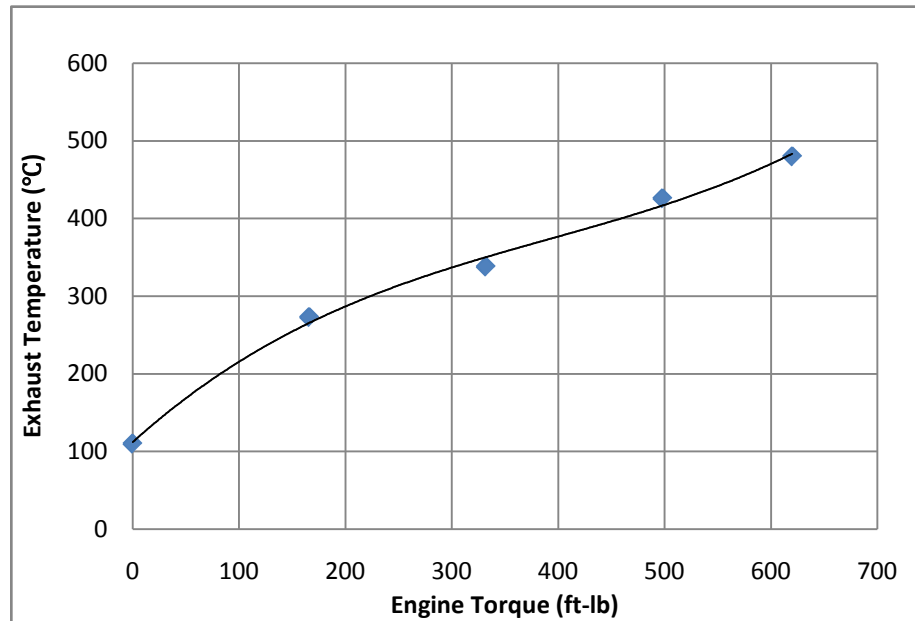
Figure 5.5. Exhaust temperature for different engine output torque.

(Data reproduced from (23))
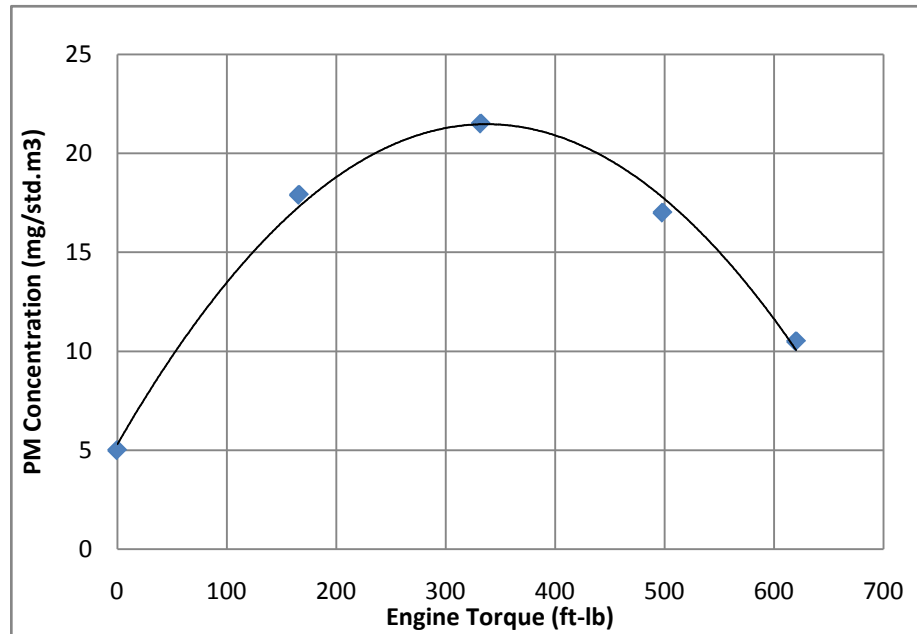
Figure 5.6. Particulate matter concentration as a function of engine torque

(Data reproduced from (23))

Based upon the correlations shown above, we are able to easily obtain the PM concentration vs. time. Figure 5.7 shows the exhaust gas flow rate as a function of time under UDDS driving cycle. This series of data are significant in filtration model and regeneration model.
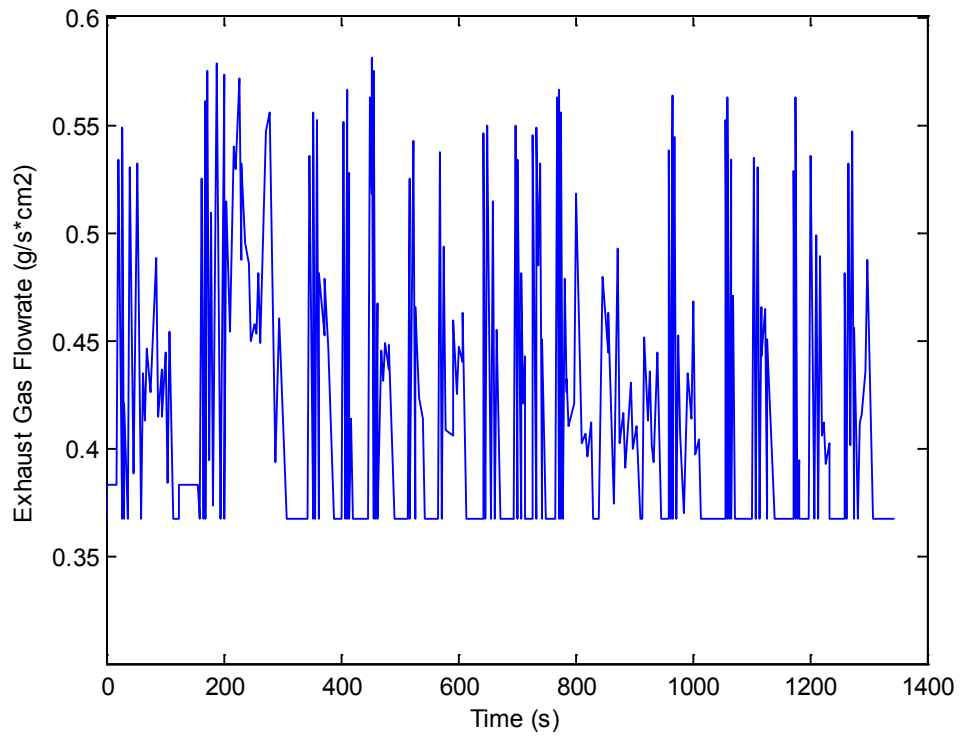
Figure 5.7. Exhaust gas flow rate as a function of time.

Figure 5.8 shows the exhaust particulate matter concentration as a function of time for

UDDS cycle, which will be used as an input parameter for the filtration model for the

UDDS driving cycle.
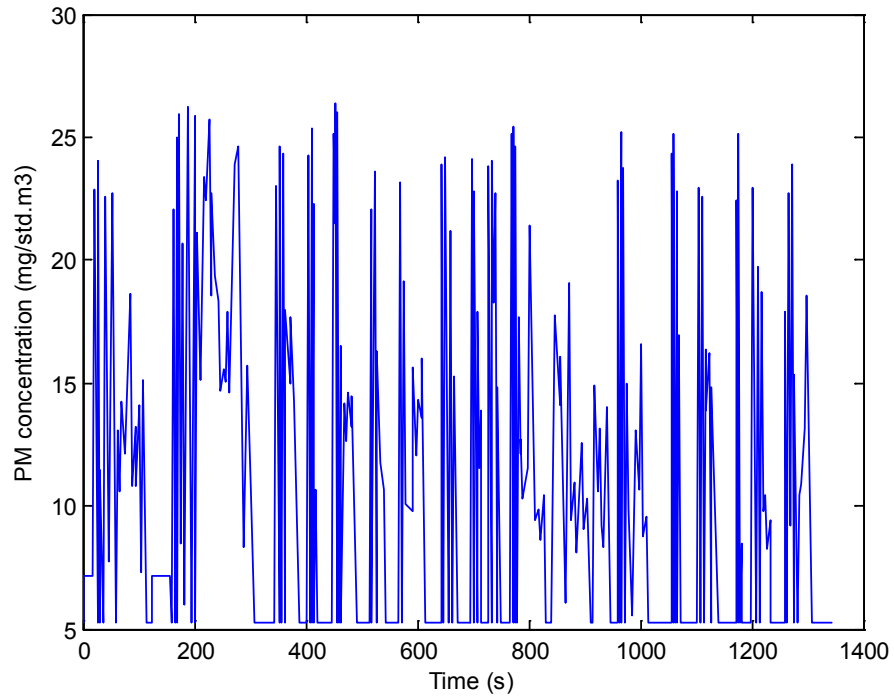
Figure 5.8. Exhaust PM concentration as a function of time.

5.3 Results and Discussion

5.3.1 Filtration during UDDS driving cycle

In chapter 3, we present a filtration model of DPF with constant input parameters, which are constant exhaust gas flow rate (G_f=0.42 g/cm^{2}s), constant inlet temperature

(T_{inlet}=435 K) and constant inlet PM concentration (C_{in}=12.75 g/m³ (Std)).

In this chapter, these three input variables will be switched to UDDS driving cycle data which fluctuates with time (shown in Figure 5.7, Figure 5.3 and Figure 5.8, respectively.).

Figure 5.9 shows the filtration efficiency of the DPF as a function of time over a time of 5360 seconds, which is equal to the time of 4 driving cycles. Comparing with the figure shown in chapter 3 for uniform conditions (Figure 3.6), it can be noticed that it takes a longer time (4400s) than that in chapter 3 (3800s) for overall filtration efficiency to achieve unity. The same result is also shown in Figure 5.10. It takes 600 seconds longer for a unit collector diameter to become constant under UDDS driving conditions than for uniform input conditions, which is shown in Figure 3.7.
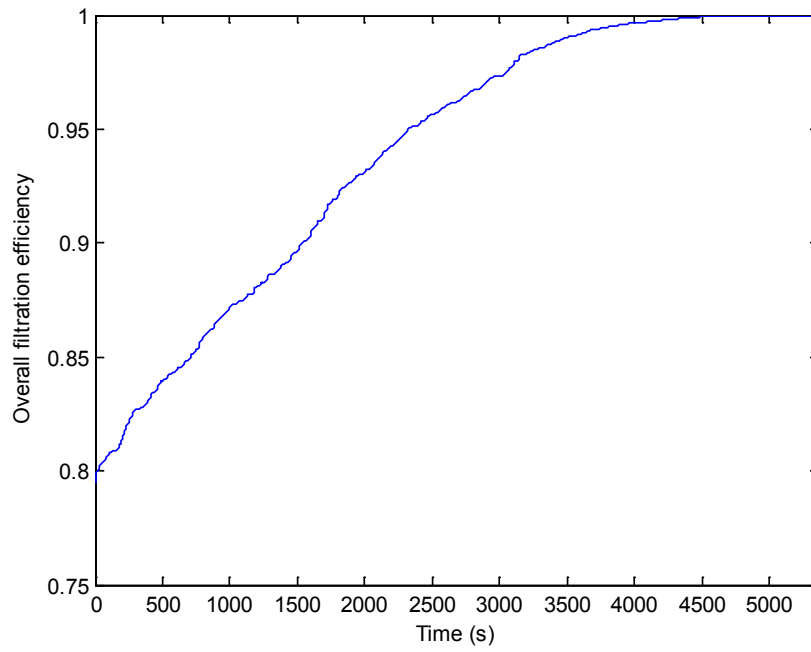
Figure 5.9. Overall filtration efficiency as a function of time under the UDDS driving cycle.
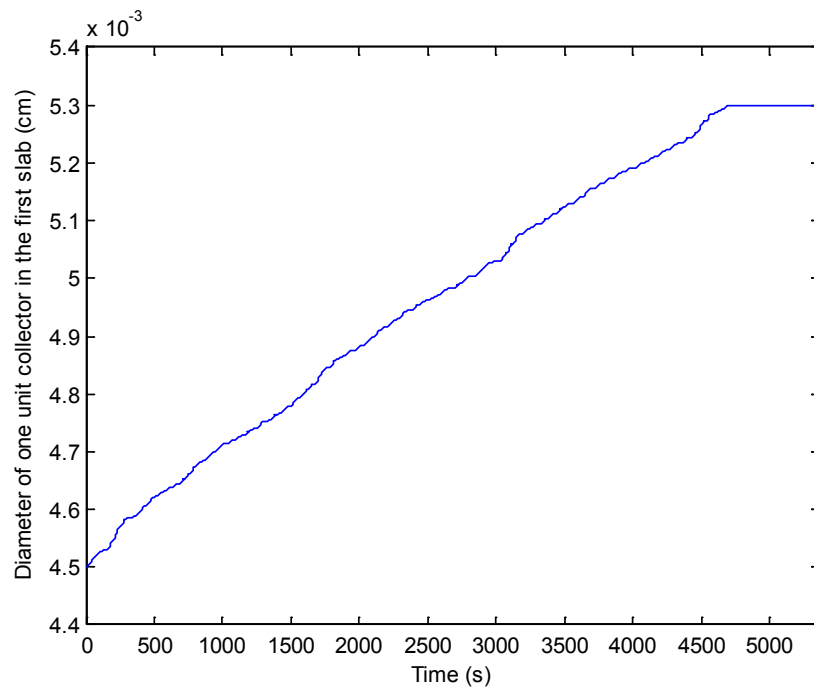
Figure 5.10. Single unit collector diameter in the first slab under the UDDS driving cycles.

Some other comparisons are also presented in this chapter. We perform the accumulated mass, single unit collector diameter, and porosity of the wall for each slab as a function of time, which are shown in Figures 5.11-5.13, respectively. From Figure 5.11, it can be found that during the first three cycles, the mass accumulated in each slab under the UDDS cycle conditions is less than that of constant input conditions (Fig. 3.8). However, during the fourth cycle, the mass in each slab is the same for both of the conditions since the particulates will only deposit on the surface of the substrate wall of the DPF. Therefore, the mass in the wall will remain identical for both of the conditions.
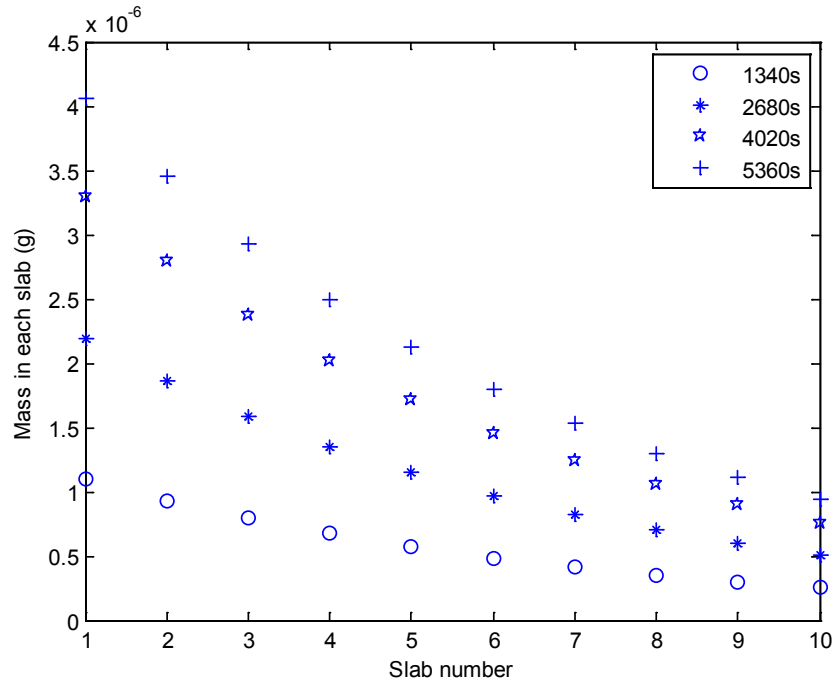
Figure 5.11. Accumulated mass in each slab as a function of time.

Due to the same filtration process shown above, under UDDS driving conditions, the diameter of single unit collector becomes smaller. On the other hand, the porosity for each slab inside the substrate wall becomes larger because of the less mass accumulated inside the deeper slab. Results are shown in Figures 5.12 and 5.13 below.
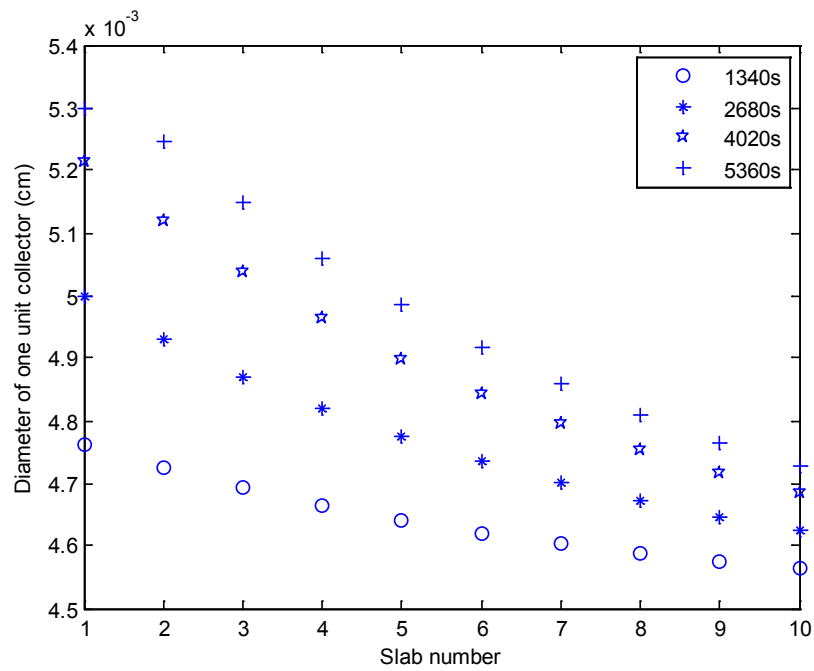
Figure 5.12. Single unit collector diameter for each slab as a function of time.
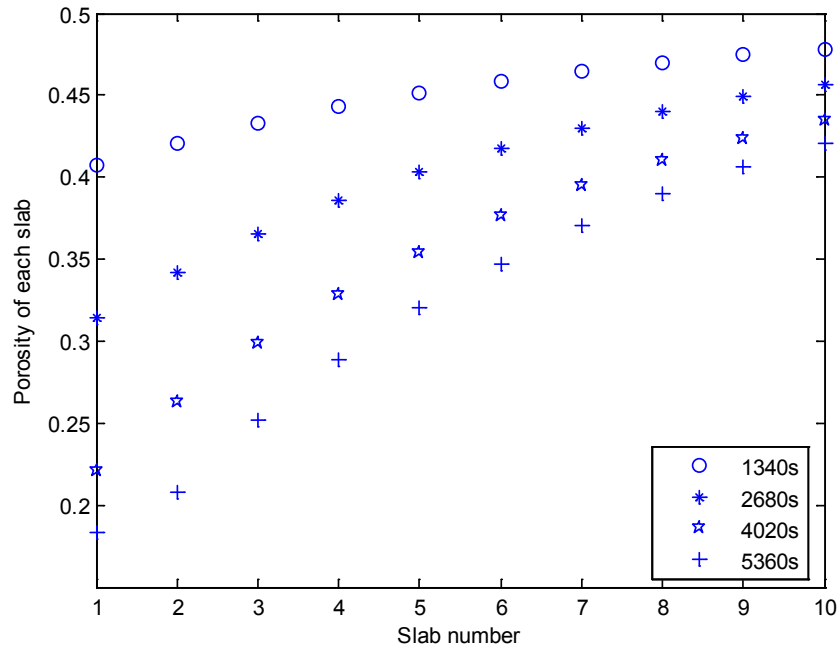
Figure 5.13. Porosity for each slab as a function of time.

5.3.2 Regeneration during UDDS driving cycle

Fuel economy during DPF regeneration is one of the most important issues in diesel engine emission control. Therefore, in this study we try to find out the best way and time to regenerate the filter. For active regeneration, the heat used to regenerate the filter is from an additional heater. Usually, the heater power will be turned off after the regeneration is complete; however, the method that will be presented here is to shut down this additional heater before the regeneration of the DPF is completed and to use the heat from diesel engine exhaust gas directly.

First, the UDDS driving cycle is referred in this study. The duration of one single UDDS driving cycle is 1340 seconds and we initiate the regenerations at different time points during the cycle and supply external heat for the regeneration for the same amount of time (120s). The inlet temperature is controlled to achieve a set point of 710K, which is 275K higher than the average exhaust temperature of the UDDS cycle (435K). Moreover, the exhaust gas flow rate is another one of the most important inlet variables for the regeneration model and it can affect the regeneration efficiency. Since the average exhaust gas flow rate during different regenerations is different, the regeneration efficiency varies between cases, as shown in Figure 5.14. However, as mentioned above, the heater was shut down after 120 seconds during the regeneration, and the regeneration will last for another 120 seconds while the inlet temperature is equal to the exhaust gas temperature.

The duration of the UDDS driving cycle is 1340s. We start the regeneration at seven different time points during the UDDS cycle: 0s, 60s, 120s, 180s, 300s, 800s, and 1200s, respectively. The regeneration efficiency as a function of time of each case is shown in Figure 5.14. From figure 5.14, we can find out that the regeneration efficiency is lower when the regeneration takes place before 120 seconds (at the beginning of the UDDS). Also it can be noticed that the regeneration efficiency is the highest (99.6%) when the regeneration took place at 180 seconds. In the next

subsection, for each case we will plot:

a) The maximum temperature in the inlet channel during the regeneration;

b) Temperature along the inlet channel at different time;

c) Deposit thickness along the inlet channel at different time;

d) Pressure drop along the inlet channel for variable time.
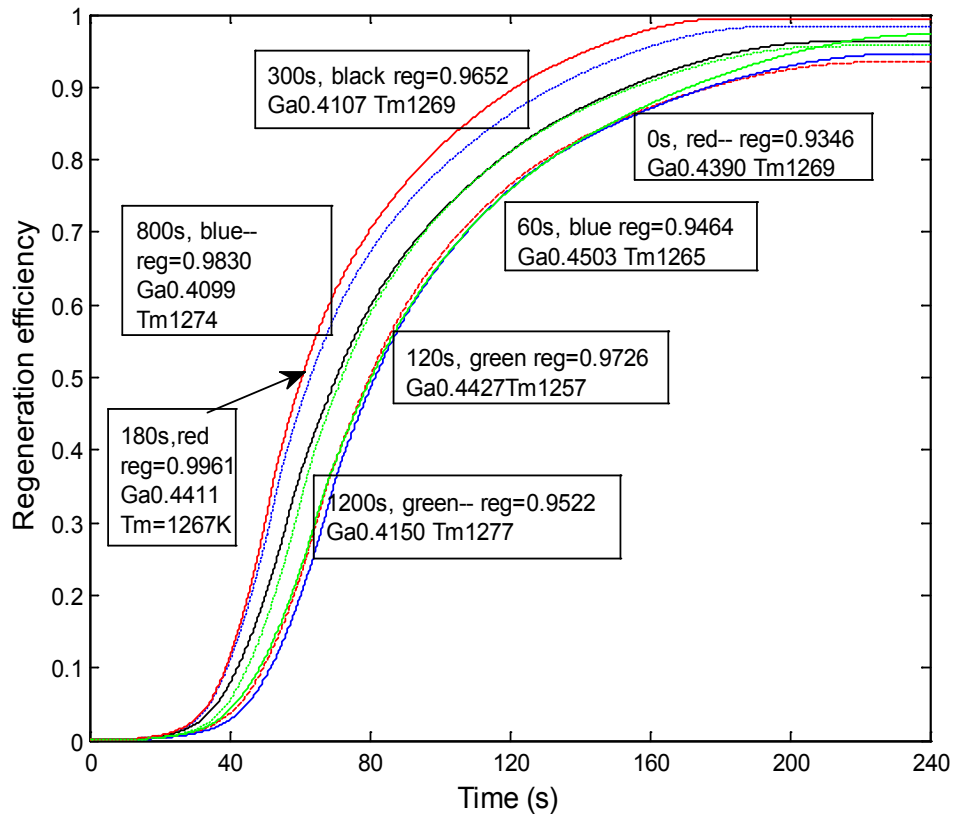
Figure 5.14. Regeneration efficiency as a function of time for different starting time. Reg: regeneration efficiency. Ga: average gas flowrate. Tm: maximum temperature (K) during the regeneration.

Case 1- Regeneration begins at t=0 in the UDDS cycle

Figures 5.15-5.18 show those four kinds of plots mentioned above in the condition of starting the regeneration at the very beginning of the UDDS driving cycle (0s). From the figures shown below, it can be noticed that, under this condition, the regeneration efficiency is 93.5% and the maximum temperature during the regeneration is 1271K which occurs at about 140s.

Figure 5.15. The maximum temperature in the inlet channel as a function of time.

(Regeneration starts at 0s in the UDDS)

Figure 5.16. Temperature along the inlet channel during the regeneration. (Regeneration

starts at 0s in the UDDS)

Also, from the thickness profile and pressure drop profile (Fig.5.17 and Fig.5.18) we

can notice the regeneration starts from the very leading-edge of the filter. However,

from the deposit thickness profile during the regeneration, it can be noticed that there

are more particulates remaining near the end of the filter channel at t= 240s which can

cause higher local pressure drop shown in Figure 5.18. Such a higher local pressure

drop is not desirable for the DPF. Therefore, the regeneration should not be initiated at

this time point (t=0s).
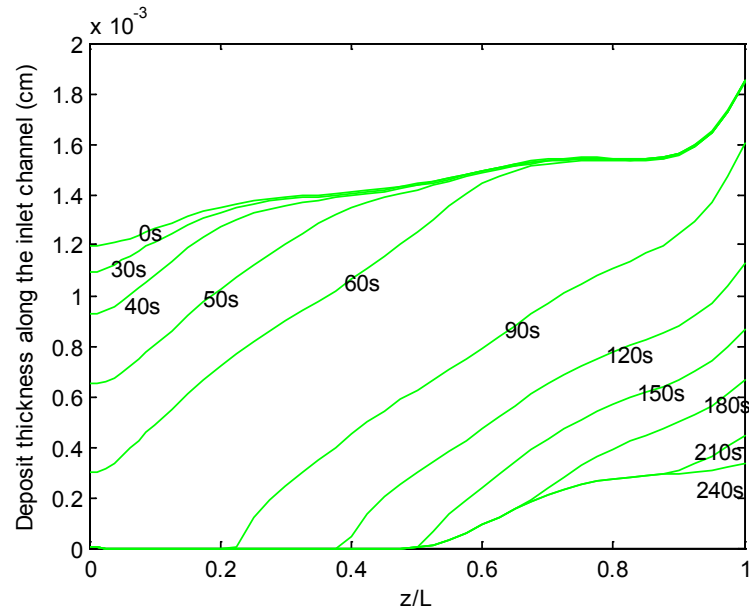
Figure 5.17. Deposit thickness along the inlet channel during the regeneration. (Regeneration starts at 0s in the UDDS)

Figure 5.18. Pressure drop along the inlet channel during the regeneration. (Regeneration starts at 0s in the UDDS)

Case 2- Regeneration begins at t=60s in the UDDS cycle

In case 2, the starting time of the regeneration is 60s during the UDDS driving cycle. Since there are no large difference for the exhaust conditions, the results shown in this case is similar with case 1 (t = 0s). The maximum temperature during the regeneration is 1265K and the regeneration efficiency is 94.6% compared to 93.5% of case 1. Similar to this case, the regeneration for case 2 is also a leading-edge ignition. From Figure 5.14, it can be noticed that when we initiate the regeneration either at 0s or 60s, the plots of the regeneration are almost identical.

Figure 5.19. The maximum temperature in the inlet channel as a function of time.

(Regeneration starts at 60s in the UDDS)
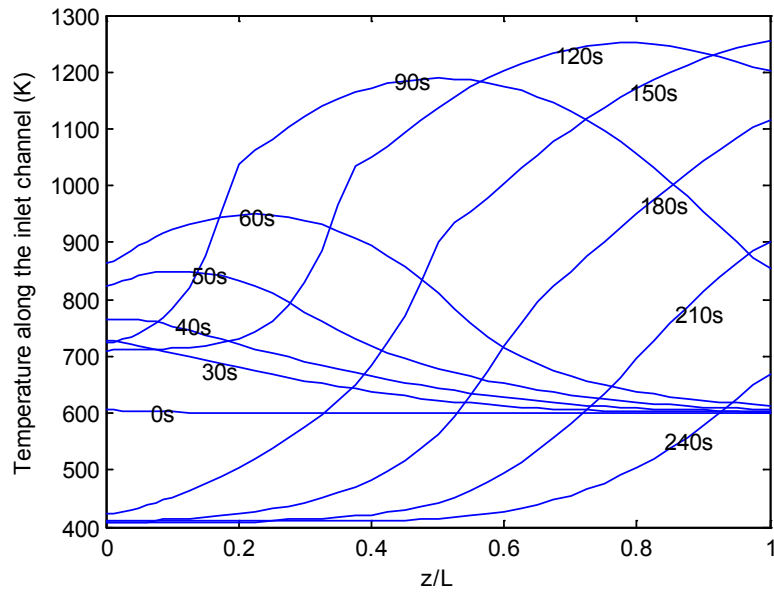
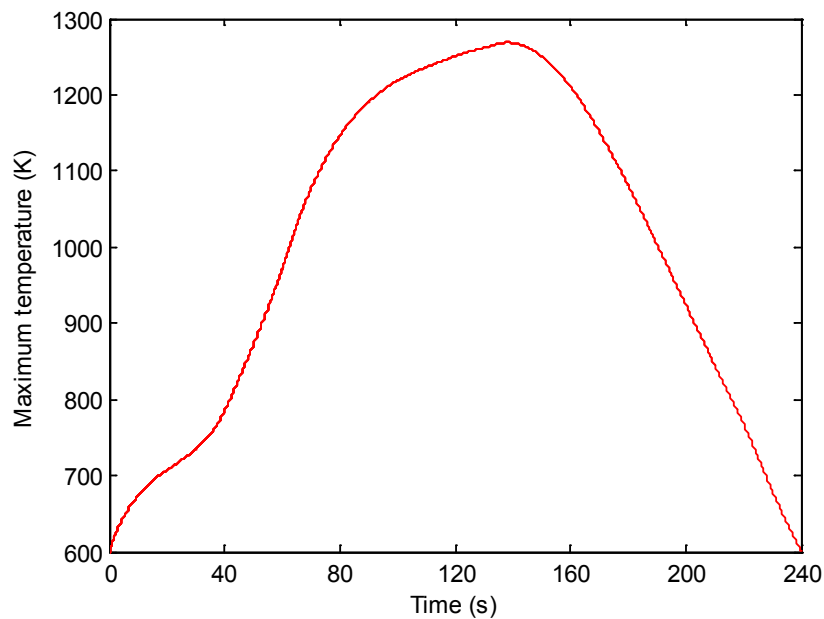**Figure 5.20. Temperature along the inlet channel during the regeneration. (Regeneration starts at 60s in the UDDS)**
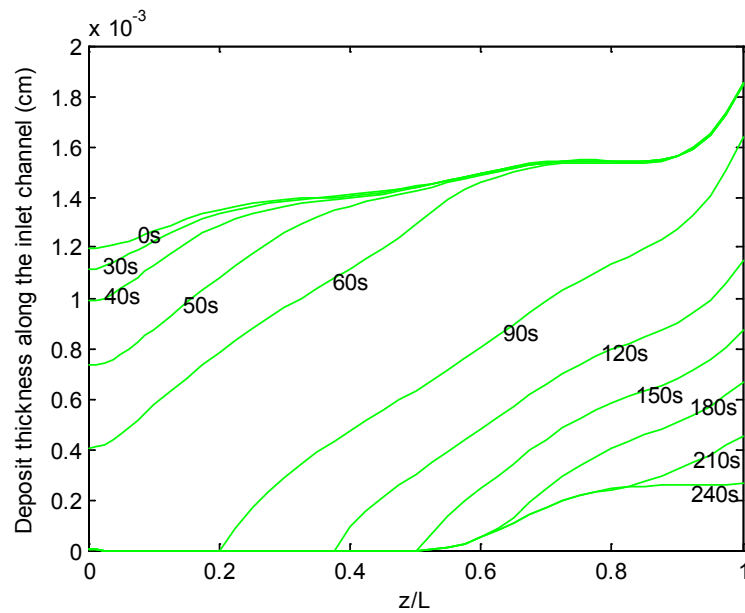
Figure 5.21. Deposit thickness along the inlet channel during the regeneration. (Regeneration starts at 60s in the UDDS)

Again, the regeneration under this condition is not completed. Some particulates remain on the substrate wall near the end of the filter channel. Similarly, the remaining deposit layer can result in higher pressure drop and may cause the crack of the DPF during subsequent filtration and regeneration cycles. By analyzing the results of these two conditions (t=0s, t=60s), the regeneration of DPF should not be initiated during the first minute into the UDDS driving cycle due to the low regeneration efficiency.

Figure 5.22. Pressure drop along the inlet channel during the regeneration. (Regeneration starts at 60s in the UDDS)

Case 3- Regeneration begins at t=120s in the UDDS cycle

Similar results are shown for case 3 (Fig.5.23-Fig.5.26). The regeneration was initiated

at 120 seconds of the UDDS driving cycle and the regeneration efficiency is 97.3%.

But the maximum temperature is a little lower (1257K). From Figure 5.14, we can find

the regeneration efficiency is almost the same as that in the first two cases during the

first 120s. However, the regeneration efficiency increases faster than in the cases when

the regeneration starts at 0s and 60s. From Figure 5.1 and Figure 5.7, we are able to

find out that during the regeneration for these three cases, there is period during which

the vehicle stops (speed is equal to zero) and thus the gas flow rate is very low.

Figure 5.23. The maximum temperature in the inlet channel as a function of time.
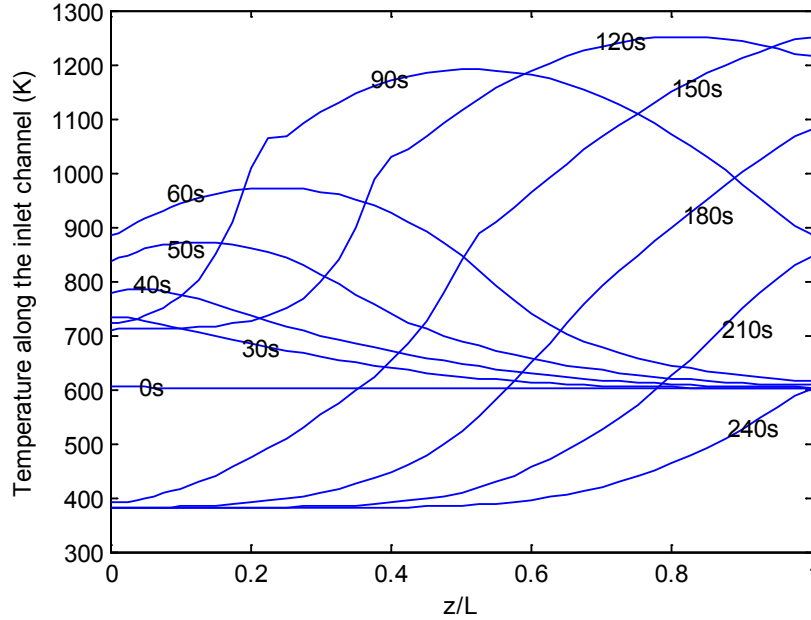
(Regeneration starts at 120s in the UDDS)

For case 3, the regeneration efficiency is higher than that of the first two cases. However, form Figure 5.25 and Figure 5.26, it can be noticed that there are still some particulates remaining on the wall near the end of the filter. Although the amount of the remaining deposit is small, the regeneration should not be initiated at this time, either.

Figure 5.24. Temperature along the inlet channel during the regeneration. (Regeneration starts at 120s in the UDDS

Figure 5.25. Deposit thickness along the inlet channel during the regeneration. (Regeneration starts at 120s in the UDDS)
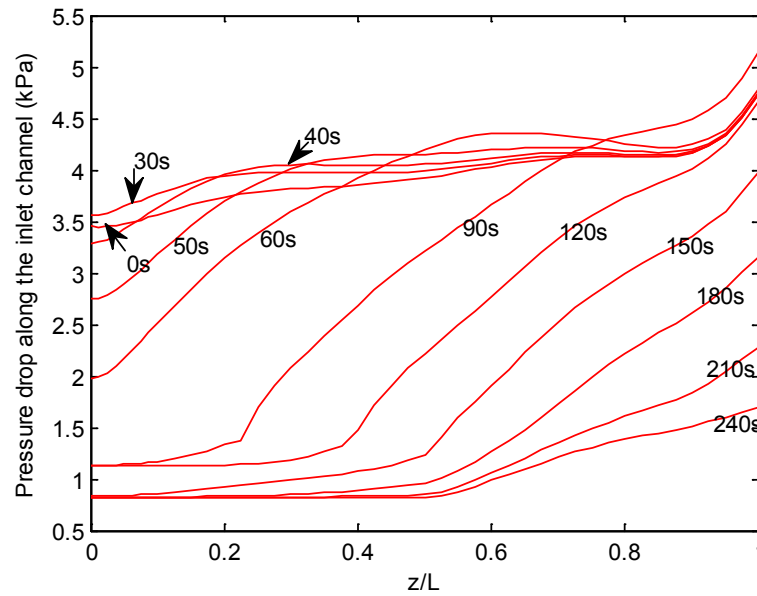

Figure 5.26. Pressure drop along the inlet channel during the regeneration. (Regeneration starts at 120s in the UDDS)

Case 4- Regeneration begins at t=180s in the UDDS cycle

In case 4 (Figure 5.27-Figure 5.30) the starting time of the regeneration is at 180s. From the figures shown below we can find out that the maximum temperature is 1275K which occurs at t = 105s during the regeneration. And from figure 5.14, we can notice the regeneration efficiency is 99.6% which is the highest of these seven cases studied here. In addition, from Figure 5.1 and Figure 5.7, it can be noticed that during the regeneration under this condition, there are no stops and the average vehicle speed is the highest.
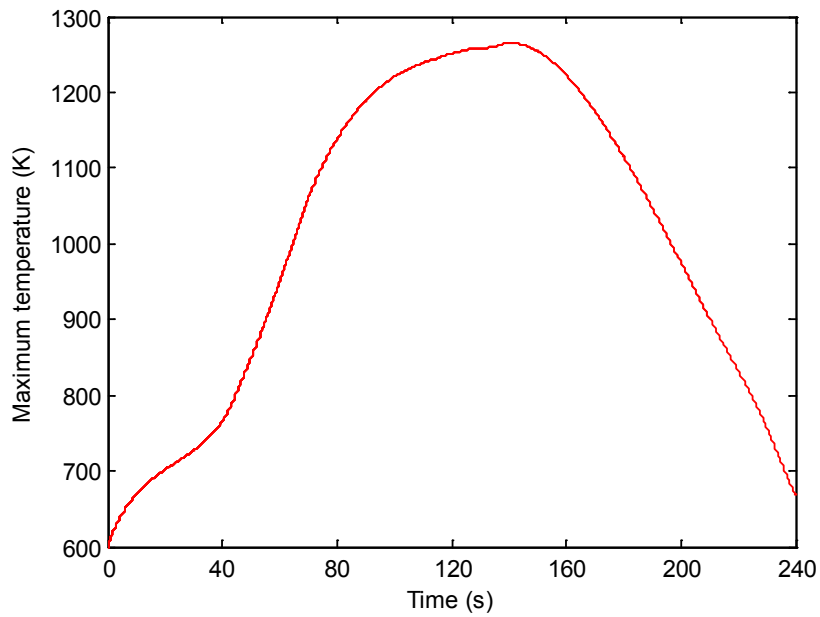

Figure 5.27. The maximum temperature in the inlet channel as a function of time.

(Regeneration starts at 180s in the UDDS)

125

From the temperature profile shown in Figure 5.28, it can be found that the temperature along the channel is quenched down to about 470K which is equal to the average temperature of the exhaust gas from the engine. Also, from Figure 5.29 and Figure 5.30, one can find that there is no particulate remaining in the filter channel. Moreover, the local pressure drop along the channel is desirable after the completed regeneration. In this study, we can conclude that the best time to initiate the regeneration is at 180s into the UDDS driving cycle.
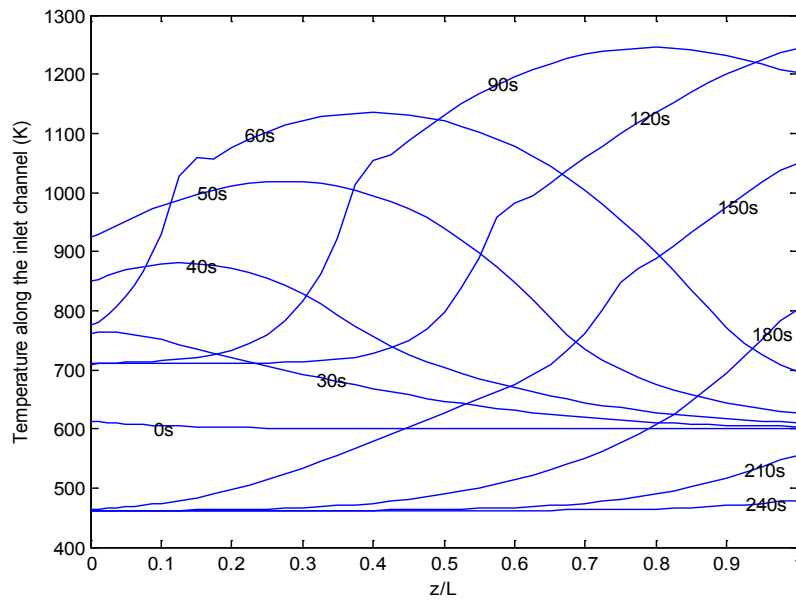
Figure 5.28. Temperature along the inlet channel during the regeneration. (Regeneration starts at 180s in the UDDS)

Figure 5.29. Deposit thickness along the inlet channel during the regeneration. (Regeneration starts at 180s in the UDDS)
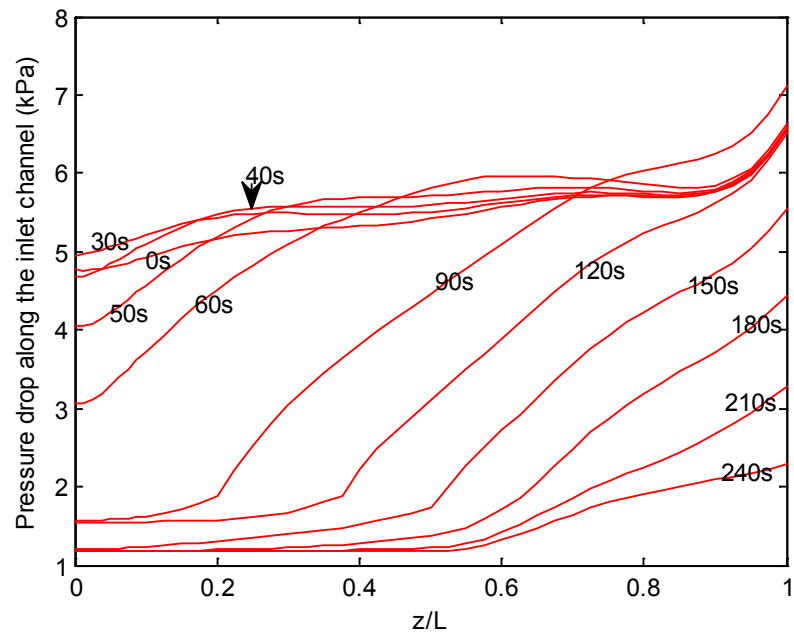

Figure 5.30. Pressure drop along the inlet channel during the regeneration. (Regeneration starts at 180s in the UDDS)

127

Case 5- Regeneration begins at t=300s in the UDDS cycle

In case 5 (Figure5.31-Figure 5.34), the starting time of the regeneration is at 300s of the UDDS driving cycle, the maximum temperature and the regeneration efficiency are 1272K and 97.2%, respectively. In this case, there are two stops during the regeneration (from Figure 5.1) which may impact the regeneration process as it did during case 3. Figures 5.33 and 5.34 display the deposit thickness and pressure drop along the inlet channel during the regeneration, respectively. From the results shown in these two figures, we are able to find that the regeneration under this condition is not completed. As discussed above, the regeneration should not be initiated at this time into the UDDS driving cycle (t=300s).
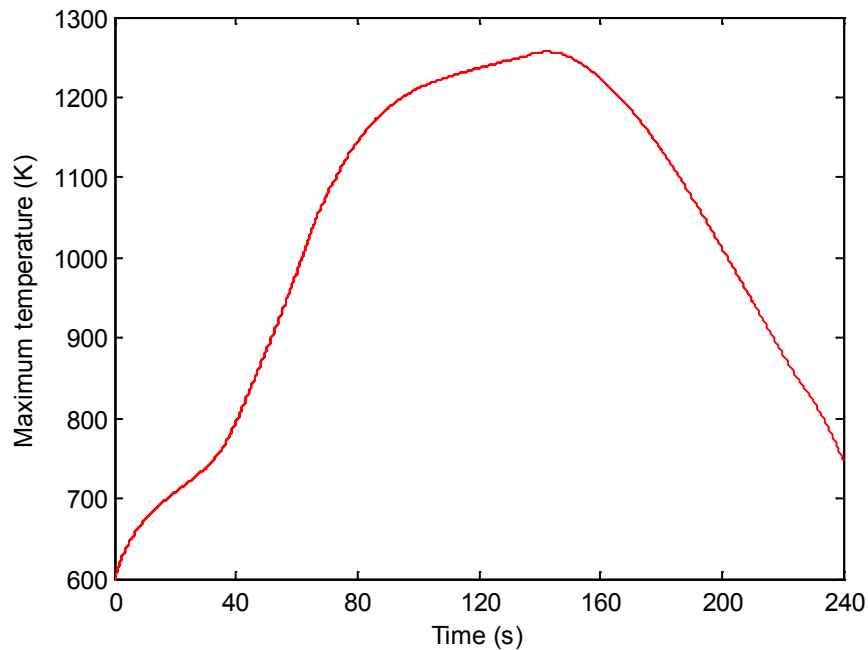

Figure 5.31. The maximum temperature in the inlet channel as a function of time.
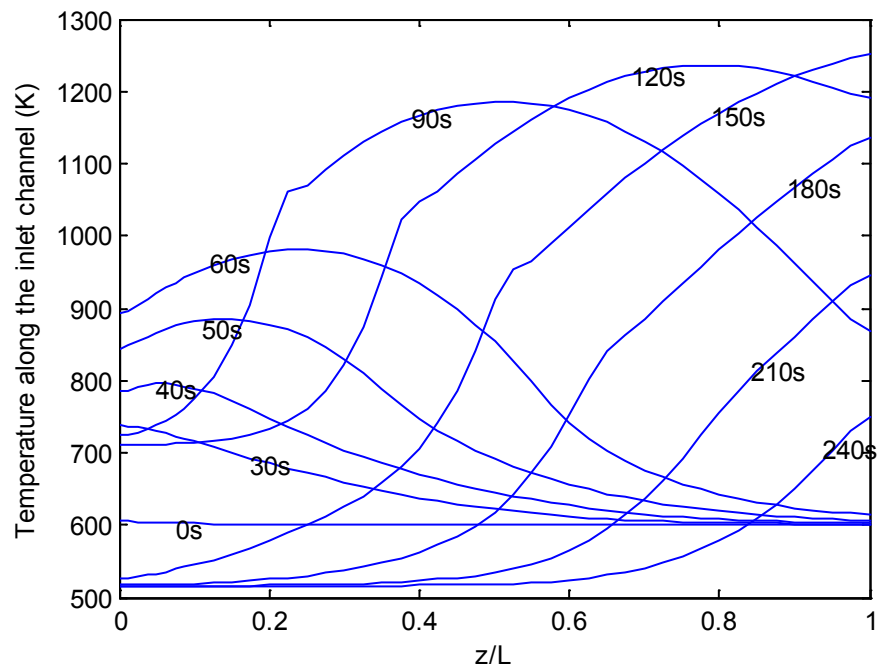
(Regeneration starts at 300s in the UDDS)

Figure 5.32. Temperature along the inlet channel during the regeneration. (Regeneration starts at 300s in the UDDS)
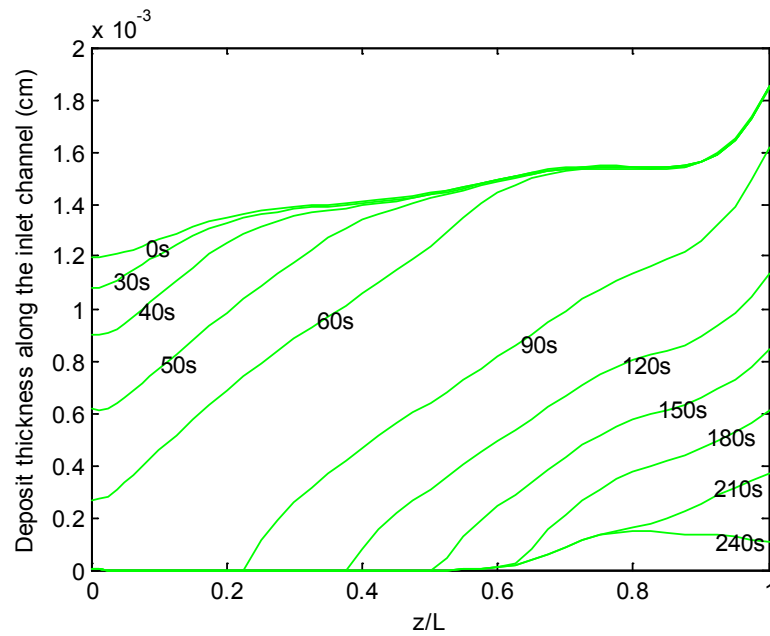

Figure 5.33. Deposit thickness along the inlet channel during the regeneration. (Regeneration starts at 300s in the UDDS)
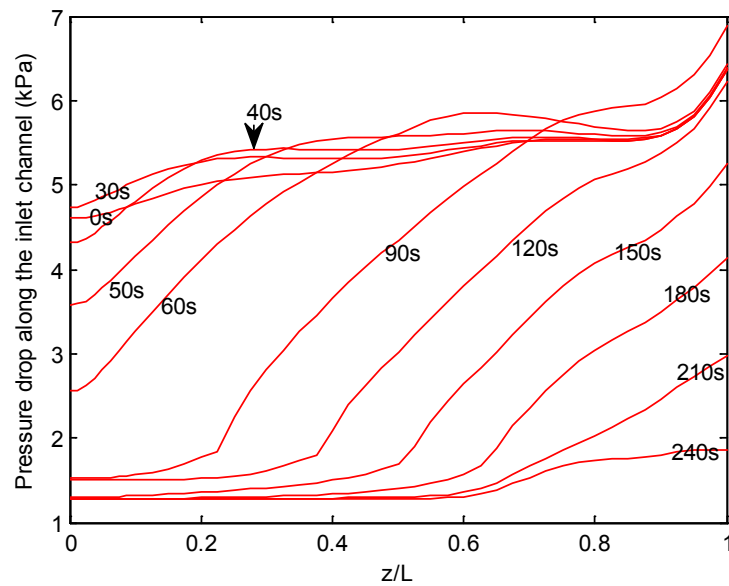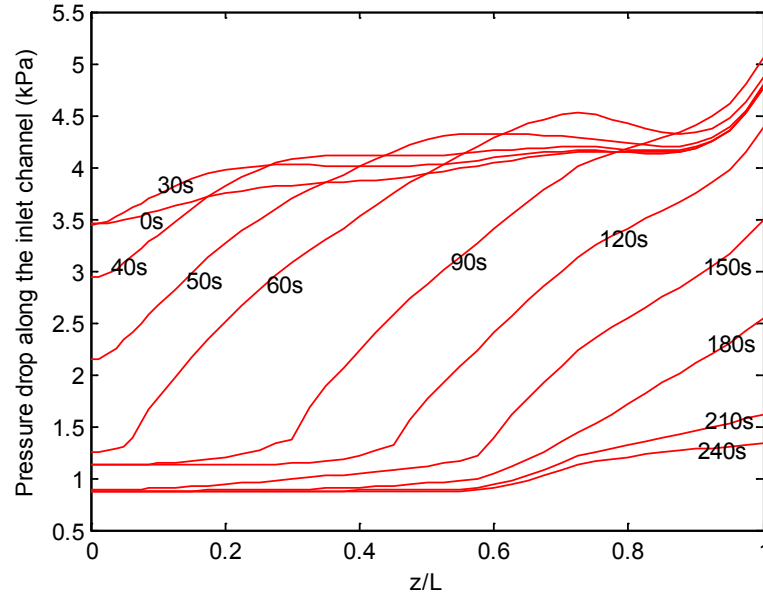
Figure 5.34. Pressure drop along the inlet channel during the regeneration. (Regeneration starts at 300s in the UDDS)

Case 6- Regeneration begins at t=800s in the UDDS cycle

In case 6 (Figure 5.35-Figure 5.38) the starting time of the regeneration is at 800s. The maximum temperature is 1274K which takes place at about 110s during the regeneration and the regeneration efficiency is 98.3%. From Figure 5.14, we can notice that the regeneration efficiency is the second highest of these seven cases. Although the average speed of this case is almost the same as those for cases 1, 2, 3, and 5, there are no stops during the regeneration. The gas flow rate is continuous during the regeneration and it results in a higher regeneration efficiency. The

regeneration under this condition is almost completed and the temperature in the channel was quenched down after the whole regeneration process.
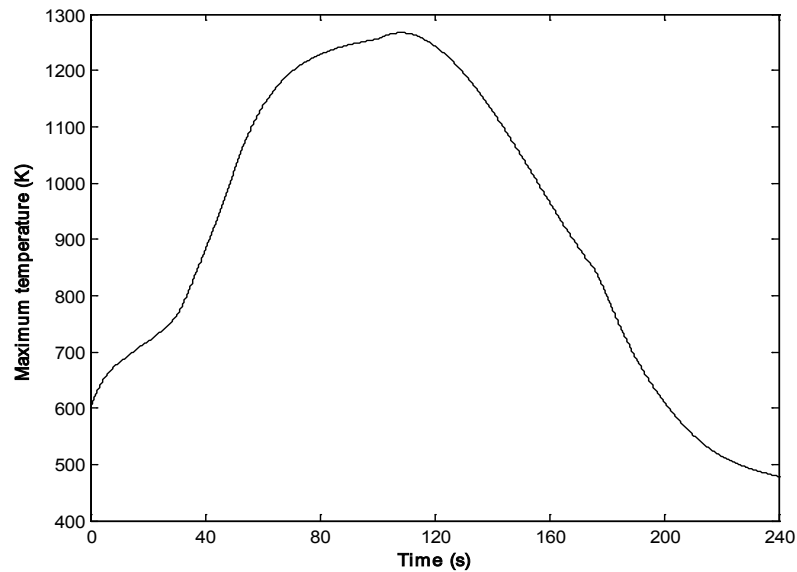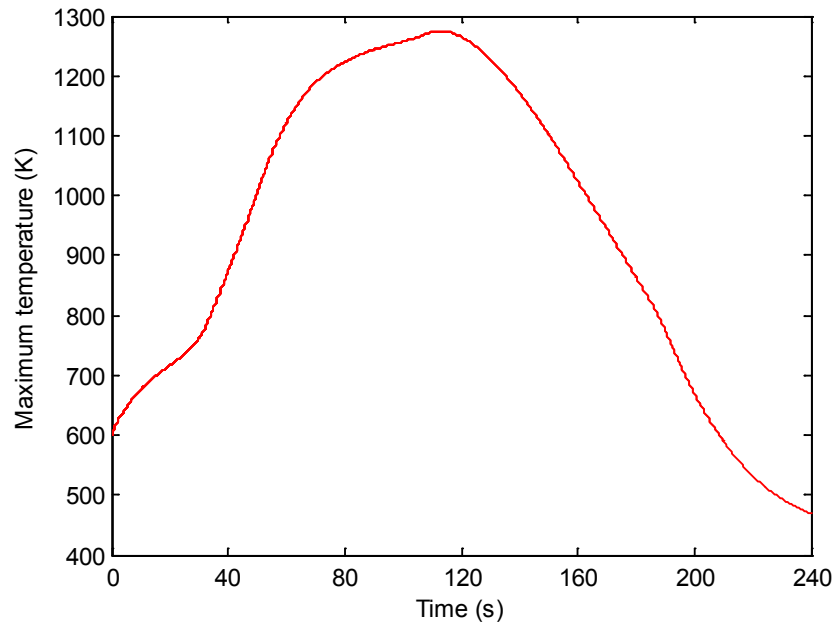

Figure 5.35. The maximum temperature in the inlet channel as a function of time.

(Regeneration starts at 800s in the UDDS)
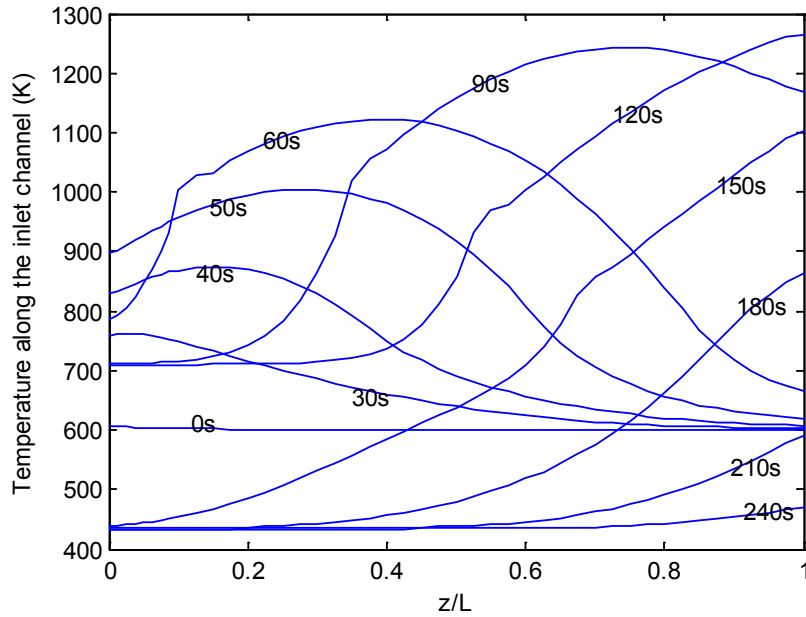
Figure 5.36. Temperature along the inlet channel during the regeneration. (Regeneration starts at 800s in the UDDS)

As mentioned above, the regeneration efficiency for this case is the second highest in these seven cases. From the figures shown below (Fig.5.37 and Fig. 5.38), we can find there are still some unburned particulates depositing near the end of the filter. As the local pressure drop there is acceptable, we may draw the conclusion that around 800s of the UDDS driving cycle is another desirable time to start the regeneration of DPF, although the regeneration efficiency is a little lower than that of the highway driving without stops period (case 3).
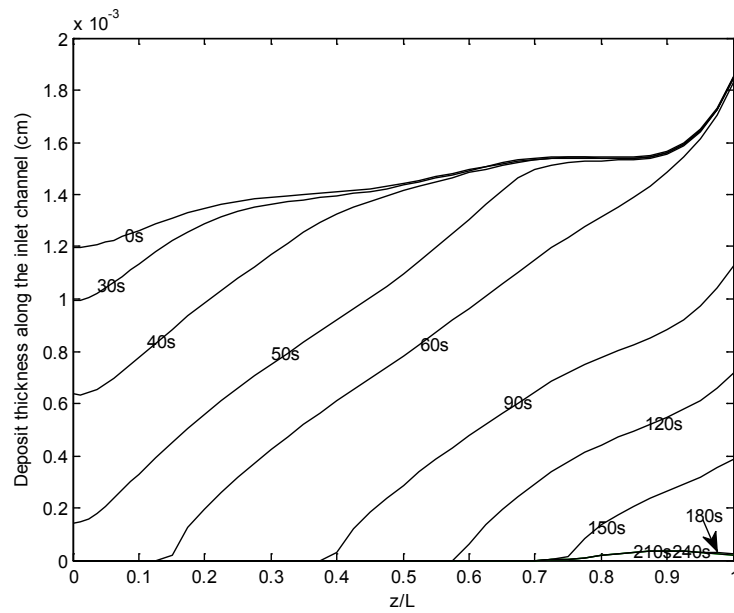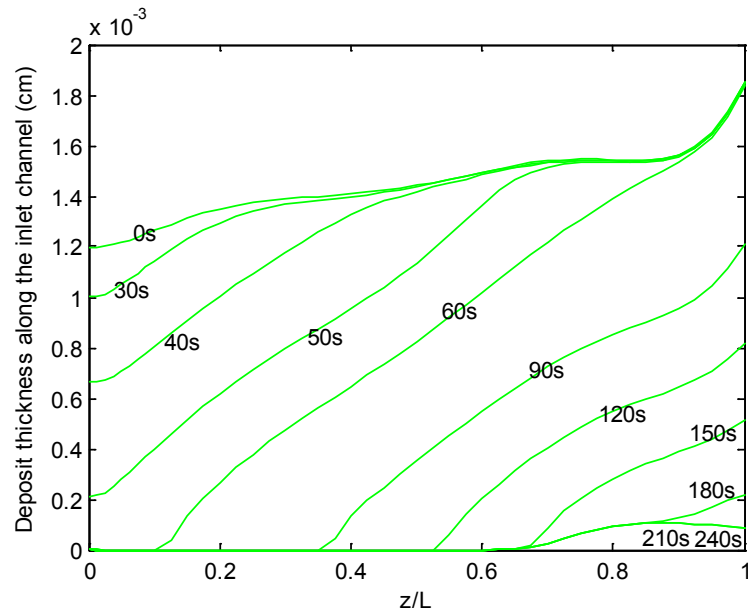
Figure 5.37. Deposit thickness along the inlet channel during the regeneration. (Regeneration starts at 800s in the UDDS)
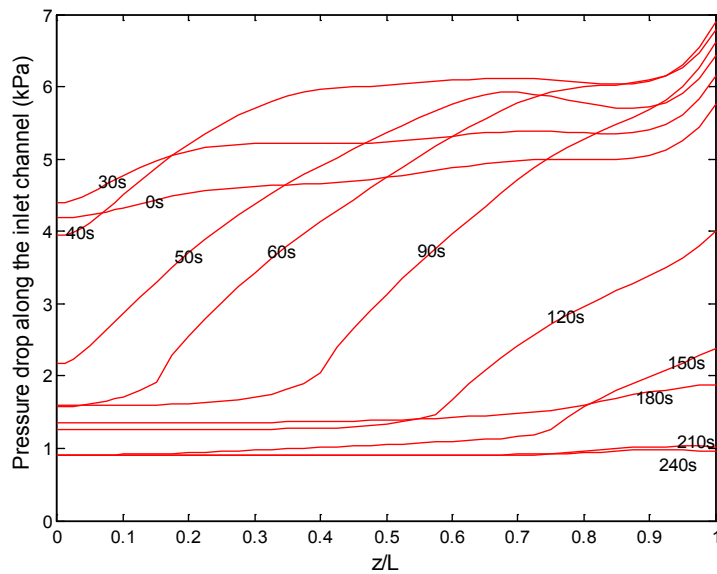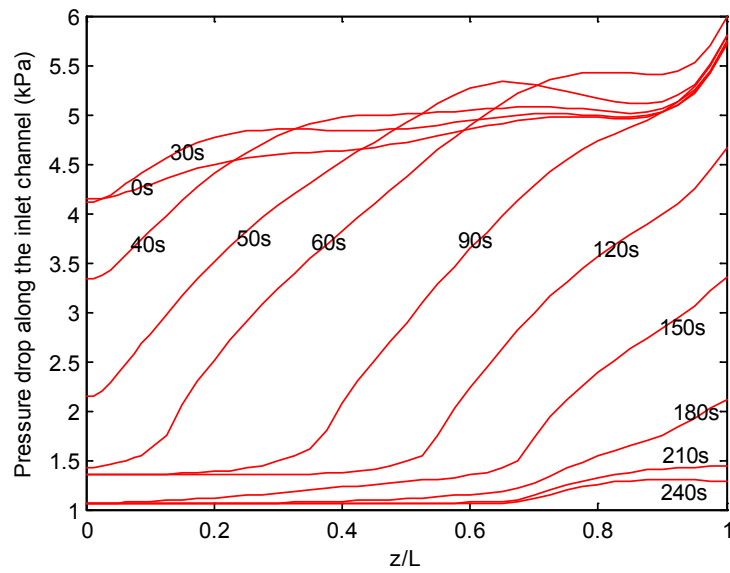

Figure 5.38. Pressure drop along the inlet channel during the regeneration. (Regeneration starts at 800s in the UDDS)

Case 7- Regeneration begins at t=1200s in the UDDS cycle

In the final case, the starting time of the regeneration is at 1200s, and the maximum

temperature is 1277K and the regeneration efficiency is 95.7%. In this case, there are

also two stops during the regeneration process. Moreover, from Figure 5.14 it can be

easily found that the regeneration efficiency for cases when we initiate the

regeneration after 60s is much higher than that when the ignition took place before 60s.

Therefore, if possible, the regeneration should be initiated after about 60s of the

UDDS driving cycle and the regeneration efficiency is the highest when we start the
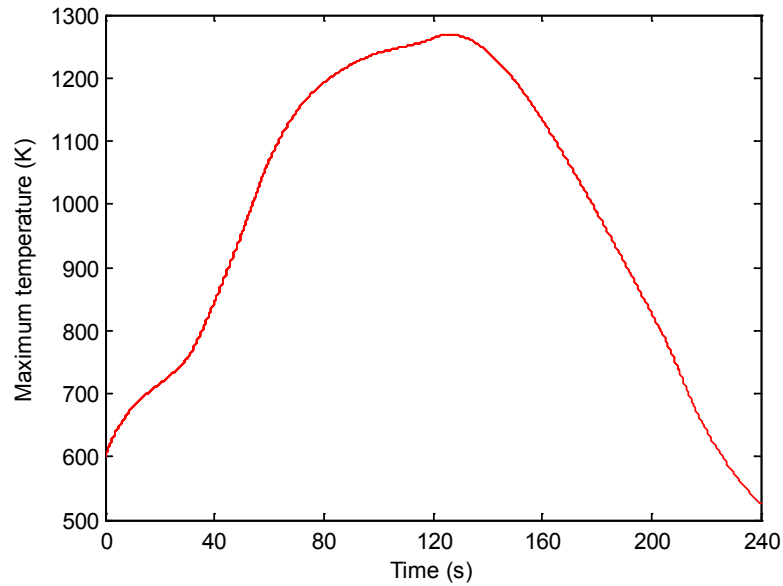
regeneration at 180s.
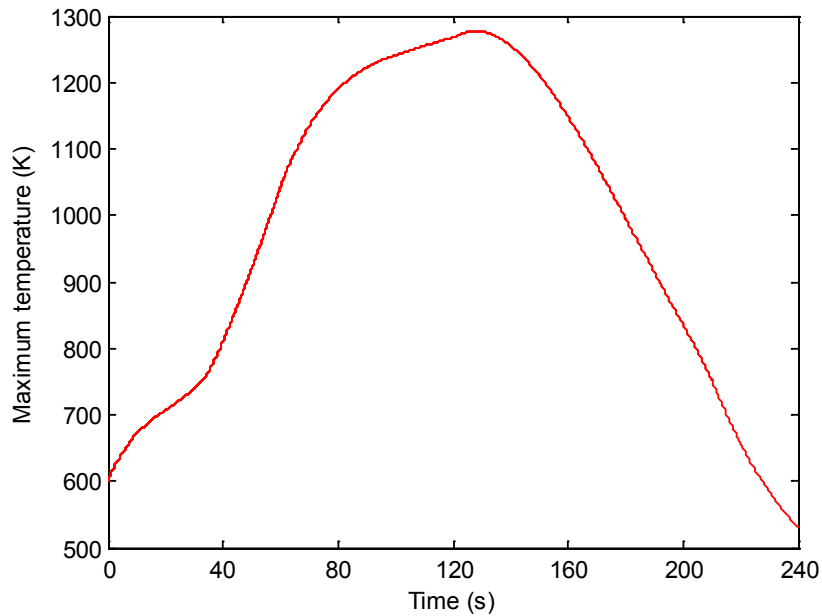
Figure 5.39. The maximum temperature in the inlet channel as a function of time.

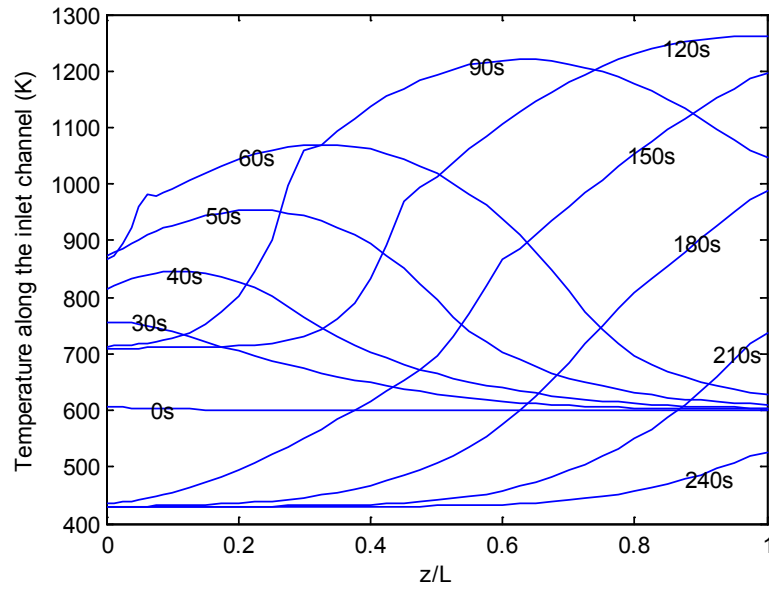**(Regeneration starts at 1200s in the UDDS)**
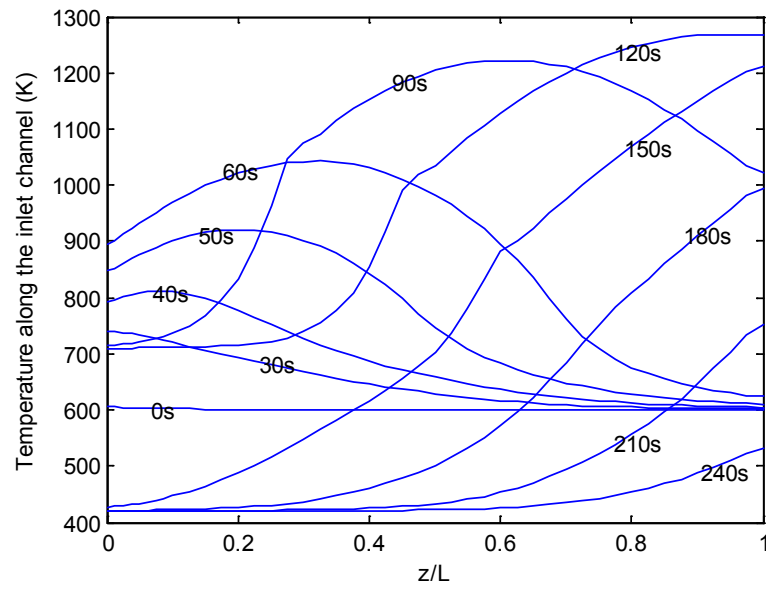
Figure 5.40. Temperature along the inlet channel during the regeneration.(Regeneration starts
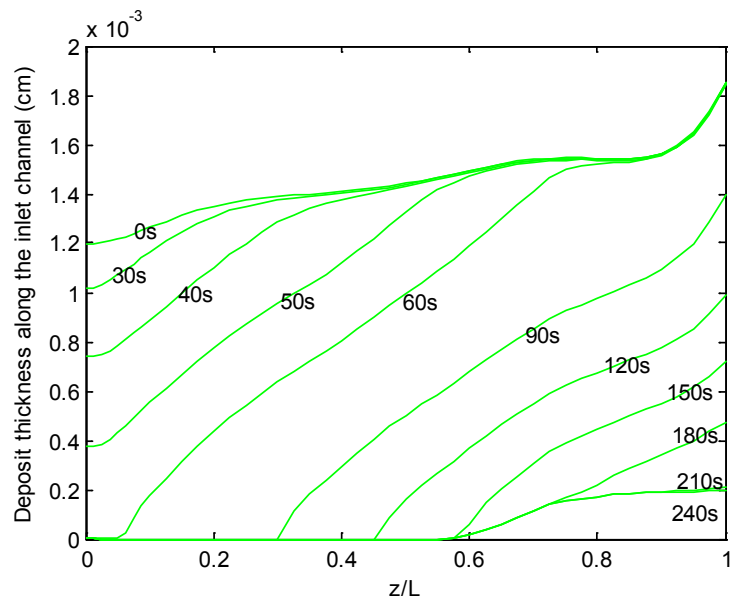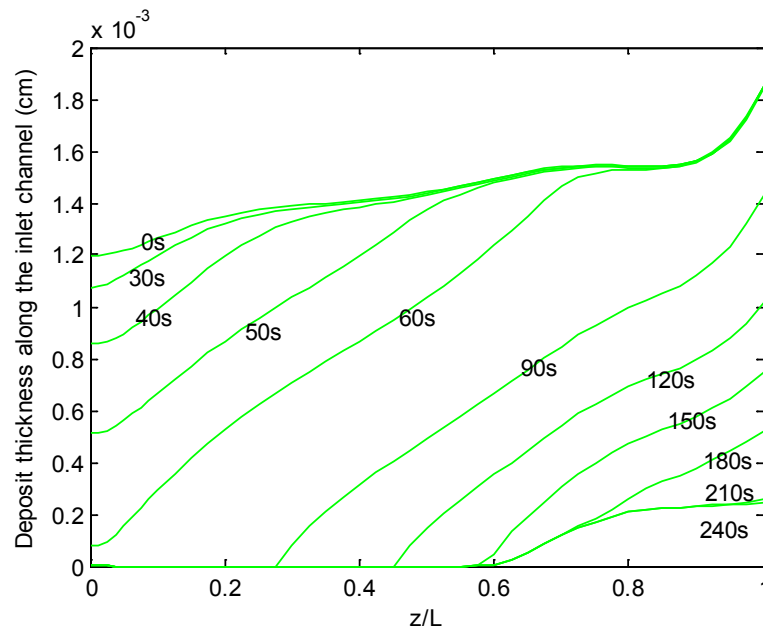
at 1200s in the UDDS)

Figure 5.41. Deposit thickness along the inlet channel during the regeneration. (Regeneration

starts at 1200s in the UDDS)

135
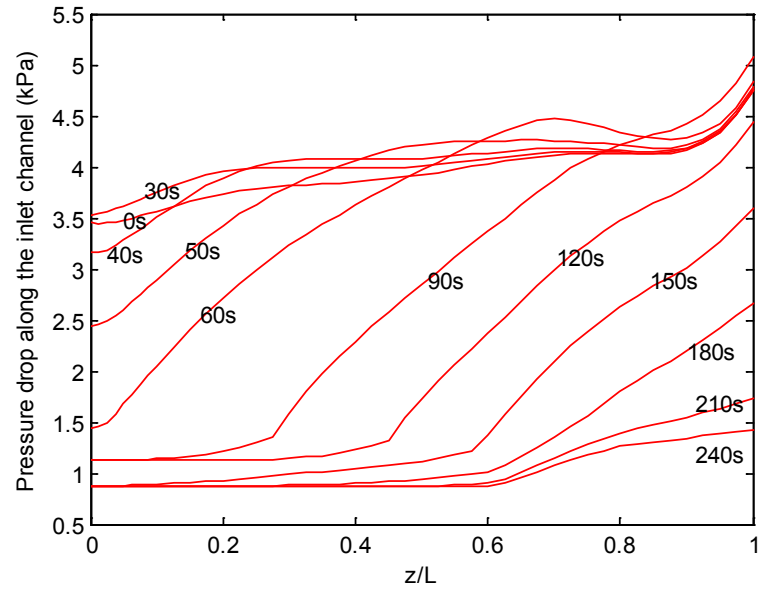
Figure 5.42. Pressure drop along the inlet channel during the regeneration. (Regeneration starts at 1200s in the UDDS)

5.3.3 Analysis

Based upon the results shown above, we may conclude that it is better to initiate the regeneration after 60 seconds during the UDDS driving cycle because the regeneration efficiency is higher during the same ignition duration. Also, we can find that for the same ignition duration, the regeneration efficiency is the highest when the regeneration took place at 180 seconds in the UDDS driving cycle.

136

Investigation of Figure 5.14 shows there are three portions in the UDDS driving cycle which are highway driving without stops (180s-320s), city driving without stops (20s-120s and 770s-950s), and start-and-stop city driving (330s-770s and 950s-1400s). Thus, the case starting at 180s corresponds to an extended period of highway driving without any stops and the regeneration efficiency is the highest during this driving period (~99%). During the city driving without stops, the regeneration efficiency is lower which is about 98%. During the start-and-stop city driving period, the regeneration efficiency is the lowest (~ 96%) because of the discontinuity of gas flow rate related to the vehicle speed. However, the particular case shown in case 2 is the city driving without stops from 20s-120s. During this period, the duration is only 100s and there are two longer stops (each one is about 40 seconds) on both sides of this period. Therefore, the regeneration efficiency during this period is the lowest.

5.4 References

(22).   Thornton M, Webb CC, Weber PA, Orban J, Slone E. Fuel Sulfur Effects on a Medium-Duty Diesel Pick-Up with a NO_x Adsorber, Diesel Particle Filter Emissions Control System: 2000-Hour Aging Results. SAE Journal. 2006;2006010425.

(23).   Dabhoiwala RH. An Experimental and Modeling Study of Two Diesel oxidation Catalyst- Catalyzed Particulate Filter Systems and the Effects of a Cracked Filter on its Performance.   M.S. Thesis. 2007. Michigan Technological University. Houghton (MI).

Chapter 6 New Driving Cycles

6.1 Formulas of New Driving Cycles

As mentioned in the Chapter 5 and from the investigation of Figure 6.1, we found there are three kinds of driving periods in the UDDS driving cycle which are highway driving without any stops (180s-320s), city driving without any stops (20s-120s and 770s-950s), and start-and-stop city driving periodic (330s-770s and 950s-1400s). In this chapter, we develop three simple functions to approximate the vehicle speed in the UDDS driving cycle. Equations 6.1-6.3 show the vehicle speed for highway driving without any stops, city driving without any stops, and start-and-stop city driving, respectively. In Equation 6.3, we assume the stopping period is 10 seconds.
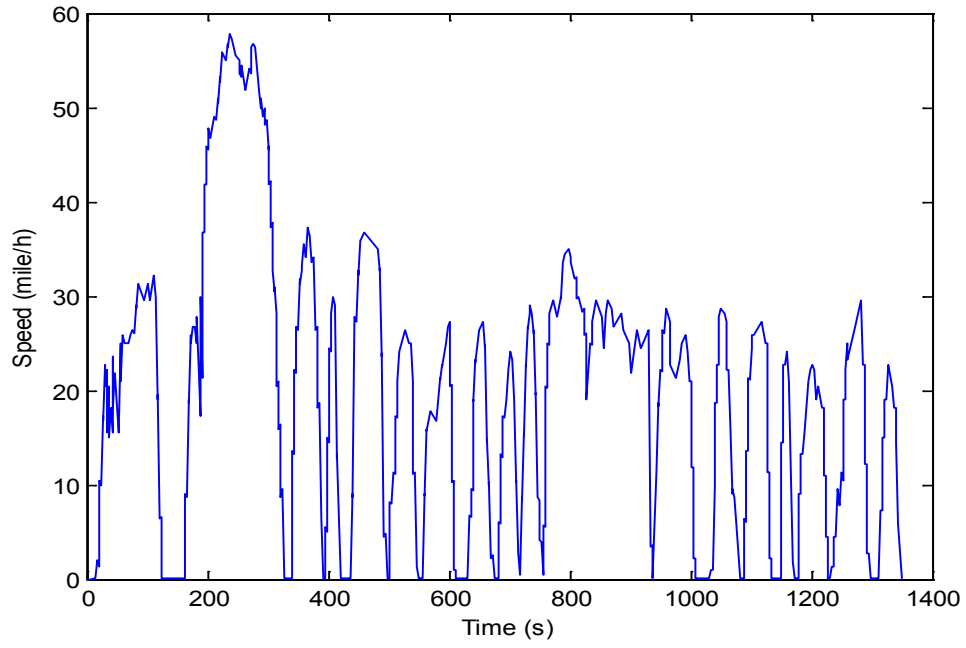
Figure 6.1. Vehicle speed as a function of time for Urban Dynamometer Driving Schedule

(UDDS). (Data reproduced from (1))

$$vs(t) = 54 + 4 \times \sin\left(\frac{2\pi t}{100}\right) \tag{6.1}$$

$$vs(t) = 28 + 2 \times \sin(2\pi t/80) \tag{6.2}$$

$$vs(t) = \begin{cases} 25 \times (\sin(2\pi t/100))^2, & 50n < t < 40 + 50n \\ 0, & \text{Otherwise} \end{cases} \quad n = 0, 1, 2 \ldots 27 \tag{6.3}$$

Figures 6.2-6.4 display the vehicle speed as a function of time for highway driving without any stops, city driving without any stops, and start-and-stop city driving, respectively.
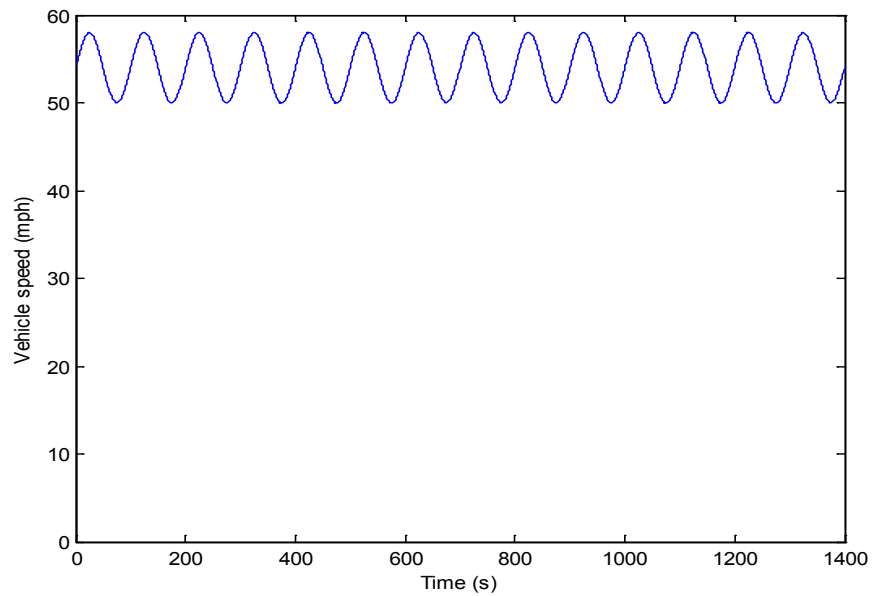
Figure 6.2. Vehicle speed (highway driving without any stops) vs time for new driving cycle.
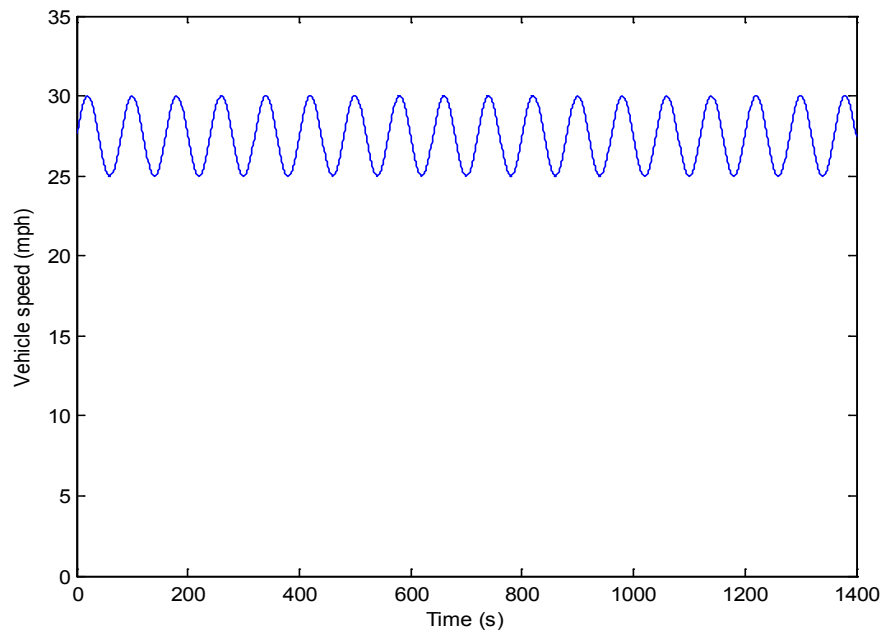
Figure 6.3. Vehicle speed (city driving without any stops) vs time for new driving cycle.
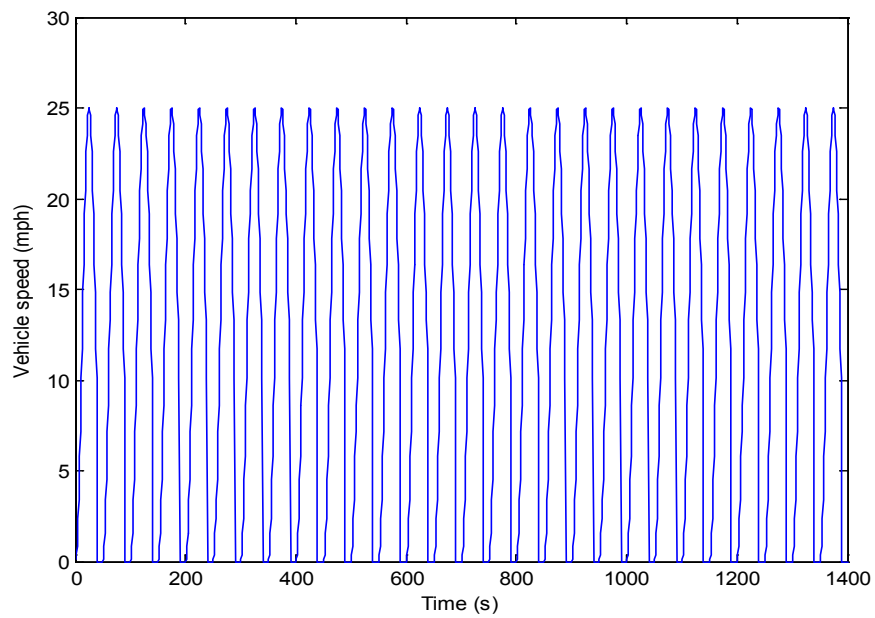
Figure 6.4. Vehicle speed (start-and-stop city driving) vs time for new driving cycle.

6.2 Comparison with UDDS Driving Schedule

Figure 6.5 shows the regeneration efficiency as a function of time using these simple driving cycles. It can be noticed that the regeneration efficiency of all of these cycles exhibit similar trends to the results of Figure 5.14: highway driving without stops gives the best performance followed by city driving without stops, and finally city driving with stops.
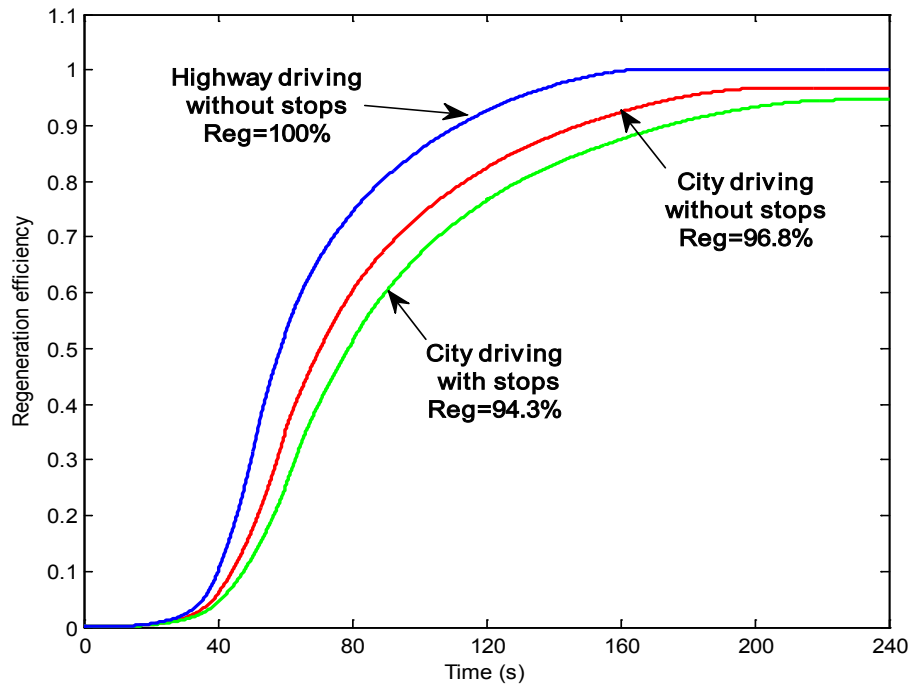
Figure 6.5. Regeneration efficiency as a function of time. (Reg: regeneration efficiency.)

We can also use these new simple driving cycles to predict temperature, deposit thickness, and pressure drop profiles during the regeneration process for each driving period.

Highway Driving Without any stops

Figure 6.6 shows the maximum temperature during the regeneration. Because of the higher gas flow rate, the maximum temperature (1272K) happens earlier than the result for UDDS driving conditions (Figure 5.27) which is around 100 seconds.

Figure 6.6. The maximum temperature in the inlet channel as a function of time. (Highway

driving without any stops)

144

Figure 6.7 shows the temperature along the inlet channel during the regeneration during highway driving without stops. From Fig. 6.7, it can be seen that the maximum temperature during the regeneration happens at about 90s, and the filter channels will be quenched after 180s. In Figure 6.8, it can be noticed that all of the particulate deposit is burned off at 180 seconds. The regeneration efficiency reaches 100% after 160s (see Figure 6.5). The reason is that under this driving condition the gas flow rate is higher due to the higher vehicle speed, which results in an earlier completion of regeneration. Moreover, the clean filter pressure drop (1.4kPa at t = 180s) is higher due to the higher gas flow rate, as seen in Figure 6.9.
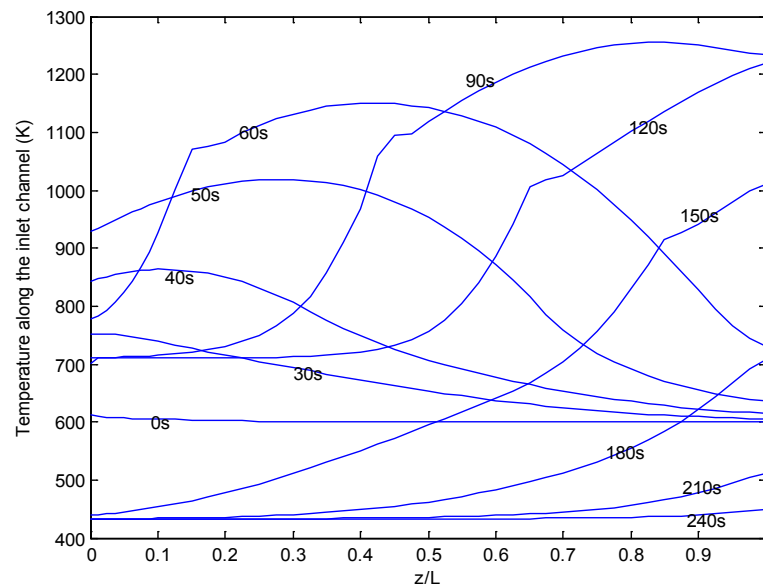
Figure 6.7. Temperature along the inlet channel during the regeneration. (Highway driving without any stops)

Figure 6.8. Deposit thickness along the inlet channel during the regeneration. (Highway driving without any stops)
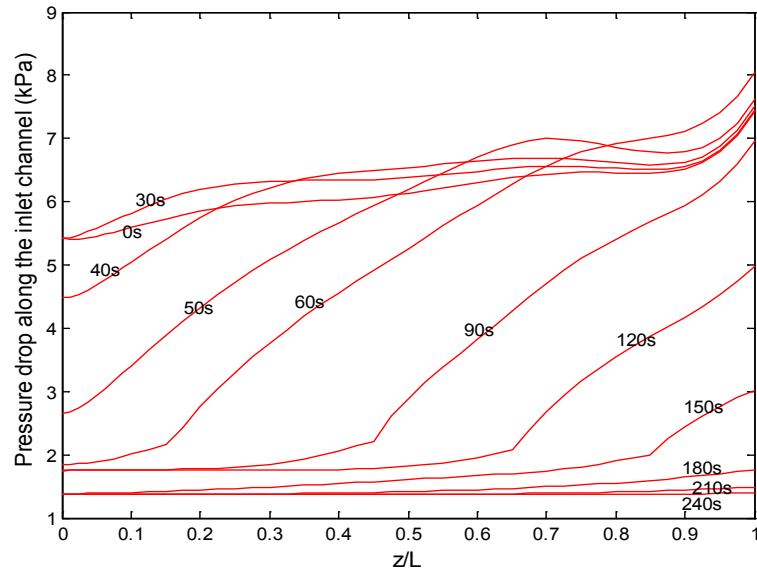
Figure 6.9. Pressure drop along the inlet channel during the regeneration. (Highway driving without any stops)

146

City driving without any stops

Under city driving without stops driving condition, the average vehicle speed is about 27 miles per hour which is lower than that for highway driving without stops condition and it leads to a lower gas flow rate. As mentioned before, less thermal energy will be supplied from this lower gas flow rate; therefore, the process of regeneration is slower and the regeneration efficiency is lower than that of highway driving without stops condition which is equal to 96.8%. From Figures 6.10 and 6.11, one can find that the maximum temperature occurs at t = 120s near the end of the channel. Also the channels will be quenched after 180s as seen in Figure 6.11.
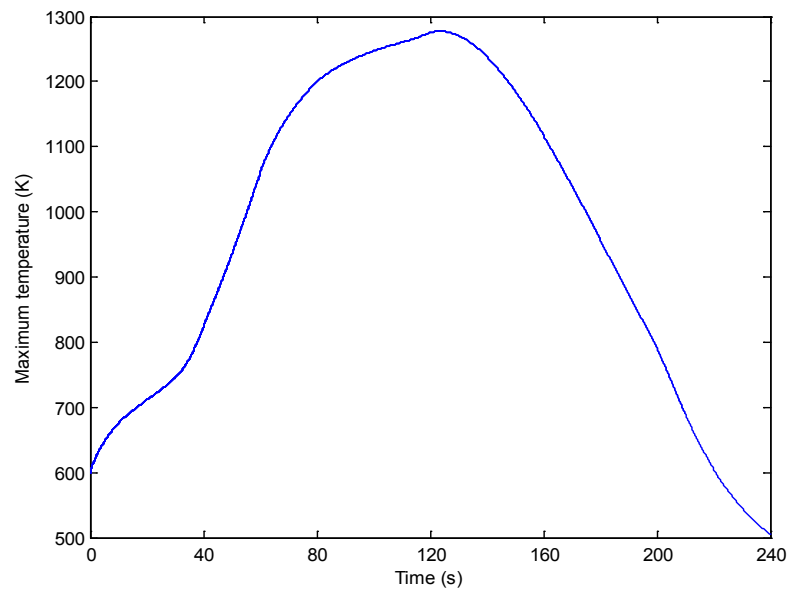
Figure 6.10. The maximum temperature in the inlet channel as a function of time. (City driving without any stops)

147
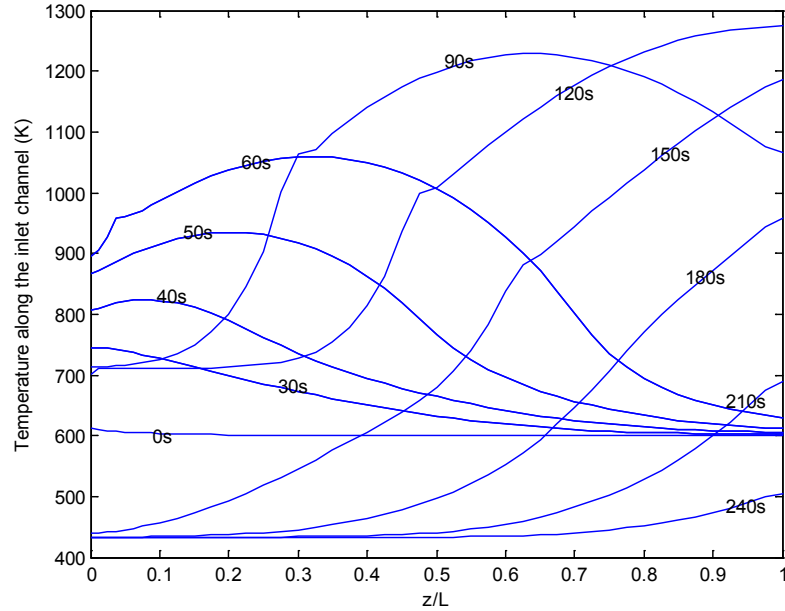
Figure 6.11. Temperature along the inlet channel during the regeneration. (City driving without any stops)

There are some particulates remaining at the end of the channel after 240s (see Figure 6.12). This is because the additional energy supplied by the fuel is too low to complete the regeneration of the DPF. Moreover, the remaining particulates may result in a higher local pressure drop which may crack the DPF. Therefore, a completed regeneration of the DPF is necessary. Figure 6.13 shows the local pressure drop in the inlet channel during the regeneration under this driving condition. From Figure 6.13, we are able to find that the local pressure drop near the end of the filter is higher which is caused by the remaining deposit layer mentioned above.
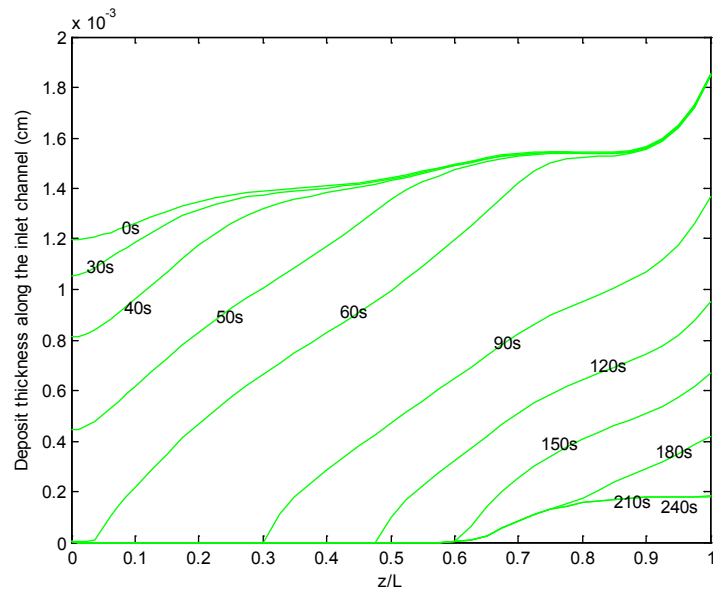
Figure 6.12. Deposit thickness along the inlet channel during the regeneration. (City driving without any stops)
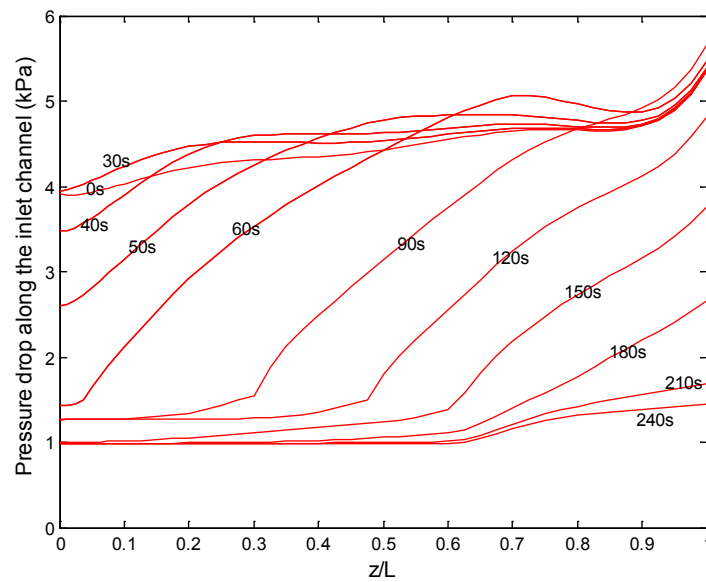
Figure 6.13. Pressure drop along the inlet channel during the regeneration. (City driving without any stops)

City Driving with Stops

Under the city driving with stops condition, there are several stops during the cycle. The average gas flow rate for this driving condition is low and the amplitude of the gas flow rate curve fluctuates more which affects the regeneration efficiency.

From Figure 6.5, it can be noticed that the regeneration efficiency is the lowest (94.3%) under this driving condition. In Figure 6.14, the maximum temperature occurs at about 40 seconds later than that of highway driving without stops (at t = 140s). Figure 6.15 shows the temperature profile along the inlet channel during the regeneration. Moreover, from Figure 6.16, we can find that there are more particulates remaining at the end of the filter after the regeneration process. During the next filtration cycles, more and more particulates will be deposited on this remaining particle layer which may result in higher local pressure drop as seen in Figure 6.17. Also, this situation requires more thermal energy to burn off the thicker deposit layer and more energy will be released from the reaction which may crack the DPF. Therefore, it is not desirable to initiate the regeneration under city driving with stops condition.
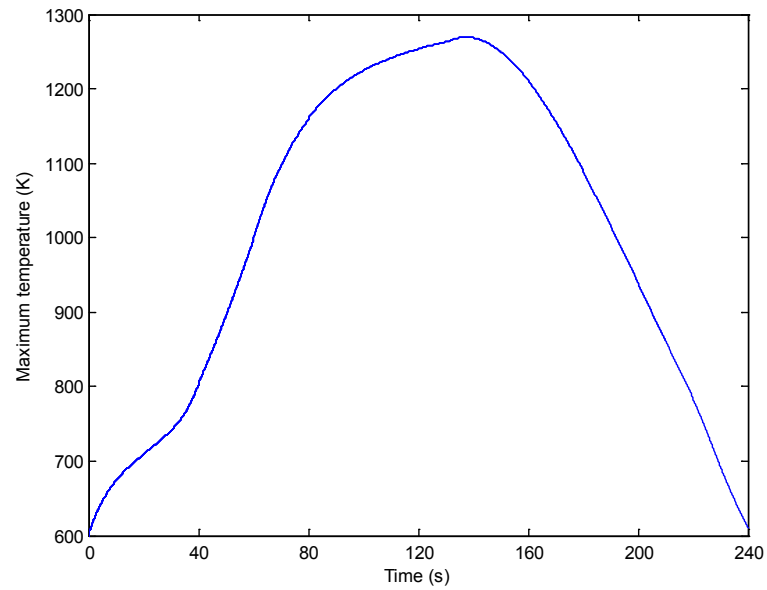
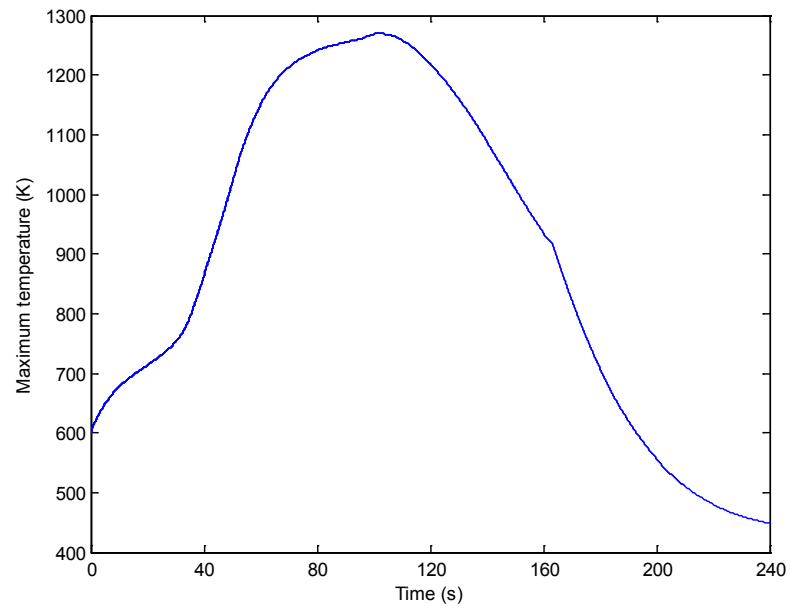**Figure 6.14. The maximum temperature in the inlet channel as a function of time. (City driving with stops)**
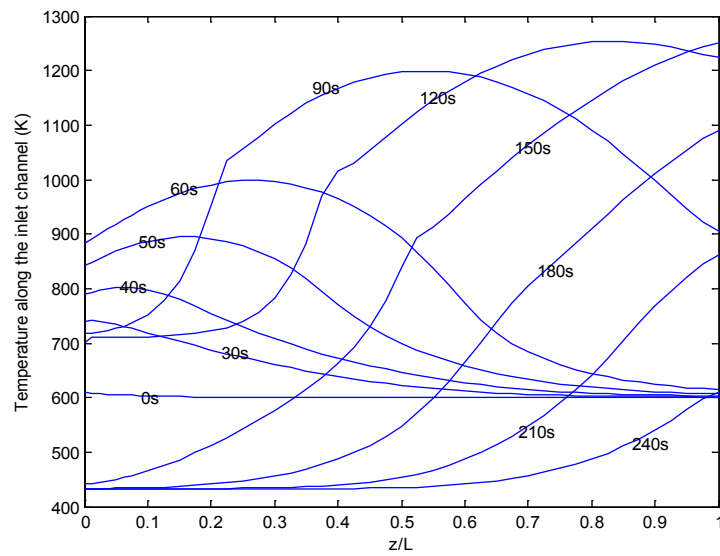
Figure 6.15. Temperature along the inlet channel during the regeneration. (City driving with stops)

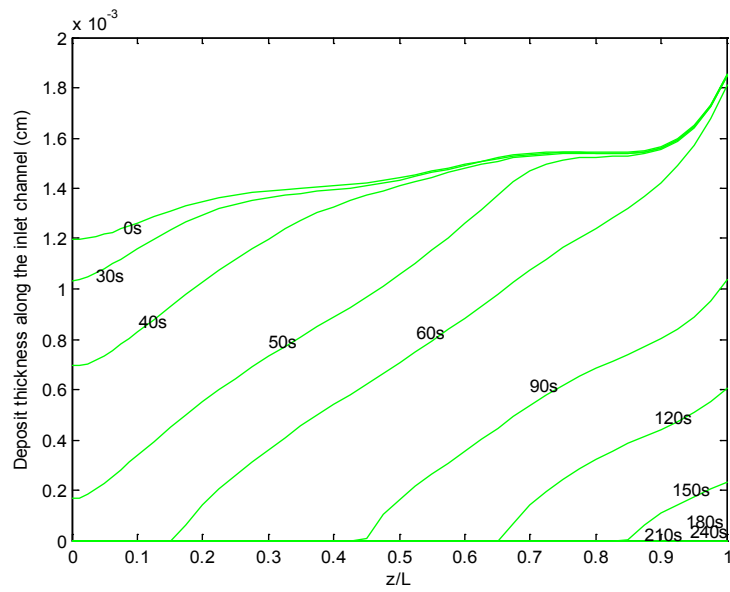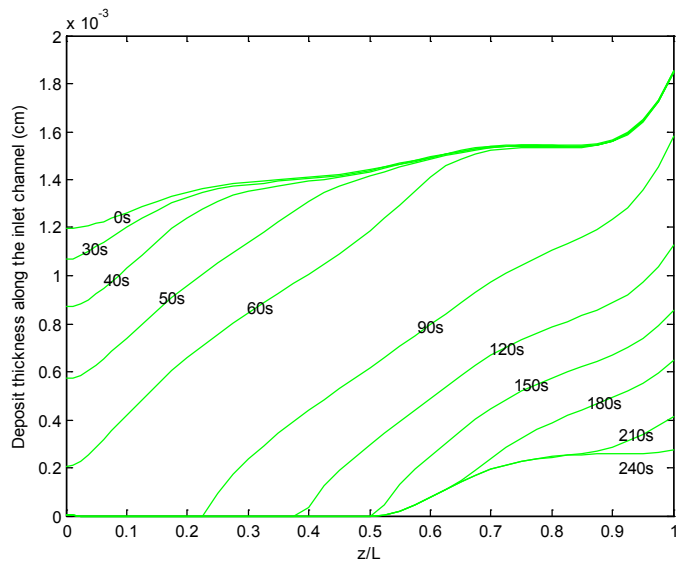**Figure 6.16. Deposit thickness along the inlet channel during the regeneration. (City driving with stops)**
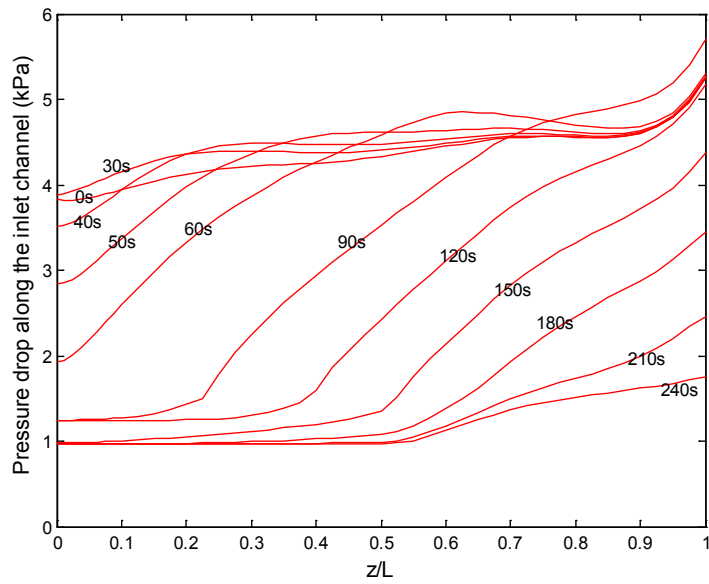
Figure 6.17. Pressure drop along the inlet channel during the regeneration. (City driving with stops)

152

By comparing these three simple driving conditions with the UDDS driving cycles, we can find that the regeneration efficiency of all of these three simple cycles shows similar trends to the results of UDDS driving cycle: highway driving without stops gives the best performance followed by city driving without stops, and finally city driving with stops. Thus, simpler transient simulations can be used in place of complex driving cycles to predict DPF regeneration performance.

Chapter 7 Findings and Conclusions

7.1 Summary

Diesel Engine and Diesel Particulate Filter (DPF)

Due to their high thermal efficiency, diesel engines have an excellent fuel economy and less carbon dioxide emission compared with gasoline engines. However, diesel engines produce a large amount of particulate matter (PM) which can imperil human health.

In order to reduce the PM from diesel engines to meet the emission standards in the U.S., a diesel particulate filter (DPF) is used as an aftertreatment device which is equipped on diesel engine vehicles. A wall-flow monolith filter is widely used because of its high filtration efficiency and high thermal capacity. These wall-flow monolith filters are made of a porous ceramic material and consist of a large number of channels with the opposite ends plugged.

Filtration in DPF

In general, there are two types of filtration: "deep bed filtration" and "cake filtration." During the filtration, mass accumulated by "deep-bed" filtration is much less than that of "cake" filtration, however, the filtration efficiency increases more remarkably during "deep-bed" filtration. This is because most of the pores in the substrate wall are blocked by the particulates accumulated inside so that particles are not able to pass through the blocked wall and get into the outlet channel of the DPF. Then, since the walls will not allow particulate to pass through them, the filtration efficiency approaches 100% which results in the "cake" filtration mechanism (4). The filter wall is divided into a series of layers, and we use a "unit collector" filtration theory in this study (17). In each layer, the diameter of the "unit collector" will increase only due to deep bed filtration. Because particulates will be trapped in each slab and since the mass which goes into the next slab will decrease, the mass accumulated decreases with transverse position through the filter wall. As such, the diameter of the unit collectors decreases which leads to an increased porosity of each slab.

Pressure Drop in DPF

The pressure drop across the DPF is one of the most important critical parameters in the design of a DPF regeneration strategy. The total pressure drop for a loaded filter

can be divided into four parts: pressure drop of inlet channel, pressure drop of outlet channel, pressure drop across the soot layer, and pressure drop across the substrate wall (17).

A thicker deposit thickness causes a higher pressure drop and there also may be a large heat released from the regeneration which may cause a crack in the DPF. Also, the additional particulate needs more thermal energy to complete the regeneration. Therefore, a reasonable pressure drop is required for the DPF during both filtration and regeneration. It is noted that a larger gas flow rate will also lead to a higher pressure drop. Finally, the larger gas flow rate may quench the thermal regeneration mechanism in the DPF.

UDDS Driving Cycles

The Urban Dynamometer Driving Schedule is a driving cycle to test the diesel engine vehicles under real-world driving conditions (22, 23). In order to find out the best desirable regeneration conditions, we performed transient simulations using the UDDS driving cycles to provide inlet conditions to our models with the goal of determining the best inlet temperature, gas flow rate, deposit thickness, regeneration duration, and the time to start the regeneration. By comparing the vehicle speed and the number of

stops during the driving period, we divide the UDDS driving cycle into three parts which are highway driving without stops, city driving without stops, and start-and stop city driving.

We choose 710K as the inlet temperature of our models since it results in leading-edge regeneration in the DPF. In order to complete the regeneration, 120 seconds is chosen as the regeneration duration. A deposit layer thickness of 11-14 μm is desirable since either too big or too small of an amount of particulates will need more thermal energy to reach a higher regeneration efficiency. We also found that the regeneration should be initiated during the portion of the UDDS that corresponds to highway driving without stops since the regeneration efficiency is the highest. On the other hand, regeneration during start-and-stop city driving results in the lowest regeneration efficiency.

New Driving Cycles

We developed three simple sinusoidal functions to approximate the vehicle speed under the UDDS driving cycle for each driving period: highway driving without stops, city driving without stops, and start-and-stop city driving. We are able to use these new simple driving cycles to predict temperature, deposit thickness, and pressure drop

profiles during the regeneration process. For each case, the simulation results exhibit similar trends to the results of UDDS driving cycles.

Comparisons between this research and industry

In the industry, CDPFs are widely equipped on larger size diesel engines, while smaller size diesel engines still use bare DPF. Therefore, for the larger size diesel engines, there are two different regeneration types: passive regeneration and active regeneration.

In this work, we simulate the regeneration under non-uniform deposit thickness in the DPF to analyze the impact of deposit thickness on the pressure drop which is a very important parameter during the regeneration of DPF. However, in reality, the deposit thickness in (c)DPF is uniform over many driving cycles, especially before the regeneration.

Before regeneration, the total soot load is about 6.5 g/L (100% load) in the industrial area. If loaded greater than 6.5 g/L, the (c)DPFs might crack or even melt due to the larger heat released from the active regeneration. Moreover, in the regeneration, the lower inlet temperature is preferred in the industry because higher temperature peak

during the regeneration is avoided to maintain the reliability and durability of the aftertreatment devices. In our research, we consider more about energy efficiency so we short the regeneration duration and use higher inlet temperature. While, in the industry, there are more concerns about the balance between energy efficiency and the durability of the equipments so that they can reduce the cost of the service of productions.

7.2 Future Work

In this work, we have shown the filtration and regeneration process of DPF under the "real-world" driving conditions—Urban Dynamometer Driving Schedule. Similar results were predicted from the use of three simple driving cycles. We have determined desirable variables of our filtration model, pressure drop model, and regeneration model under UDDS driving cycle.

Also in this work we found that gas flow rate is the significant variable in the regeneration model and the regeneration efficiency increases with increasing gas flow rate. Therefore, we will consider adding a by-pass system to increase the gas flow to

improve regeneration performance under non-ideal operating conditions.

In addition, different series of on-road diesel engine exhaust data and variable driving cycles should be integrated with the model.

In a recent development, Catalyzed Diesel Particulate Filters (CDPFs) are widely used as the aftertreatment of diesel vehicles instead of DPFs. For the CDPF, the substrate walls of the filter are coated with catalyst and this kind of can increase the filtration efficiency and the regeneration efficiency of a variety of diesel engine emissions, including NOx, CO, hydrocarbons, and PM. The modeling work here can be extended to the study of CDPFs.

To aid in this effort, a better understanding of the chemical conversion and the mechanism of the regeneration in CDPF is desired which will be helpful for the improvement of filtration efficiency and regeneration efficiency.

As discussed in the previous subsection, we will try lower inlet temperature and longer regeneration duration of the regeneration of (c)DPFs in the future works. Another important parameter during the regeneration is the soot loading in the DPF. A better

knowledge of (c)DPFs soot loading is critical for the aftertreatment system. In recent,

a new technology - RF (Radio Frequency) - is being developed to measure the soot

level in (c)DPFs   based sensing techniques. In the future work, we may have a better

understanding of this new technology in order to measure the soot loading more

accurately.

References

(1). Emission test cycles – DieselNet [Internet]. Urban Dynamometer Driving Schedule (UDDS). Available from http://www.dieselnet.com/standards/cycles/ftp72.html

(2). Zheng HS, Keith JM, Ignition analysis of wall-flow monolith diesel particulate filters. Catalysis Today. 2004:98(3):403-412.

(3). Blackman PG. Emission Control Options to Achieve Euro IV and Euro V on Heavy Duty Diesel Engines. SAE Journal. 2008;2008280021.

(4). Foster DE, Kusaka T. Detailed Diesel Exhaust Particulate Characterization and Real-Time DPF Filtration Efficiency Measurements during PM Filling Process. SAE Journal. 2007;2007010320.

(5). Sakai H, Busch P, Vogt CD. Filtration Behavior of Diesel Particulate Filters. SAE Journal. 2007;2007010921.

(6). Johnson JH, Naber JD, Bagley ST. A Methodology to Estimate the Mass of Particulate Matter Retained in a Catalyzed Particulate Filter as Applied to Active Regeneration and On-Board Diagnostics to Detect Filter Failures. SAE Journal. 2008;2008010764.

(7). Pinturaud D, Charlet A, Caillol C, Higelin P, Girot P, Briot A. Experimental Study of DPF Loading and Incomplete Regeneration, SAE Journal. 2007;2007240094.

(8). Mizutani T, Kaneda A, Ichikawa S, Kurachi H, Vogt CD, Tanaka M, Martin A, Fujii S, Busch P. Filtration Behavior of Diesel Particulate Filters (2). SAE Journal. 2007;2007010923.

(9). Barataud C, Bardon S, Bouteiller B, Gleize V, Charlet A, Higelin P. Diesel Particulate Filter Optimization. SAE Journal. 2003;2003010376.

(10). Masoudi M. Pressure Drop of Segmented Diesel Particulate Filters. SAE Journal. 2005;2005010971.

(11). Nixdorf RD. Microwave-Regenerated Diesel Exhaust Particulate Filter. SAE Journal. 2001;2001010903.

(12). Nakatani K, Hirota S, Takeshima S, Itoh K, Tanaka T Dohmae K, Simultaneous PM and NOx Reduction System for Diesel Engines. SAE Journal. 2002;2002010957.

(13). Benker B, Wollmann A, Claussen M. Measurement of the Local Gas Velocity at the Outlet of a Wall Flow Particle Filter. SAE Journal. 2005;200524001.

(14). Furuta Y, Mizutani T, Miyairi Y, Yuki K,Kurach H. Study on Next Generation Diesel Particulate Filter. SAE Journal. 2009;2009010292.

(15). Kuki T, Miyairi Y, Kasai Y, Miyazaki M, Miwa S. Study on Reliability of Wall-Flow Type Diesel Particulate Filter. SAE Journal. 2004;2004010959.

(16). Huang D, Keith JM. Parametric and Sensitivity Analysis of Diesel Particulate Filter Regeneration. International Journal of Chemical Reactor Engineering. 2009;7 (A56).

(17). Johnson JH, Konstandopoulos AG. A Study Describing the Performance of Diesel Particulate Filters During Loading and Regeneration- A Lumped Parameter Model for Control Applications. SAE Journal. 2003;2003010842.

(18). Dullien FAL. Porous Media- Fluid Transport and Pore Structure. New York (NY). Academic Press. 1979. (Chapter 3).

(19). Lee KW, Gieseke JA. Collection of Aerosol Particles by Packed Beds, Environmental Science and Technology. 1979;13(4):466-470.

(20). Bissett EJ. Mathematical Model of the Thermal Regeneration of a Wall-flow Monolith Diesel Particulate Filter. Chemical Engineering Science. 1984;39 (7/8):1233-1244.

(21). Huang D. Parametric and Sensitivity Study of Wall-Flow Monolith Diesel Particulate Filter Regeneration. M.S. Thesis. 2008. Michigan Technological University. Houghton (MI).

(22). Thornton M, Webb CC, Weber PA, Orban J, Slone E. Fuel Sulfur Effects on a Medium-Duty Diesel Pick-Up with a NO_x Adsorber, Diesel Particle Filter Emissions Control System: 2000-Hour Aging Results. SAE Journal. 2006;2006010425.

(23). Dabhoiwala RH. An Experimental and Modeling Study of Two Diesel oxidation Catalyst- Catalyzed Particulate Filter Systems and the Effects of a Cracked Filter on its Performance.   M.S. Thesis. 2007. Michigan Technological University. Houghton (MI).

Appendix A Copyright Permissions

(Copyright permission for Figure 1.1)

<div align="center">

ELSEVIER LICENSE
TERMS AND CONDITIONS

</div>

Aug 21, 2008

This is a License Agreement between Di Huang ("You") and Elsevier ("Elsevier"). The licen
consists of your order details, the terms and conditions provided by Elsevier, and the payme
terms and conditions.

Supplier	Elsevier Limited
	The Boulevard,Langford Lane
	Kidlington,Oxford,OX5 1GB,UK
Registered Company Number	1982084
Customer name	Di Huang
Customer address	2008 E woodmar dr.
	houghton, MI 49931
License Number	2012650928134
License date	Aug 19, 2008
Licensed content publisher	Elsevier
Licensed content publication	Catalysis Today
Licensed content title	Ignition analysis of wall-flow monolith diesel particulate filters
Licensed content author	Haishan Zheng and Jason M. Keith
Licensed content date	1 December 2004
Volume number	98
Issue number	3

Pages	10
Type of Use	Thesis / Dissertation
Portion	Full article
Format	Electronic
You are an author of the Elsevier article	No
Are you translating?	No
Purchase order number	
Expected publication date	Jan 2008
Elsevier VAT number	GB 494 6272 12
Permissions price	0.00 USD
Value added tax 0.0%	0.00 USD
Total	0.00 USD

Terms and Conditions

INTRODUCTION

1. The publisher for this copyrighted material is Elsevier. By clicking "accept" in connecti
with completing this licensing transaction, you agree that the following terms and conditio
apply to this transaction (along with the Billing and Payment terms and conditions establish
by Copyright Clearance Center, Inc. ("CCC"), at the time that you opened your Rightsli
account and that are available at any time at <http://myaccount.copyright.com>).

GENERAL TERMS

2. Elsevier hereby grants you permission to reproduce the aforementioned material subject
the terms and conditions indicated.

3. Acknowledgement: If any part of the material to be used (for example, figures) h
appeared in our publication with credit or acknowledgement to another source, permissi
must also be sought from that source. If such permission is not obtained then that mater

may not be included in your publication/copies. Suitable acknowledgement to the source mu
be made, either as a footnote or in a reference list at the end of your publication, as follows:

"Reprinted from Publication title, Vol /edition number, Author(s), Title of article / title
chapter, Pages No., Copyright (Year), with permission from Elsevier [OR APPLICABI
SOCIETY COPYRIGHT OWNER]." Also Lancet special credit - "Reprinted from The Lanc
Vol. number, Author(s), Title of article, Pages No., Copyright (Year), with permission fro
Elsevier."

4. Reproduction of this material is confined to the purpose and/or media for which permissi
is hereby given.

5. Altering/Modifying Material: Not Permitted. However figures and illustrations may l
altered/adapted minimally to serve your work. Any other abbreviations, additions, deletio
and/or any other alterations shall be made only with prior written authorization of Elsevier L
(Please contact Elsevier at permissions@elsevier.com)

6. If the permission fee for the requested use of our material is waived in this instance, plea
be advised that your future requests for Elsevier materials may attract a fee.

7. Reservation of Rights: Publisher reserves all rights not specifically granted in th
combination of (i) the license details provided by you and accepted in the course of th
licensing transaction, (ii) these terms and conditions and (iii) CCC's Billing and Payment terr
and conditions.

8. License Contingent Upon Payment: While you may exercise the rights licens
immediately upon issuance of the license at the end of the licensing process for th
transaction, provided that you have disclosed complete and accurate details of your propos
use, no license is finally effective unless and until full payment is received from you (either
publisher or by CCC) as provided in CCC's Billing and Payment terms and conditions. If f
payment is not received on a timely basis, then any license preliminarily granted shall l
deemed automatically revoked and shall be void as if never granted. Further, in the eve
that you breach any of these terms and conditions or any of CCC's Billing and Payment terr
and conditions, the license is automatically revoked and shall be void as if nev
granted. Use of materials as described in a revoked license, as well as any use of th
materials beyond the scope of an unrevoked license, may constitute copyright infringeme
and publisher reserves the right to take any and all action to protect its copyright in th
materials.

9. Warranties: Publisher makes no representations or warranties with respect to the licens

material.

10. Indemnity: You hereby indemnify and agree to hold harmless publisher and CCC, and their respective officers, directors, employees and agents, from and against any and all claims arising out of your use of the licensed material other than as specifically authorized pursuant to this license.

11. No Transfer of License: This license is personal to you and may not be sublicensed, assigned, or transferred by you to any other person without publisher's written permission.

12. No Amendment Except in Writing: This license may not be amended except in a writing signed by both parties (or, in the case of publisher, by CCC on publisher's behalf).

13. Objection to Contrary Terms: Publisher hereby objects to any terms contained in any purchase order, acknowledgment, check endorsement or other writing prepared by you, which terms are inconsistent with these terms and conditions or CCC's Billing and Payment terms and conditions. These terms and conditions, together with CCC's Billing and Payment terms and conditions (which are incorporated herein), comprise the entire agreement between you and publisher (and CCC) concerning this licensing transaction. In the event of any conflict between your obligations established by these terms and conditions and those established by CCC's Billing and Payment terms and conditions, these terms and conditions shall control.

14. Revocation: Elsevier or Copyright Clearance Center may deny the permissions described in this License at their sole discretion, for any reason or no reason, with a full refund payable to you. Notice of such denial will be made using the contact information provided by you. Failure to receive such notice will not alter or invalidate the denial. In no event will Elsevier or Copyright Clearance Center be responsible or liable for any costs, expenses or damage incurred by you as a result of a denial of your permission request, other than a refund of the amount(s) paid by you to Elsevier and/or Copyright Clearance Center for denied permissions.

LIMITED LICENSE

The following terms and conditions apply to specific license types:

15. **Translation**: This permission is granted for non-exclusive world **English** rights only unless your license was granted for translation rights. If you licensed translation rights you may only translate this content into the languages you requested. A professional translator must perform all translations and reproduce the content word for word preserving the integrity of the article. If this license is to re-use 1 or 2 figures then permission is granted for

non-exclusive world rights in all languages.

16. **Website**: The following terms and conditions apply to electronic reserve and auth websites:

Electronic reserve: If licensed material is to be posted to website, the web site is to l password-protected and made available only to bona fide students registered on a releva course if:

This license was made in connection with a course,

This permission is granted for 1 year only. You may obtain a license for future webs posting,

All content posted to the web site must maintain the copyright information line on the botto of each image,

A hyper-text must be included to the Homepage of the journal from which you are licensin at http://www.sciencedirect.com/science/journal/xxxxx   or the Elsevier homepage for boo at http://www.elsevier.com , and

Central Storage: This license does not include permission for a scanned version of tl material to be stored in a central repository such as that provided by Heron/XanEdu.

17. **Author website** for journals with the following additional clauses:

This permission is granted for 1 year only. You may obtain a license for future webs posting,

All content posted to the web site must maintain the copyright information line on the botto of each image, and

The permission granted is limited to the personal version of your paper.   You are not allowe to download and post the published electronic version of your article (whether PDF or HTM proof or final version), nor may you scan the printed edition to create an electronic version,

A hyper-text must be included to the Homepage of the journal from which you are licensin at http://www.sciencedirect.com/science/journal/xxxxx , or the Elsevier homepage for boo at http://www.elsevier.com and

Central Storage: This license does not include permission for a scanned version of tl material to be stored in a central repository such as that provided by Heron/XanEdu.

18. **Author website** for books with the following additional clauses:

Authors are permitted to place a brief summary of their work online only.

A hyper-text must be included to the Elsevier homepage at http://www.elsevier.com

This permission is granted for 1 year only. You may obtain a license for future webs posting,

All content posted to the web site must maintain the copyright information line on the botto of each image, and

The permission granted is limited to the personal version of your paper.   You are not allowe

to download and post the published electronic version of your article (whether PDF or HTM proof or final version), nor may you scan the printed edition to create an electronic version,

A hyper-text must be included to the Homepage of the journal from which you are licensi at http://www.sciencedirect.com/science/journal/xxxxx , or the Elsevier homepage for boo at http://www.elsevier.com and

Central Storage: This license does not include permission for a scanned version of the material to be stored in a central repository such as that provided by Heron/XanEdu.

19. **Website** (regular and for author): "A hyper-text must be included to the Homepage of the journal from which you are licensing at http://www.sciencedirect.com/science/journal/xxxxx.

20. **Thesis/Dissertation**: If your license is for use in a thesis/dissertation your thesis may submitted to your institution in either print or electronic form. Should your thesis be publish commercially, please reapply for permission. These requirements include permission for the Library and Archives of Canada to supply single copies, on demand, of the complete these and include permission for UMI to supply single copies, on demand, of the complete thes Should your thesis be published commercially, please reapply for permission.

v1.2

21. **Other conditions:**

None